EFFECT OF ATMOSPHERIC PRESSURE AND TEMPERTURE ON A SMALL SPARK IGNITION INTERNAL COMBUSTION ENGINE'S PERFORMANCE

THESIS

Peter J. Schmick, Captain, USAF

AFIT/GAE/ENY/11-M28

DEPARTMENT OF THE AIR FORCE
AIR UNIVERSITY

AIR FORCE INSTITUTE OF TECHNOLOGY

Wright-Patterson Air Force Base, Ohio

AFIT/GAE/ENY/11-M28

EFFECT OF ATMOSPHERIC PRESSURE AND TEMPERTURE ON A SMALL SPARK IGNITION INTERNAL COMBUSTION ENGINE'S PERFORMANCE

THESIS

Presented to the Faculty

Department of Aeronautics and Astronautics

Graduate School of Engineering and Management

Air Force Institute of Technology

Air University

Air Education and Training Command

In Partial Fulfillment of the Requirements for the

Degree of Master of Science in Aeronautical Engineering

Peter J. Schmick

Captain, USAF

March 2011

AFIT/GAE/ENY/11-M28

EFFECT OF ATMOSPHERIC PRESSURE AND TEMPERTURE ON A SMALL SPARK IGNITION INTERNAL COMBUSTION ENGINE'S PERFORMANCE

Peter Schmick

Captain, USAF

March 2011

Approved:

_____	_____
Dr. Marcus Polanka (Chairman)	date
_____	_____
Dr. Paul King (Member)	date
_____	_____
Lt Col Frederick Harmon (Member)	date

Abstract

The ever increasing use of man portable unmanned aerial vehicles by the US military in a wide array of environmental conditions calls for the investigation of engine performance under these conditions. Previous research has focused on individual changes in pressure or temperature conditions of the air stream entering the engine. The need was seen for a facility capable of providing an environment representative of various simulated altitude conditions. A mobile test facility was developed to test small internal combustion engines with peak powers less than 10 hp. A representative engine was tested over a range of speeds from 2000 RPM to 9000 RPM at every 1000 RPM. The throttle was set to 50%, 75%, and 100% open at each of the speeds tested. The test engine was tested at environmental conditions representing sea level standard day conditions, 1500 m conditions and 3000 m conditions. The engine torque, fuel flow rate, and air flow rate were measured at each test point to determine the impact of combined pressure and temperature variations on engine performance. During the process of testing the engine and the test stand it was determined that the inlet air pressure had a significant impact on engine operation. The test engine failed to operate under fuel rich or fuel lean conditions caused by these pressure oscillations through the carburetor.

Acknowledgements

I would like to thank my academic advisor, Dr. Marc Polanka, and the research sponsors, Dr. Fred Schauer and Paul Litke, for allowing me the opportunity to work on this research with them. Thank you Paul and Dr. Schauer for letting me utilize your facilities and all of the advice you gave me during the last year and a half. Thank you Dr. Polanka for the many hours spent discussing this research and listening to all of the problems encountered and offering suggested solutions.

This research would not have been accomplished if it weren't for the help and guidance of several key players that work in D-Bay and 5-Stand. Dr. John Hoke and Adam Brown of ISSI along with Capt Cary Wilson were instrumental in assisting me with the experimental setup and I appreciate their patience in helping me solve many of the issues encountered. I would also like to thank them for helping to further my understanding of all of the fundamental concepts behind this research. Thanks to Dave Burris for writing the LabView program. I would like to thank Curtis Rice, Rich Rymann, and Justin Goffena for all of their always willing lab support, which included anything from helping me find materials to showing me how to use some of the machining equipment, to the proper way to install certain components. I would also like to thank them for helping to fabricate some of the test stand.

Lastly, I would like thank my fiancé for always being understanding and listening to me talk about how things were going on a daily basis, which was far too often. She supported my efforts the entire way and encouraged me to do my best.

Table of Contents

Page

Page

List of Figures

Page

Page

Page

Page

List of Tables

Page

List of Symbols

Symbol	
$\partial R/\partial x_i$	partial derivative of variable R with respect to variable x_i
δR	change in variable R
δx_i	change in variable x_i
η_c	combustion efficiency
η_f	fuel conversion efficiency
η_{mc}	mechanical efficiency
η_{th}	thermal efficiency
θ	crank angle
κ	polytropic coefficient
λ	excess air ratio (Eq. 22)
λ	delivery ratio (Eq. 8)
λ	Power (Eq. 13)
ρ	density
ρ_{mix}	mixture density
ρ_{Power}	power density
ρ_{ref}	reference density
ϕ	equivalence ratio
ψ	relative humidity
ω	air humidity ratio
a	crank radius (Figure 2)
a	auto regression coefficient (Eq. 19)
a	minor dimension in Appendix C
A	constant (Eq. 9)
A	constant (Eq. 10)
A/F	Air to fuel ratio
b	distance (Eq. 4)
b	constant (Eq. 9)
b	major dimension in Appendix C
B	bore (Figure 2)
B	constant (Eq. 10)
$c(\theta)$	compression ratio as a function of crank angle
CF	correction factor
COV_{imep}	coefficient of variation of indicated mean effective pressure
CO	carbon monoxide
CO_2	carbon dioxide
$\overline{C_P}$	average specific heat at constant pressure
CR	compression ratio
C_V	valve flow coefficient
$E(\theta)$	voltage output as a function of crank angle
EI	emissions index
F	force
F/A	Fuel to air ratio
H_c	heat of combustion

Symbol

H_2O	water, dihydrogen oxide
K_S	sensor gain
l	connecting rod length
L	stroke
	mass flow rate
$_{Air}$	mass air flow rate
m_{engine}, x	engine mass, (Eq. 9)
$_{f}$	mass fuel flow rate
$_{mix}$	mass flow rate of the mixture
MW	molecular weight
N	engine speed, RPM (Eq. 4), (Eq. 6), (Eq. 8)
N	number of samples (Eq. 20), (Eq. 34), (Eq. 35)
N_b, P_b	brake power
N_e	net output power
N_i	indicated power
NO_x	nitric oxide formations
n_R	number of revolutions per power stroke
p_D	saturated vapor pressure
p	pressure
p_{alt}	pressure at altitude
p_{in}, p_{inlet}	inlet pressure
p_{amb}	ambient pressure
P	power
q	volumetric flow
Q	energy
Q_{HV}	heating value of fuel
R	specific gas constant
Sg	specific gravity
t	time
t_{tot}	total time
T	torque (Eq. 4), (Eq. 6)
T	temperature (Eq. 10), (Eq. 13), (Eq. 22)
T_{alt}	temperature at altitude
T_S	temperature at reference condition
$V(\theta)$	volume as a function of crank angle
V_c	clearance volume
V_d	displacement volume
Vol	volume
Vol_{pp}	volume per pulse
x	number of pulses (Eq. 21)
X	percent open (Eq. xx)

List of Abbreviations

Abbreviation	
AFIT	Air Force Institute of Technology
AFRL	Air Force Research Laboratory
AGL	Above Ground Level
ASTM	American Society for Testing and Materials
ATDC	After Top Dead Center
BDC	Bottom Dead Center
BMEP	Brake Mean Effective Pressure
BSFC	Brake Specific Fuel Consumption
COTS	Commercial Off the Shelf
DI	Direct Injection
DIN	Deutsches Institut für Normung, German Institute for Standardization
HC	Hydrocarbon
IC	Internal Combustion
ICE	Internal Combustion Engine
KIAS	Knots Indicated Air Speed
LHV	Lower Heating Value
MEP	Mean Effective Pressure
MON	Motored Octane Number
MSL	Mean Sea Level
PC	Personal Computer
PT	Pressure Transducer
RC	Remote Controlled
RON	Research Octane Number
SAE	Society of Automotive Engineers
SI	Spark Ignition
TDC	Top Dead Center
TT	Thermocouple
TTL	Transistor-Transistor Logic
U.S.	United States
UAS	Unmanned Aerial System
UAV	Unmanned Aerial Vehicle
UBHC	Unburned Hydrocarbons
VDC	Voltage Direct Current
WOT	Wide Open Throttle

EFFECT OF ATMOSPHERIC PRESSURE AND TEMPERTURE ON A SMALL SPARK IGNITION INTERNAL COMBUSTION ENGINE'S PERFORMANCE

I. Introduction

The United States military uses many different types of small internal combustion engines in a wide variety of unmanned aerial system, UAS. These engines run from large multi-cylinder spark ignition engines like the Rotax 914, to mid-sized rotary Wankle type UAV Engines Ltd model 801, to single cylinder single digit horsepower engines like the Fuji B34, down to two stroke spark ignition engines like the OS91. In addition to the typical spark ignition engines the introduction of diesel engines and small scale turbine engines is beginning to occur. The size and type of engine chosen for each specific application is based upon the requirements of the mission. Larger engines are useful for long duration, large, higher altitude UASs like the Predator or Reaper. The U.S. Army uses the mid-sized UAV Engines Ltd model 801 in the Shadow UAS and the smaller Fuji B34 in the Sentinel Hawk (1). The main reasons for engine selection for a particular aircraft or mission are based on range, endurance, performance, and payload tradeoffs made during the aircraft design process.

While much research is ongoing in the development of small scale turbines and larger internal combustion engines the primary focus of this research is on engines in the small range that are generally commercial off the shelf, COTS, parts that were designed to run on high octane fuels. There is a requirement for the U.S. armed forces to go to a single fuel for all classes of UAS (2). This requirement stems from the need to simplify the fuel logistics train across all services. The fuel of choice for this single logistics train is JP-8 because of its high energy content and its current use as a fuel for manned aircraft

systems and ground vehicles. The impact of fuel type and octane rating on engine performance will be discussed in more detail in chapter II. Figure 1 gives a description of the current UAS systems as well as future systems grouped based upon mission and performance. The general focus of this research is on those systems which fall under groups 1 and 2 as well as smaller systems from group 3.

<table>
<tr><th>UAS Category</th><th>Maximum Gross Takeoff Weight (lbs)</th><th>Normal Operating Altitude (ft)</th><th>Speed (KIAS)</th><th>Current / Future Representative UAS</th></tr>
<tr><td>Group 1</td><td>0-20</td><td>< 1,200 AGL</td><td>100 kts</td><td>Wasp III, FCS Class I, TACMAV, RQ-14A/B, BUSTER, BATCAM, RQ-11B/C, FPASS, RQ-16A, Pointer, Aqua Terra, Puma</td></tr>
<tr><td>Group 2</td><td>21-55</td><td>< 3,500 AGL</td><td rowspan="2">< 250</td><td>Vehicle Craft Unmanned Aircraft System, ScanEagle, Silver Fox, Aerosonde</td></tr>
<tr><td>Group 3</td><td>< 1320</td><td rowspan="2">< 18,000 MSL</td><td>RQ-7B, RQ-15, STUAS, XPV-1, XPV-2</td></tr>
<tr><td>Group 4</td><td rowspan="2">> 1320</td><td rowspan="2">Any Airspeed</td><td>MQ-5B, MQ-8B, MQ-1A/B/C, A-160</td></tr>
<tr><td>Group 5</td><td>> 18,000 MSL</td><td>MQ-9A, RQ-4, RQ-4N, Global Observer, N-UCAS</td></tr>
</table>

Figure 1: Current U.S. Unmanned Aerial Systems Programs (2)

The development of suitable engines begins by determining the performance of the engine based on several parameters. The power and torque produced by the engine as a function of the fuel consumed is the way in which engines of different types and sized can be compared. While two stroke engines generally have a higher power output based on engine size they are generally less fuel efficient than four stroke engines. Diesel compression ignition engines have a higher efficiency and power output than four stroke

engines but are usually much heavier than similar spark ignition engines. The extra weight for a diesel engine is due to thicker cylinder walls needed to contain the much higher cylinder pressures that are created in the compression ignition engine. The higher energy content of fuels like JP-8 and Jet-A are more suited to the compression ignition engines where temperatures are allowed to go higher during combustion and knocking or auto-ignition is desired. The use of low octane fuels in spark ignition engines can lead to knocking which can damage the engine or cause heavy vibrations which could damage other parts of the aircraft. The development of new technologies such as direct fuel injection and variable spark timing have shown promise in reducing engine knock in engines running on heavy fuels.

One aspect of engine development that has not seen much research is the variation of engine performance with altitude. Most small COTS engines in use today were originally developed for the recreational remote controlled, RC, model aircraft enthusiast. These engines were designed to operate within several hundred feet of sea level. In general most of these COTS engines run using a carburetor to meter fuel in the intake of the engine. Most carburetors included on these production engines can be tuned with some difficulty for operation at higher altitudes by adjusting the needle valve setting by hand manually. The demand placed on these engines by the military in their employment of UAS systems has lead to the desire to determine engine performance based on a fixed engine tuning over a range of pressure and temperature conditions simulated operation over a range of altitudes.

I.1 Objectives

There are several objectives for the current research. This research was aimed at determining how the engine performance varies as a function of altitude using high octane fuels as a baseline for future research. A range of engine speed and load conditions will be run at multiple simulated altitude conditions for the baseline fuel. In addition the engine performance running on heavy fuels over a range of engine speed, engine load, and altitude conditions will be run for comparison. The ultimate goal is to use the information gained in this research to help engine developers and system designers build systems that are capable of running on low octane fuels over a wide range of altitudes in a consistent manner.

A secondary goal for this research is to investigate the sensitivity of engine performance based upon carburetor setting. The carburetor is tuned manually per manufacturer's instructions by rotating the needle valve in or out a specific number of turns. Because the adjustment is made manually the accuracy of the adjustment is quite crude and as such large variability in the actually setting from flight to flight can occur. The engines utilized in typical model aircraft applications and currently being used in small man portable UASs are manufactured without tight tolerances. The lack of manufacturing precision may lead to significant performance differences from engine to engine. Designing cost effective platforms with repeatable performance is important to military utility. A tertiary goal of this research is to attempt to quantify the amount of variability in engine performance that can be attributed to manufacturing differences between identical engines.

I.2 Methodology

The first step towards completing the research objectives was to design a mobile test stand capable of generating simulated altitude conditions. Once the design phase was completed parts were ordered and construction on the mobile test facility was completed. The next step in the process was to complete a series of system functionality checks. These checkouts verified that the system could be operated safely, that it was capable of generating the conditions required, and that it was capable of recording the necessary measurements to complete the performance analysis.

The capability of the test stand was determined through a series of tests. The first test was completed by running the main flow path to determine the ability of the stand to generate low pressures within the chamber. The pressures were achieved by varying the compressor speed and the control valve positions in increments until the compressor drive motor reached its power limit. Based upon the ambient temperature pressure tests the next step was to couple the coolant system with the pressure system. The coolant flow rate was incrementally increased while the system pressure was incrementally reduced. The combined pressure and temperature testing set the capability limits of the mobile test facility.

Once the limits of the test facility were determined a representative test engine was placed in the chamber. Performance testing of representative engine was completed in several steps. The first step was to determine sea level performance of the engine. Sea level performance was determined by incrementally varying engine speed from 2000 to 8500 RPM at set throttle positions. The throttle position was then changed and the engine speed was again run through the range of speeds. Four throttle positions were

used to generate a sea level engine performance map. After the sea level testing was completed attempts were made to determine engine performance at two additional altitudes of 5000 ft and 10000 ft. Performance maps at the additional altitudes were not completed due to limitations of the test facility. The test engine was tested at lower than sea level pressured to determine how engine inlet pressure impacts engine performance. The lower pressure load tests were completed by fixing the engine speed and throttle setting and varying the inlet pressure of the engine. The lower pressure load tests showed trends in engine performance as the inlet pressure decreases.

The impact of carburetor tuning was observed during the course of performing engine load tests. Carburetor tuning was critical to completing the full range of sea level engine performance tests. Future testing of carburetor tuning should involve careful variation of carburetor needle position in small steps at fixed engine speed and throttle position to determine the impact to engine torque and power. In order to determine the full impact of carburetor tuning the needle position test should be repeated for a range of engine speed and throttle positions.

II. Theory and Previous Research

II.1 Engines

Internal combustion engines come in many sizes and types which can make it hard to apply research done on one test engine to classes of engines. Engine size is usually based upon the total displacement volume of the engine. Large engines are categorized as those with a total displacement volume greater than 300 cm^3 and small engines are those with a displacement volume less than about 150 cm^3. There are two main engine designations that differentiate engine operation; the number of strokes and the type of ignition. The number of strokes that an engine uses determines how many movements of the piston occur for each power stroke of the engine. A four stroke engine has four movements for each power stroke that occurs while a two stroke has only two. A four stroke engine has an intake, compression, expansion, and exhaust stroke which enables the engine to get rid of most of the burned combustion products before replacing them with a fresh charge in the cylinder. A two stroke engine has only two strokes, the compression and expansion. The intake of a fresh charge occurs simultaneously with the exhausting of the burned products. This simplification means that at the cost of generally lower efficiency you get a power stroke more frequently leading to a higher power density. Power density is defined in Eq. (1) as the engine rated power divided by the mass of the engine.

$$\rho_{Power} = \frac{P}{m_{engine}} \tag{1}$$

Smith, Boruta, Jerovsek, and Meitner (3) give two metrics for describing engine loading and engine compactness. Smith et al define engine loading in terms of horsepower, hp, per volume which allows researchers to compare how much power is being generated independent of engine type. Smith et al define power density in a slightly different form than Eq. (1) as horsepower per pound, but this represents a similar metric for the engine. Table 1 gives a comparison of several state of the art engines and their related metrics given by Smith et al. Typical spark ignition and diesel engines have power densities between about 0.3 and 1.0 hp/lb with a power to volume ratios between 1.00 and 2.70 hp/in^3.

Table 1: Engine Comparison Chart (5)

Engine	Type	Power (hp)	Displacement (in^3)	Volume (ft^3)	Weight (lbs.)	hp/lb	hp/in^3
Yanmar 6L43-EPT	Diesel	480	354	32.7	1411	0.3402	1.36
Yanmar 4BY 150	Diesel	150	122	18.3	551	0.2720	1.23
Delta Hawk DH200A4/U4/R4	Diesel	200	202	8.0	327	0.6116	1.00
Rotax 914 UL2	SI	100	74	4.7	166	0.6024	1.35
UAV AR682R	SI Rotary	95	36	2.0	124	0.7661	2.64
UAV AR801R	SI Rotary	50	18	1.0	65	0.7692	2.70
ZanZottera 498iA	SI	39	30	0.75	41	0.9512	1.30

The second designation is the type of ignition used in the engine. Spark ignition engines use a spark plug or glow plug to provide the additional energy needed for the fuel air mixture to reach the activation energy level needed to start combustion. Compression ignition engines compress the fuel air mixture so that the temperature rise caused by compression exceeds the ignition temperature of the mixture. In compression ignition engines the compression ratio defined in Eq. (2) is between two and three times higher than that used in spark ignition engines (4).

$$CR = \frac{V_d + V_c}{V_c} \tag{2}$$

where V_d is the displacement or volume swept by the piston from bottom dead center, BDC, to top dead center, TDC, and V_c is the clearance volume. The clearance volume is the volume of the cylinder when the piston is at TDC and is the minimum cylinder volume. Figure 2 shows the relationship between the components that translate power from the combustion chamber into the output shaft. The crank angle, θ, shown in Figure 2 is a way to relate the change in chamber volume to various engine parameters discussed in the next section.

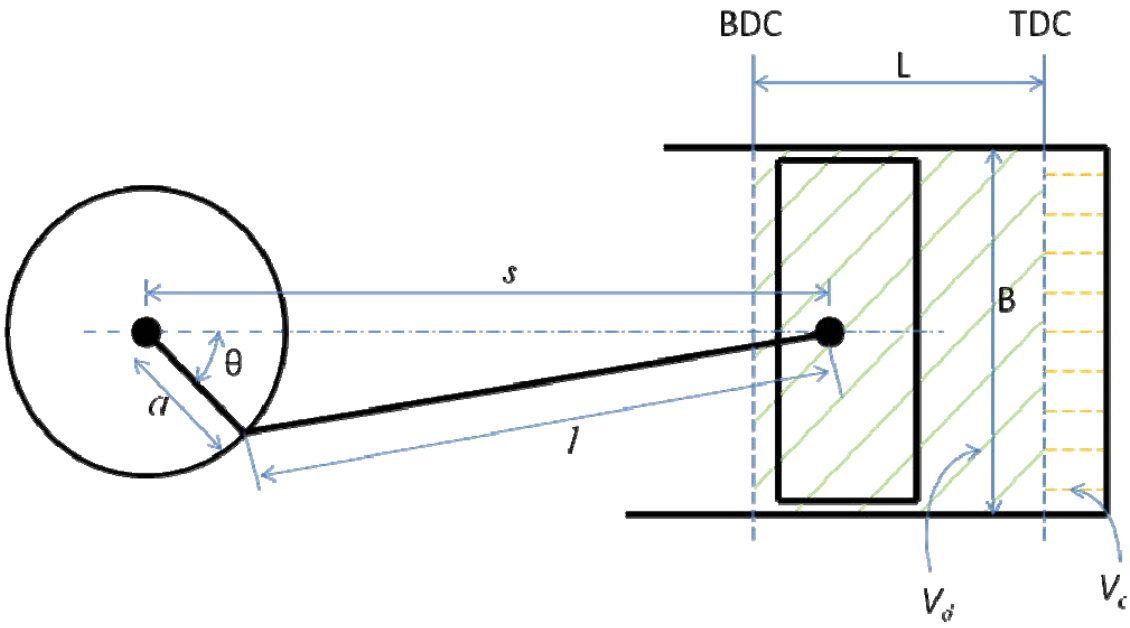

Figure 2: Geometry of cylinder, piston, connecting rod, and crankshaft where B=bore, L=stroke, *l*=connecting rod length, *a*=crank radius, θ=crank angle (adapted from 4).

Several other engine descriptions are important in describing the engine being used in a given research or UAS application. A naturally aspirated engine is one that uses air from the surrounding environment directly without the aid of a pump. A carbureted

engine uses the principles of a venturi or system of venturis to produce the required fuel flow. The carburetor meters the fuel based on a pressure difference created by the venturi. This fuel flow mixes with the air stream in the intake of the engine before it reaches the cylinder. Fuel injection uses a mechanical device to meter pressurized fuel through an orifice into either the intake or the cylinder. Fuel injected into the intake stream is generally termed port fuel injection while fuel injection into the cylinder is generally called direct fuel injection, DI.

The intake process in a two stroke engine is somewhat different than for a four stroke engine due to the need to increase the intake pressure of the fuel air charge above the exhaust pressure in order to enhance exchange of gas within the cylinder during simultaneous intake and exhaust period called scavenging. Scavenging in a two stroke engine is accomplished in several ways and is based upon the geometry of the ports and way in which the fresh charge intake pressure is increased. The three main types of scavenging are cross-scavenged, loop-scavenged, and uniflow-scavenged configurations. Uniflow scavenged engines bring the fresh charge in one end of the cylinder and exhaust it at the opposite end of the cylinder using a variety of ports and valves. Cross-scavenged and loop-scavenged engines use an arrangement of ports in the cylinder wall near BDC which open and close as the piston moves up and down within the cylinder. The main difference between cross-scavenged and loop-scavenged engines is the arrangement of the ports. Cross-scavenged engines have the intake port directly across the cylinder from the exhaust port and use some upward angle in the intake and exhaust ports to force the flow up into the cylinder. Loop-scavenged engines use multiple intake ports generally set perpendicular to the exhaust port. In loop-scavenged engines the intake ports are usually

set so that the incoming flow impinges on a wall or on the opposing incoming flow from the opposite intake port. Figure 3 shows a general diagram of the three types of scavenging processes. The flow path into and out of cylinder is extremely important in two stroke engine design and can have a large impact on engine performance and fuel efficiency (4).

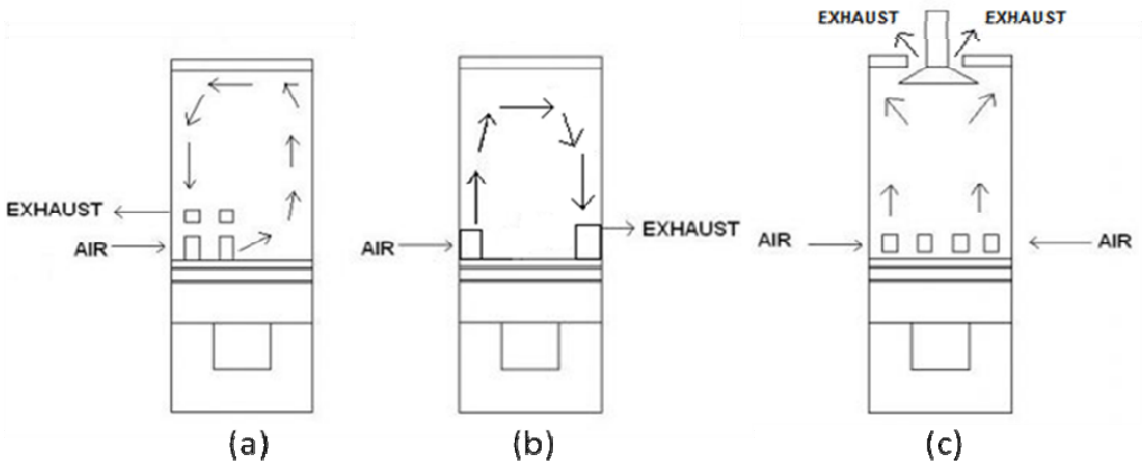

Figure 3: Common types of scavenging; (a) loop-scavenging, (b) cross-scavenging, (c) uniflow-scavenging configurations (adapted from 5).

The compression of the fresh charge in a two stroke engine can be accomplished using an external pump such as a roots type blower or a centrifugal compressor or it can be accomplished using the piston and the crankcase to form an internal compressor. For small single cylinder two stroke engines commonly found in RC airplane applications and used for small engine applications such as chain saws generally crankcase compression is used to save space and reduce weight. One major drawback to most two stroke engines is that the oil used to lubricate the piston and reduce cylinder wear must be mixed with the fuel and is burned as part of the combustion process. In four stroke engines the oil is contained within a separate area and is a closed loop system which is easier for maintenance and logistics.

II.2 Comparison of Engine Parameters

In order to compare one engine to another across the wide variety of engine types a set of performance parameters is needed. The most basic performance parameters are fuel consumption, power, and torque. Power and torque are based upon engine size and type. The amount of power required to hold the dynamometer at a fixed speed can be measured, and is called brake power, P_b. Using a load cell at a fixed distance on the dynamometer torque can be measured. A shaft encoder on the dynamometer shaft can measure speed directly. In order to relate engines of different sizes the fuel consumption, or fuel mass flow rate, $\dot{m}_f$, is divided by the engine power as in Eq. (3), and is called the brake specific fuel consumption, BSFC. BSFC is a measure of the fuel used per amount of energy produced per unit time and is related to how well the energy can convert the available chemical energy stored in the fuel into useful shaft work.

$$BSFC = \frac{\dot{m}_f}{P_b} \tag{3}$$

Torque, *T*, is defined as a force, *F*, times a distance, *b*, given by Eq. (4) and is the measure of an engines ability to do work. Power is the rate at which an engine performs work and is defined by Eq. (5) as torque times the angular speed of the engine. The angular speed of the engine is the rotational rate in revolutions per unit time, N, times the number of radians per revolution, 2π. The engine load required by an ICE is due to the torque required to move a propeller or other device through some amount of rotation. This load as well as throttle setting will determine the engine RPM. As engine load and engine speed increase the total amount of fuel and air running through an engine will

increase leading to changes in BSFC and emissions. In a two stroke carbureted engine changes in engine speed and throttle setting will have an impact on the scavenging of the engine. Engine load and engine speed can also impact combustion efficiency, but it is not necessarily a linear dependence and is more likely attributed to the equivalence ratio driven by the engine speed and throttle setting (4).

$$T = F * b \tag{4}$$

$$P_b = 2\pi * N * T \tag{5}$$

The torque available at the output shaft is the engines ability to do work and can be related across engine sizes and type by defining the work per cycle of an engine divided by the cylinder volume. This quantity is termed mean effective pressure, MEP, since it has units of pressure and is given as Eq. (6). The term n_R is the number of crank revolutions per power stroke per cylinder and is equal to two for a four stroke engine, and one for a two stroke engine. From Eq. (6) it can be seen that since for a given engine the only quantity that changes is the torque at the output shaft which leads to maximum BMEP at the maximum torque value. Maximum power does not occur at the maximum torque value because it is a function of torque and engine speed. The BMEP value for the maximum engine power output will be 10% to 15% lower than the maximum BMEP value (4).

$$\text{BMEP} = \frac{P_b * n_R}{V_d * N} = \frac{2\pi * T * n_R}{V_d} \tag{6}$$

Fuel conversion efficiency, η_f, is a measure of how well the engine is able to convert the chemical energy stored in the fuel and convert it into useful shaft work. Fuel conversion efficiency is defined as work per cycle divided by the amount of fuel inducted

per cycle times the fuel heating value, Q_{HV}, and is given by Eq. (7). In four stroke engines the volumetric efficiency is used to describe the engines ability to induct air into the cylinder during operation. Two stroke engines do not have a defined induction process so volumetric efficiency is not applicable and will not be used to compare engines or past research.

$$\eta_f = \frac{P_b}{\dot{m}_f * Q_{HV}} = \frac{1}{BSFC * Q_{HV}} \tag{7}$$

In addition to the thermodynamic or fuel conversion efficiency defined in Eq. (7), two stroke engines use a parameter called the delivery ratio to describe their operating characteristics. Delivery ratio, λ, from Haywood (4), is defined as the mass of delivered air or mixture per cycle divided by the reference mass show as Eq. (8). For spark ignition two stroke engines the mixture mass is used to define the delivery ratio. The reference mass is the density of the mixture at the inlet conditions times the engine speed and the displacement volume, and the actual mixture mass delivered is simply the sum of the fuel mass flow rate and the air mass flow rate. Higher delivery ratios are desired and indicate that the engine is exhausting a higher percentage of burned products and replacing them with fresh charge.

$$\lambda = \frac{\dot{m}_{mix}}{\rho_{mix} * N * V_d} \tag{8}$$

II.3 Scaling Laws/Issues

The use of small internal combustion engines for UAS applications requires that designers understand the implications of scaling the engine size and its impact on engine

performance and combustion. Cadou et al have done considerable research on small scale internal combustion engines (6, 7, 8, and 9) and how the power and efficiency of the engine can be estimated based upon engine mass. Cadou et al (6) propose a power scaling law on a log-log scale in the form $P=Ax^b$ where x is the mass of the engine and A and b are constants shown as Eq. (9).

$$P = 9901.3x^{0.7633} \tag{9}$$

Figure 4 from Reference 6 shows the relationship between engine mass and output power. Cadou, Moulton, and Menon attempted to derive a similar log linear relationship between engine weight and engine efficiency but the data available from engine manufactures did not support this relationship for engines below 1 kg.

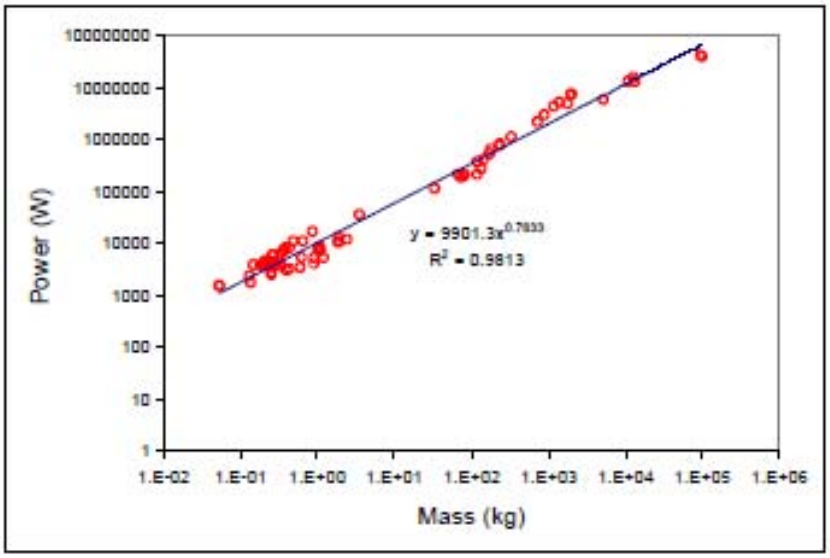

Figure 4: Power output versus engine size (6)

The research by Cadou et al (6) was designed to test small scale internal combustion engines in order to determine appropriate scaling laws based on actual test data rather than relying on manufactures reported values. The researchers built a test system capable of measuring engine speed, engine torque, engine brake power, and fuel

consumption. The engine torque was measured using a cradle system connected to a load cell where the moment arm between the load cell and the cradle can vary in length to accommodate different engine sizes. The engine brake power was measured using a Magtrol HB-880 double hysteresis brake where the power absorbed is proportional to the voltage signal supplied to the brake. The engine speed was measured using an ElectroSensors system consisting of 16 magnetic poles attached to the power takeoff shaft and a proximity switch with senses the poles as they pass. The fuel consumption was measured by taking a series of mass measurements of the fuel tank over fixed periods of time. The researchers used a least squares fit to the mass measurements to determine the fuel mass flow rate. Cadou et al used a two stroke spark ignition OS46FX engine to test first the accuracy of the test system and second to test how running the engine under fuel rich and fuel lean conditions would impact the engine performance. The tests performed over a range of engine speeds at wide open throttle showed that torque and power both increase as the engine is operated in a leaner condition. The engine efficiency also increases as the engine is run in a leaner condition. The maximum power output measured for this engine was 0.5 hp which was only about 30% of the manufacturer's estimate of 1.65 hp. The researchers also noted that the noise associated with the fuel mass measurements meant that there was about a 2% error bar around the engine efficiency calculated.

Menon, Moulton, and Cadou (8) also illustrated one other important aspect related to small internal combustion engines. The variation in performance between engines of the same design and variation in the performance of a single engine over multiple tests was shown to be significant. Using two AP Engines Yellowjacket engines with a

displacement of 2.45 cm^3 and a mass of 150 g Menon et al (8) showed how two identical engines from the same manufacturer perform differently. The engines were run with a constant mixture setting leaned per the manufacturer's instructions at a wide open throttle, WOT, over a range of engine speeds from 7000 to 14000 RPM. The fuel mass flow rate was measured using an FMTD4 nutating microflowmeter manufactured by DEA Engineering. The air mass flow rate was measured using a TSI model 4021 mass flowmeter with an operating range of 0-300 L/min and a linear 0-4 VDC output signal. Power and torque were measured as described above from Reference 7 using the same dynamometer developed in the previous work. The goal of this work was to determine power and efficiency values within 10% of the actual value for use in understanding how engine performance scales with engine size.

Menon et al (8) showed in Figure 5 that a given engine's performance over repeated tests was repeatable within the measurement uncertainty. The slight variation in the data between tests on the same engine was due to torque sensor calibration drift and slight changes in needle valve setting between runs. Figure 5 also shows the very large difference in performance between the two engines tested in this research. The reasons for the variation in performance between identical engines operating at the same conditions were not identified by the authors. One reason for the differences may be manufacturing tolerances by the engine builder. A second cause for this variation may be due to the differences in the carburetors on each engine and how they supply the fuel and air mixture to the engine.

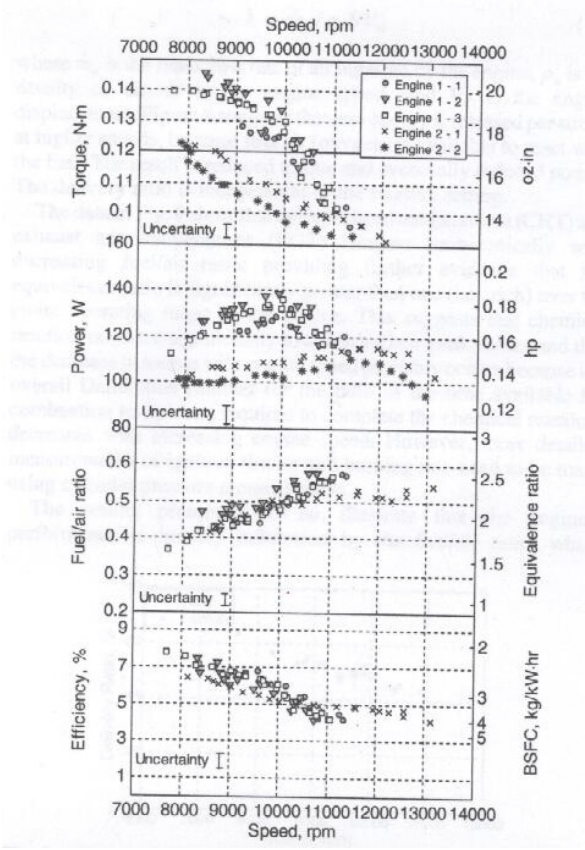

Figure 5: Engine Performance at constant mixture setting and WOT; two different engines and five different tests (8).

Menon et al (8) also investigated the impact of delivery ratio on engine performance. They used a slight variation of Eq. (8) where the mass flow and density of air was used instead of mixture mass flow and mixture density. The slight changes due to this adjustment would not impact the overall conclusions reached. Menon et al showed in Figure 6 that the delivery ratio decreases as engine speed increases independent of mixture setting. Figure 6 shows delivery ratio plotted against engine speed for two different mixture settings. The authors explain that the decrease in delivery ratio with increasing engine speed is due to an increase in fuel to air ratio with engine speed. The increase in fuel to air ratio means that less energy is released per cycle as less air is available to react with the fuel in the combustion chamber during each cycle. The

decrease in delivery ratio is shown to be independent of mixture setting. The independence of delivery ratio with mixture setting is expected because the mass flow of the mixture into the engine would scale proportionally to the engine speed and is not dependent on the amount of fuel metered by the needle valve on the carburetor.

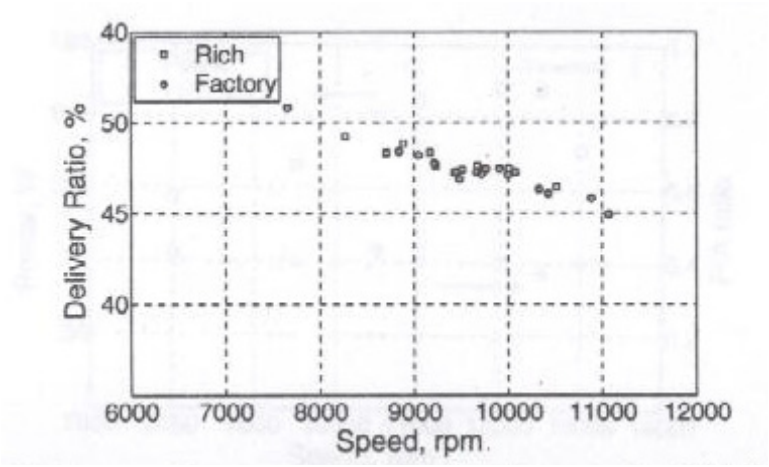

Figure 6: Delivery ratio as a function of engine speed at WOT for two different mixture settings (8).

Another important aspect of engine scaling is the relationship between engine size and frictional losses. As the engine size decreases generally the surface to volume ratio increases which would lead one to conclude that frictional losses would increase as the engine size decreases. Cadou and Menon (9) showed for three different small IC engines that engine thermal efficiency, η_{TH}, was somewhat independent of engine mass. This result is unexpected and is attributed by the authors to differences in the fuel systems on each of the engines. Using the same test setup described previously, Cadou and Menon ran the three engines at wide open throttle over a large range of engine speeds while measuring Power, Torque, fuel flow rate and air flow rate. From these measurements the authors were able to calculate BSFC, thermal efficiency, and air to fuel mixture ratio. The main impact of this study was the determination that the fuel supply system can have

a very large impact on the engine efficiency and performance. The authors also noted that the measure peak power of each engine were on the low end of the manufactures reported data but followed the previously noted power law relationship.

Shin, Chang, and Koo (10) studied the effect of altitude variation on engine fuel efficiency and frictional losses. The main focus of their research was to tune an engine prediction code. By tuning the code the researchers felt that they would be able to predict some general guidelines which would help developers design a long endurance miniature unmanned aerial vehicle, UAV, engine. Tests were conducted on an ENYA Company Model R155-4c 25.4 cm^3 four-stroke glow-plug combustion engine. The researchers modified the engine to be a four-stroke spark ignition engine run on gasoline with the addition of a separate lubrication system. The engine frictional losses were measured by using an electric motor to turn the piston and measure the torque required at different engine speeds. Figure 7 shows the measured motored mean effective pressure as a function of engine speed for the test engine. The wide range of data points for engine speeds below about 5000 RPM is attributed to the large cycle to cycle variations that occur in small IC engines. The reasons for these large variations will be discussed in more detail in section II.6.1. The tests showed that there is no one correlation that will work to predict frictional losses across the engine speed range from 3000 RPM to 10000 RPM. The overall result of these frictional loss tests was to come up with a correlation to predict power and torque as a function of engine speed. The code developed by the authors was able to predict the power and torque over a range of engine speeds when compared to test data. The results from the motoring tests allowed the authors to include

frictional losses in an engine prediction code which was used to investigate the impact of altitude on fuel consumption, power, and torque.

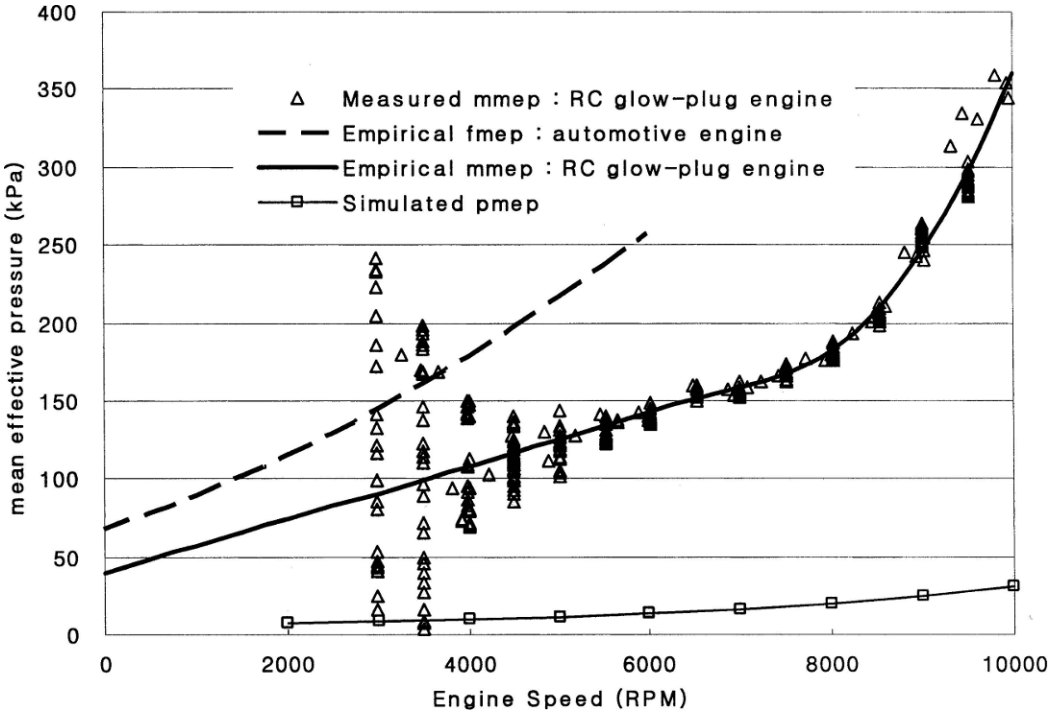

Figure 7: Measured friction losses of the test engine in comparison with those of a typical automotive engine (10).

II.4 Pressure Impact

The effect of atmospheric pressure on the performance of a two-stroke engine was presented by Harari and Sher (11). In this study an attempt to build upon the correlations previously made in other papers was accomplished by including the effect of atmospheric pressure on the predicted output power. The work by Harari and Sher was done using a Sachs type SF2-350 Pistion-port engine with 2x350 cm^3 opposed-piston crankcase scavenged, Schnürle type, two-stroke engine. Engine power and torque were measured using a Hofmann eddy-current dynamometer type 12d. Exhaust gas composition was measured using a SGA-9000 infrared gas analyzer. The ambient pressure was controlled by a vacuum pump at the exhaust and by throttling the intake air using a differential

pressure gauge between the intake and exhaust. The data collected covered a speed range from 6000 RPM to 9000 RPM and a pressure range from 44 kPa to 100 kPa. The pressure range tested equates to a range from sea level up to 7000 km. The maximum engine power has an approximate linear dependence upon the ambient pressure. Harari and Sher plotted maximum torque as a function of engine speed for a wide range of inlet pressure conditions and is shown as Figure 8. The general torque curve increase from low RPM up to a maximum and then decreases with increasing engine speed. Figure 8 shows that at sea level this engine follows this expected pattern while with decreasing inlet pressure the maximum torque begins to behave very non-linearly.

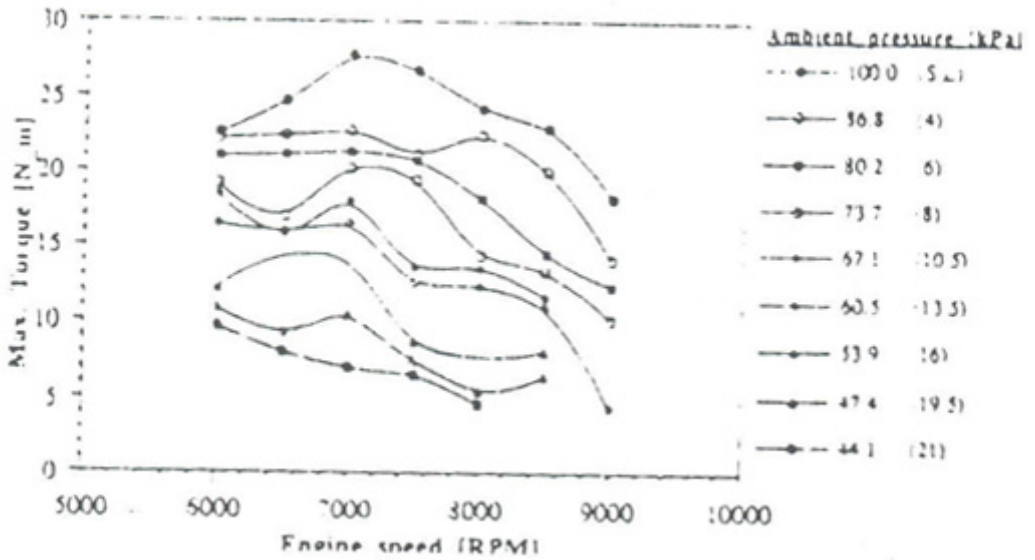

Figure 8: Maximum engine torque vs. engine speed and ambient pressure (11).

Harari and Sher replotted the data in Figure 8 as maximum torque versus ambient pressure and showed that as the inlet pressure decreases the maximum torque for all engine speeds also decreases. The authors were attempting to determine a correction factor, CF, which could be used to determine engine power as a function of ambient

temperature, *T*, and pressure, *p*. The general form of the correction factor is listed as Eq. (10) and can be used to predict engine power, P_b, as Eq. (11).

$$CF = \left(\frac{p - p_V}{(p - p_V)_S} \right)^A \left(\frac{T_S}{T} \right)^B = \frac{1 - \omega}{1 - \omega_S} \left(\frac{p}{p_S} \right)^A \left(\frac{T_S}{T} \right)^B \tag{10}$$

where p_V is the water vapor partial pressure, ω is the air humidity ratio, and the subscript *S* denotes reference sea level static conditions. *A* and *B* in Eq. (10) are constants that are correlated from experimental data.

$$P_b = (P_b)_S * CF \tag{11}$$

When plotted on a log scale the peak power was shown to have a linear dependence on ambient pressure while the correction factor depends significantly on engine speed. These results lead the authors to conclude that the correction factor should be a function of ambient pressure raised to a power proportional to engine speed. The constant *A* in Eq. (10) is determined by the authors to be near 1.0 for low engine speeds while for maximum engine speed *A* should be 2.0 (11). From the experimental data the author suggests that the engine torque or BMEP falls 50% when the ambient pressure decreases from 100 kPa to 50 kPa. One of the conclusions reached by Harari and Sher is that the scavenging efficiency and the delivery ratio decrease with decreases in ambient pressure and is one of the main reasons that power and torque decrease while BSFC increases.

Shin, Chang, and Koo (10) established that their computer code could predict the power and torque of the test engine over a range of engine speeds. The authors then used the code to simulate engine performance at three altitudes, sea level, 3 km, and 5 km. Using the code they predicted the effect of altitude on brake mean effective pressure and engine brake power. Figure 9 and Figure 10 show these predictions and as expected the

engine power and BMEP decrease as altitude increases. Shin et al used the code to predict brake specific fuel consumption, BSFC, of the engine at the same altitudes. Test data collected from the experiment described previously at sea level conditions when compared to code predictions of BSFC was not as good as the power and pressure predictions. The authors give several reasons for the differences including errors in the measurements made with the air-fuel sensor and possible leakage in the exhaust manifold which may have allowed fresh air into the system.

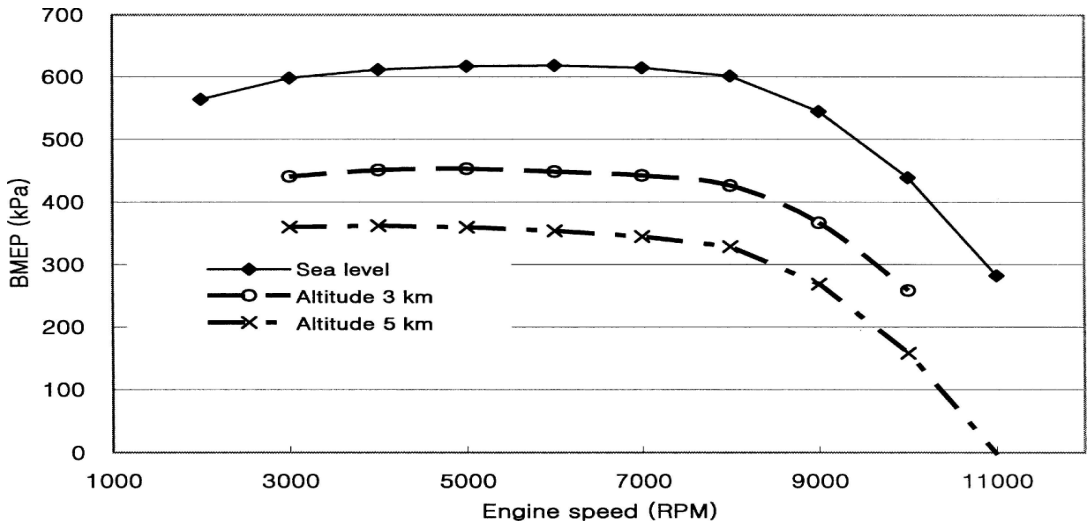

Figure 9: Simulation results of BMEP with altitude (10).

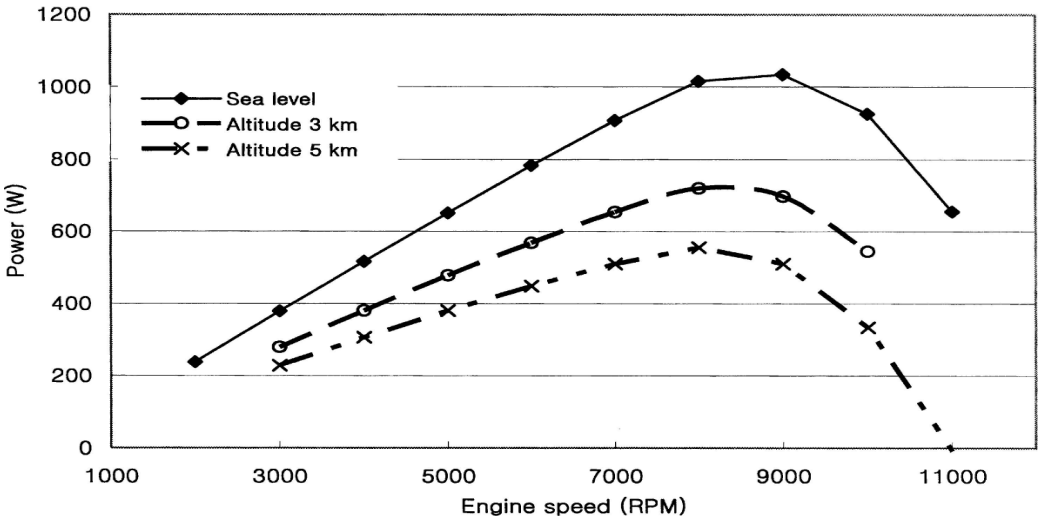

Figure 10: Simulation of engine power with altitude (10).

II.5 Temperature Impact

Watanabe and Kuroda (12) studied the effect of inlet air temperature on the power output from a two-stroke crankcase compression gasoline engine. Their effort was focused on determining a correlation for the power output of the engine as a function of the absolute inlet temperature in a range of 4.5 °C to 40 °C. The test engine was a 60 cm^3 Schnuerle scavenging type engine and was run over a speed range from 1000 RPM to 4000 RPM. The authors used six electric heaters with a total capacity of 900 W to heat the inlet air allowing a maximum carburetor inlet air temperature of 50 °C. Air flow rate was measured upstream of a surge tank with a round nozzle. The surge tank was 690 times the size of the engine volume and had a gummy diaphragm attached to reduce pressure and flow pulsations to allow for more accurate air flow measurements. Engine power was measured using a 2 hp electric dynamometer and was corrected back to standard conditions using Eq. (12).

$$\left(N_b\right)_S = \frac{p_S}{p} N_b \tag{12}$$

where N_b is break power, p is the atmospheric pressure, and the subscript s denotes reference conditions. The authors derived a relationship between the power output and the scavenging pressure to show that as the temperature decreases the power will decrease due to a decrease in scavenging pressure with increasing ambient temperature. This result also compares well with compressor theory where an increase inlet temperature for a fixed inlet temperature will result in a lower outlet pressure. Watanabe and Kuroda based upon established theory of how four stroke engine power scales with temperature assumed a form show as Eq. (13).

$$P_b \propto \left(\frac{1}{T}\right)^{\lambda} \tag{13}$$

where brake power, P_b, is proportional to the inlet temperature to a power, λ. From the test data for engine output power the exponent λ falls between 0.5 and 0.9, where λ=0.5 represents the four stroke engine theory. The exponent in the equation given was dependent upon the temperature of the inlet air flow and engine speed. The author's correlation was compared with the established DIN 6270 correlation which has the form given by Eqs. (14) thru (16).

$$N_e = (N_e)_0 * \alpha \tag{14}$$

$$\alpha = \mathrm{K} + 0.7(\mathrm{K} - 1)\left(\frac{1}{\eta_{mc}} - 1\right) \tag{15}$$

$$\mathrm{K} = \frac{N_i}{(N_i)_0} = \left(\frac{T_0}{T}\right)^{3/4} * \frac{p - \psi\ p_D}{(p - \psi\ p_D)_0} \tag{16}$$

where N_e is the net power output, N_i is the indicated power output or brake power, η_{mc} is mechanical efficiency, p is atmospheric pressure, p_D is saturated vapor pressure, ψ is the relative humidity, and the subscript 0 indicates reference conditions. These equations along with the authors' correlations and the experimental data are shown in Figure 11.

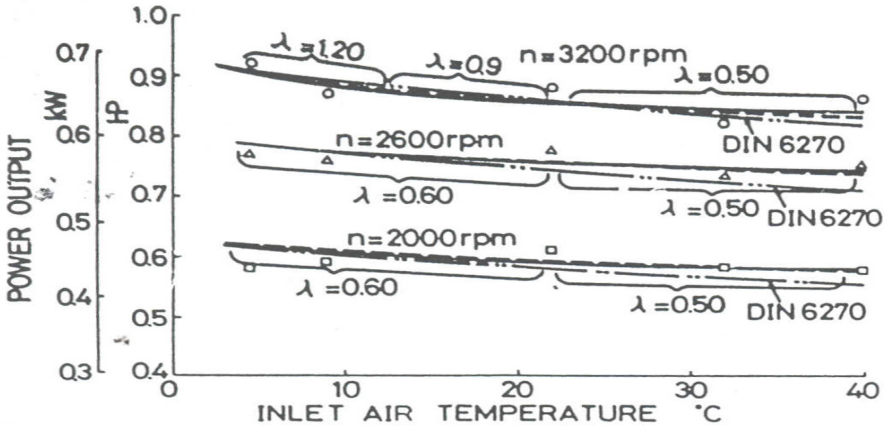

Figure 11: Values of λ in Eq. (13), i.e., $P_b \propto (1/T)^{\lambda}$ (12).

Watanabe and Kuroda (12) assert that the use of a constant temperature cooling airflow around the engine may have impacted the data. They state that a cooling airflow heated to the same temperature as that of the inlet airflow would cause the power drop due to the temperature increase to be more significant and possibly fall closer to the DIN 6270 lines in Figure 11.

Temperature has also been shown to have a large impact on the formation of several important combustion products or emissions. Combustion products such as Nitric Oxides, NO_X, unburned hydrocarbons, UBHC, and Carbon Oxides, CO_2 and CO, are all important in relation to combustion efficiency and the ever increasing pressure to reduce greenhouse gases produced by internal combustion engines. Nitric Oxide compounds, NO_X, emissions have been shown to vary proportionally to the temperature at which the reaction occurs (13-14). This relation has been show to be independent of engine or fuel type. Flynn et al (13) showed that there is an approximate minimum temperature under which conditions are such that a chemical combustion reaction will not occur thus NO_X will not be produced. Flynn also showed the impact of temperature on the production of UBHCs, where reduced combustion temperatures will increase the amount of UBHC in the emissions.

The reduction of NO_X emissions has been approached from a variety of angles. Most approaches attempt to reduce the combustion event temperature in order to reduce the production of NO_X. This attempt in the past has come at the price of increasing carbon monoxide, CO, emissions. CO is an incomplete combustion product and increased combustion temperatures increase the rate at which CO can be converted to carbon dioxide, CO_2. This is a well know trade off that has been documented for

different types of engines. Chen (14) was able to show that by injecting an aqueous mixture of ethanol and water in addition to the standard fuel injection one could reduce NO_X emissions without significantly impacting CO or unburned hydrocarbon, UBHC, emissions.

Wilson (15) ran several experiments in an effort to determine the effects of fuel heating and ultimately mixture temperature on the torque and BSFC of a small internal combustion engine. The tests utilized a Fuji B-34 single cylinder four stroke spark ignition engine with stock timing as the test engine. Power and torque were measured using a Magtrol model 1WB65 eddy current dynamometer. The fuel flow rate was measured using a Max Machinery model 213 mass flow meter. Wilson built a fuel heater constructed from a copper block that utilized two 750 W Watlow strip heaters and a Watlow temperature controller to heat the fuel to the desired temperature. Fuel temperature was measured with a thermocouple downstream of the heating element to get an accurate measurement of fuel temperature into the carburetor. Wilson (15) ran three independent tests in order to determine fuel temperature on engine torque and BSFC. The first test was run by simply heating the fuel to the desired temperature while measuring BSFC and torque. The second test compared the heated fuel data from test one with data obtained by adjusting the carburetor high speed needle with fuel at ambient temperature. The last test consisted of heating the fuel to a specific temperature and adjusting the high speed needle on the carburetor. The conclusion from these tests presented by Wilson is that heating the fuel alone has little impact on the overall engine performance. Wilson also concluded that the impact of equivalence ratio on engine performance is significant and can be greatly impacted by carburetor setting and fuel

temperature. Based on the results from Wilson (15) for heated fuel tests no conclusions can be made about how much the air temperature will impact the engine performance. Equivalence ratio in the engine will be impacted by the air and fuel densities which are directly related to the temperature of the mixture, so it is expected that inlet air temperature will have a direct impact on engine performance.

II.6 Measurement/Accuracy of Parameters Required

II.6.1 Pressure

The accuracy of pressure measurements can be crucial to calculating important engine parameters such as heat release, combustion event timing, and combustion stability. Pressure measurements along with temperature measurements can be used to determine the state of the air entering the carburetor and exiting in the exhaust gas flow. The accuracy of these measurements is important in determining the impact that changes in intake pressure have on the performance of the engine. Cylinder pressure can vary widely from cycle to cycle and are impacted by changes to inlet pressure and temperature, composition of the charge stemming, and changes in the fuel to air ratio. Turbulent flow in the cylinder would cause changes to the flow pattern causing differences in the amount of charge being short circuited and altering the percent of residual charge. Knocking conditions would also cause variations in cylinder pressure based on the location of the knock center and the severity of the knock.

Intake and exhaust gas pressures can be used to help reference or peg the pressure signal being transmitted by the pressure transducer for in cylinder measurements. The signal measured by the in cylinder pressure transducers can change due to the high heat

flux associated with combustion in the area of the pressure transducer. In order to accurately translate the transducer voltage signal into an absolute pressure one or more points in the signal versus time curve must be related to an independent pressure measurement. Several methods for pegging the cylinder pressure measurement are discussed by Lee, Yoon, and Sunwoo (16) who proposed a new method based upon a modified least squares method which utilizes a variable polytropic coefficient. Lee et al propose that the reference should be based upon the assumption of polytropic compression where Eq. (17) allows the calculation of the pressure at an arbitrary crank angle based upon a reference condition.

$$\frac{p(\theta)}{p(\theta_{ref})} = \left[\frac{V(\theta_{ref})}{V(\theta)}\right]^{\kappa} = c(\theta) \tag{17}$$

where θ is the crank angle degree and the subscript *ref* represents an arbitrary reference condition. The modified method proposes the calculation of the polytropic coefficient on a cycle-by-cycle basis and considering it a fixed value for each independent cycle. Solving Eq. (17) for κ gives the estimation of the polytropic coefficient of each cycle as Eq. (18).

$$\tilde{\kappa}_i = \frac{\ln[p(\theta)/\, p(\theta_{ref})]}{\ln[V(\theta_{ref})/V(\theta)]} \tag{18}$$

The use of Eq. (18) allows for the solution of the measurement bias and the reference pressure for each cycle based on applying a linear least-squares method from the solution of Eq. (20). The work by Lee et al (16) also uses a first order auto-regressive filter to help improve the robustness of the resulting polytropic coefficient of the form of

Eq. (19). The variable *a* in Eq. (19) represents the auto-regressive coefficient and was set at 0.2 for the study completed by Lee et al.

$$\tilde{\kappa}_i = a\,\tilde{\kappa}_{i-1} + (1-a)\,\tilde{\kappa}_i \quad 0 < a < 1 \tag{19}$$

$$w = \left(X^T X\right)^{-1} X^T y \tag{20}$$

where the variables in Eq. (19) are

$$w = \begin{bmatrix} E_{bias} \\ K_s\, p(\theta_{ref}) \end{bmatrix} \qquad y = \begin{bmatrix} E(\theta_1) \\ E(\theta_2) \\ \mathrm{M} \\ E(\theta_N) \end{bmatrix} \qquad X = \begin{bmatrix} 1 & c(\theta_1) \\ 1 & c(\theta_2) \\ \mathrm{M} & \mathrm{M} \\ 1 & c(\theta_N) \end{bmatrix}$$

and $E(\theta)$ is the voltage at a specific crank angle, K_s is the sensor gain, and $c(\theta)$ is equal to the right hand side of Eq. (17) and N is the total number of sample points used in the calculation for a single pressure cycle. Lee et al showed based on simulated engine pressure data and experimental measurements from a four cylinder 2.0 L direct injection diesel engine that the modified least squares method had better noise rejection capability and higher accuracy through the calculation of the two norms of the sensor offset calculation error. The two norm, also referred to as the Euclidean norm, is the length or size of a vector and is defined as the square root of the sum of the squares of every value in the vector. The sensor offset calculation error two norm is equivalent to saying the error bounds of the calculated sensor offset. The calculation error two norm for the modified lease squares method was 0.96. The three point pegging method discussed by Lee et al had a two norm of 1.68 while the two point method and the regular least squares methods were both above 2.33. In addition to the two norm calculated from simulated engine data, experimental pressure measurements were taken and each of the methods

was used to calculate peg drift and the influence on the center of gravity of difference pressure. Difference pressure is the difference in pressure between the measured combustion pressure and the measured motored pressure. Lee et al showed that the modified least squares method had a 4% smaller standard deviation in peg drift and a 60% lower standard deviation in the difference pressure center of gravity.

Wilson (15) did not reference his cylinder pressure data and instead relied only on normalizing the data based upon the maximum pressure per cycle. Uncalibrated and normalized data allowed Wilson to investigate the impacts of spark timing on the location of peak cylinder pressure but did not allow him to directly compare the impact of fuel type on peak pressure. In addition the in cylinder pressure measurements were able to show signs of knocking combustion even though the measurements were not referenced. The use of spark plug measuring sensors such as the one used by Wilson (15) is discussed further by Bertola et al (17) and Walter et al (18). Bertola et al (17) investigated the effect of transducer placement and type on measurement values. The experiment was conducted on a modern four cylinder spark ignition engine with homogeneous charge operation. The test engine was 0.5 liters with four valves per cylinder. Bertola et al used both face sealing and shoulder sealing piezoelectric pressure sensors located in five separate positions within the cylinder head. The data collected during the test was filtered by selecting representative cycles instead of averaging the data over many cycles. The reason given for this was averaging the data would make the data less meaningful by smoothing out the peaks. Bertola et al showed the effect of locating the pressure sensor very near the cylinder wall which tends to increase the initial pressure rise due to the shock interactions with the wall. The authors also showed that locating the pressure

sensor in the squish gap area of the cylinder tends to increase the initial pressure rise. The authors (17) propose that the best position for measuring knocking conditions in the cylinder is in the center of the cylinder. This location provides for the ability to measure knocking occurring in any location throughout the cylinder with the least interference or magnification from the cylinder walls or the squish gap. Bertola et al also investigated the impact that an indicating bore has on the measured pressure signal. Using different sensors mounted in the same location within the cylinder head the authors were able to show that sensors using an indicating bore showed signs of signal amplification due to oscillations within the indicating bore. The amplitude of the enhanced signal was dependent on the dimension of the indicating bore. The authors recommend a flush mounted pressure sensor in order to reduce this induced error associated with the indicating bore.

II.6.2 Temperature

Temperature measurements are important in order to determine the entrance and exit conditions of the air, fuel, and exhaust gas mixtures. Temperature measurements along with pressure measurements can be used to determine the state of the mixture, including the heating value of the mixture which can then be used to determine thermal efficiency. In addition to thermal efficiency the temperature measurements are needed in order to determine the correlation between altitude atmospheric conditions and engine performance. Thermocouples are utilized to measure the temperature of the important quantities. Thermocouples are available in several different types including washer type, grounded, ungrounded, and exposed. Washer type thermocouples can be used to measure

surface temperatures like engine head temperatures. Grounded thermocouples have a quicker response time than ungrounded thermocouples but are susceptible to electrical noise and ground loops. Exposed junction thermocouples are best for use when measuring gas temperatures by allowing the junction to be in direct contact with the test gas. Wilson (15) used Omega K-type thermocouples for all temperature measurements. K-type thermocouples have a temperature range of -200 °C to 1250 °C with standard limits of error of either 2.2 °C or 0.75% of the scale above 0 °C and 2.2 °C or 2.0% of the scale below 0 °C (19).

II.6.3 Flow Meters

Flow meters are an important part of any combustion test experiment. The rate of both fuel and air mass flows can be used to determine the fuel to air ratio in the engine. The accurate measurement of these two flow rates is important because these values are used to calculate several secondary parameters such as thermal efficiency, and brake specific fuel consumption. Errors in the measurement of fuel flow rate can have a significant impact on the reported BSFC value. BSFC is used to compare engines of various sizes and types and is an important value that should be calculated accurately. Typical liquid flow meters use the liquid to turn a shaft based on a specific volume of fluid. As the shaft rotates a transmitter sends a signal which can be used along with the density of the fluid to calculate an accurate mass flow. For small internal combustion engines the required mass flow rate of fuel is low and so care must be taken to size the liquid flow meter. If the volume of fluid required to turn the meter is high then fewer pulses are sent to the data acquisition system per unit time. With few pulses the time

between pulses can vary significantly leading to errors in the actual mass flow rate of the fuel. Menon et al (8) gave a table of typical fuel flow rates for small internal combustion engines which ranged from 0.5 g/s up to about 4 g/s. These small flow rates are sometimes hard to measure with standard off the shelf liquid flow meters. Menon et al (8) choose to use a FMTD4 nutating microflowmeter by DEA Engineering which is capable of measuring 0.02 cm^3 of fluid per 5 V pulse. The fuel flow rate can be calculated directly, Eq. (21), from the number of pulses, x, times the volume per pulse, Vol_{pp}, divided by the total time, t_{tot}. Menon et al used a scale as a backup device to measure mass flow by taking readings at specific time intervals.

$$\dot{m}_f = \frac{xVol_{pp}}{t_{tot}} \tag{21}$$

Air mass flow measurements can be done in several ways including thermal mass flow meters, orifice meters, venturi meters, or a variety of other methods. The basic principle behind many types of mass flow meters is based upon measuring a pressure drop between two points with fixed areas and fixed fluid temperature. Using Bernoulli's equation the pressure drop and the area difference can be used to compute a volumetric flow rate which multiplied by the density of the fluid calculated from the pressure and temperature can be converted into a mass flow rate. Thermal flow meters use the principles of heat transfer to measure the mass flow rate of the fluid moving past a heater element. The temperature change sensed by the meter is directly correlated to the mass flow rate of the gas or liquid. Menon et al (8) used a TSI model 4021 mass flowmeter that was capable of measuring 0-300 standard liters per minute with a linear 0-4 VDC

output signal. Thermal flow meters operate accurately only under steady conditions so care must be taken to damp out any flow perturbations caused by the engine.

II.6.4 Power, Torque, Speed

From Eq. (4) and Eq. (5) the relationship between power, torque, and speed is established. The accuracy of any one of these measurements can impact the overall performance calculations of an engine. Brake mean effective pressure is based upon measured power, and engine speed. Power can be calculated based upon measured torque and engine speed. Brake specific fuel consumption is proportional to engine output power and fuel flow rate. Thermal efficiency of the engine is also based upon measure power, fuel flow rate, and fuel heating value. Cadou et al (6-9) utilized a Sensotek model 31 load cell to directly measure engine torque based upon a fixed measure location. Engine load was applied using a Magtrol model HB-880 double hysteresis brake affixed to the engine through a gearing system. Cadou et al (8) asserts that utilizing this setup allows for a more accurate measurement of the torque because there are no losses associated with a power train. The setup also offers the ability to adjust the sensitivity of the torque measurement based upon the length of the moment arm to which the load cell is affixed. The largest uncertainty in power and thermal efficiency values comes from the torque measurement error and care should be taken to reduce this error (8).

Wilson utilized a Magtrol 1WB65 eddy current dynamometer which outputs both engine power and engine torque. The Magtrol has a 0.5% error at full load (15) and contributed a very large error to reported BSFC values at low torque settings. Wilson

also reported that the data acquisition system was not fully utilizing the available torque values. The original setup only ran at 1 Hz but the Magtrol was outputting the torque signal at 120 Hz. An upgrade to the acquisition software was made that read the torque signal at 120 Hz and reported an average value at 1 Hz which gave a more accurate representation of the average torque.

II.7 Other Research

II.7.1 Spark/Valve/Injection Timing

Engine performance in internal combustion engines can be affected by a wide variety of parameters. Some of the most important parameters involving the combustion event include spark timing, and valve timing or injection timing. Spark timing directly impacts when the combustion event will begin during normal operating conditions in spark ignited engines. If the spark event occurs early or late relative to TDC then the peak pressure will not occur at the optimum value of 16° ATDC (4) and maximum brake torque will not be generated. Valve or injection timing is important because it directly impacts the mixing process. The combustion process will occur along the boundary between the fuel and air. If the fuel is not mixed uniformly with the air before the combustion process is started then incomplete combustion may result. If the fuel or fuel/air mixture is introduced into the cylinder late in the compression stroke then less energy will be imparted into the gas. If the fuel or fuel/air mixture is introduced to early into the cylinder then autoignition may occur causing damage to the engine. For two-stroke crankcase scavenged engines similar to the test engine utilizing carburetors there are no valves or direct injection. Crankcase scavenged engines rely on mixing of the fuel

and air in the crankcase prior to introduction into the cylinder and allow for a relatively long mixing time. Spark timing for this type of engine will have the greatest impact on engine performance.

Wilson (15) investigated the impact of spark timing on BSFC and torque by varying the spark advance from the stock timing at fixed engine load conditions. With the engine running at a fixed throttle setting and engine speed the spark advance was varied between 60° BTDC and 10° ATDC. The spark timing was corrected from a given input timing to the actual spark timing based upon an average error value for each engine speed. Wilson showed that as expected the fuel flow rate at a given engine speed was approximately constant and was independent of spark timing advance. The data also showed that the timing advance which gave the maximum torque also corresponded to a minimum in the engine BSFC. Figure 12 shows the relationship between engine speed and spark timing for both minimum BSFC and maximum torque. From the results of the tests Wilson calculated an average decrease in BSFC of 9.36% across the range of engine speeds and an average increase in torque of 4.45% with optimized spark timing over the stock timing. Wilson recommended addition work to determine that actual impact on BSFC and torque by carefully optimizing spark timing with fixed equivalence ratio and mixture temperature to isolate the effects of spark timing on engine performance.

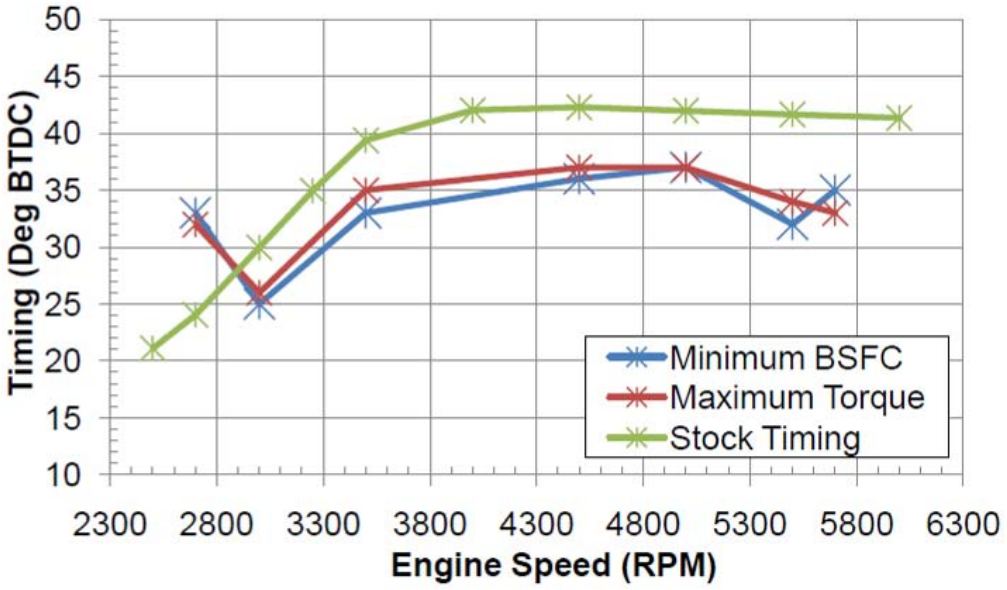

Figure 12: Optimum spark advance (BTDC) for maximum torque and minimum BSFC vs. stock with n-Heptane (15).

II.7.2 Geometry

Cylinder geometry will have a large impact on engine performance and can include engine compression ratio, engine port arrangements, engine clearance volume size and shape, spark plug location, piston diameter, piston head shape, and piston stroke among other things. Engine intake and exhaust design can also have an impact on engine performance based on how area changes and cyclical pressure changes can be amplified as pipe oscillations. Heywood (4) states that variations in mixture motion within the cylinder at the time of spark, variations in the amount of fuel and air fed into the cylinder, and variations in the mixing of fresh mixture and residual gases within the cylinder are the causes for cycle to cycle differences in engine performance. All of the reasons listed by Heywood for cyclic variations are directly related to engine geometry.

Beshai, Deniz, Chomiak, and Gupta (20) studied the impact of chamber geometry on cycle by cycle variations in an optically accessible square piston spark ignition test

engine. The single cylinder test engine runs on propane and can be modified to change the compression ratio and piston head shape with the use of caps placed on top of the standard flat top piston. The researchers collected data over a minimum of 100 cycles in order to obtain a representative sample for statistical analysis. Beshai et al (20) used the maximum heat release rate to compare how the modified piston cap would compare to a flat top piston. The flat top piston consistently had a maximum heat release rate over the modified piston. In addition the coefficient of variation was calculated for the heat release rates for the flat top piston and the modified piston. The coefficient of variation for the flat top piston heat release rate was between 0.175 and 0.306 while the coefficient of variation for the modified piston was between 0.516 and 0.792. This result shows that chamber geometry can have a large impact on the local flow on a cycle by cycle basis and that care should be taken to minimize this flow variation in order to increase heat release rates and maximize engine performance.

Ceviz (21) studied the effect that intake plenum volume has on engine performance over a range of engine speeds. The study was conducted using an engine with a maximum power of 62 kW at 5800 RPM and a compression ratio of 9.2. The standard engine was run at five specific speeds of 1250, 1500, 2000, 2500, and 3000 RPMs with three different intake plenum volumes. The first experiment was run with the original intake manifold, the second had a 90 cm^3 addition, and the third with a 180 cm^3 addition over the original size. In cylinder pressure was measured with a Kistler 6117BFD17 spark plug piezoelectric pressure transducer and was sampled at 100 kHz. Intake manifold pressure was measured using a Delco Electronics 1 bar manifold absolute pressure sensor which has a 6.0 ms response time and was positioned 6.5 cm upstream of

the intake valve. Both in cylinder pressure and manifold pressure were averaged over 50 consecutive cycles to eliminate the effects of cyclic variations. Cylinder pressure data was pegged by assuming that the pressure in the cylinder at bottom dead center after the intake stroke equals the mean intake manifold pressure. During the tests, engine speed was controlled by changing throttle position with a fixed engine load. No data was given for experiments with volume additions greater than 180 cm^3 because those tests resulted in a decrease in engine performance according to the author. Ceviz (21) showed that the increase in intake plenum volume resulted in an increase in brake torque, Figure 13, over the range of engine speeds tested.

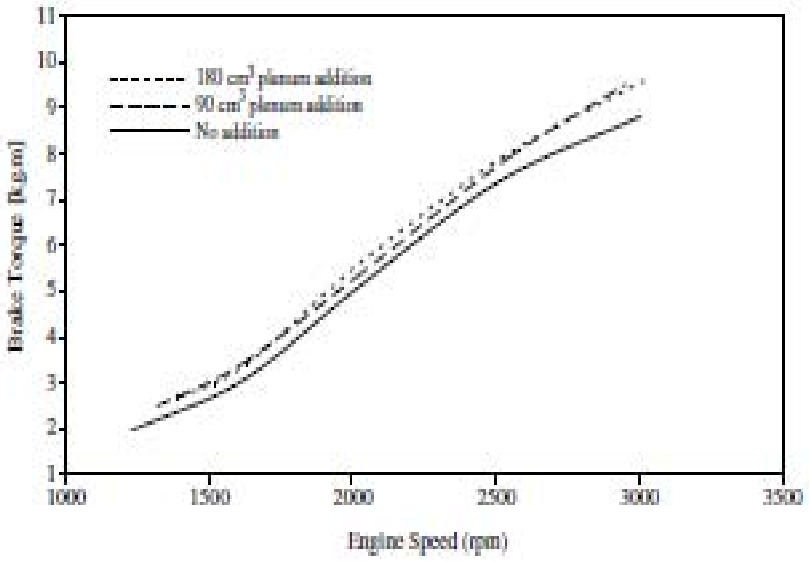

Figure 13: Variation of brake torque with engine speed for three different intake plenum volumes (21).

Figure 14 shows that a 90 cm^3 increase in plenum volume resulted in a decrease in BSFC for engine speeds below 2500 RPM and was consistent with the BSFC produced when running the engine above 2500 RPM with the original intake plenum. The 180 cm^3 addition resulted in a decrease in BSFC over both the 90 cm^3 addition and the original

volume for engine speeds below 2300 RPM. For engine speeds above about 2500 RPM the large volume addition resulted in higher specific fuel consumption. The author (21) attributes this increase in BSFC at higher engine speeds to an increase in intake manifold pressure with increased plenum volume and engine speed.

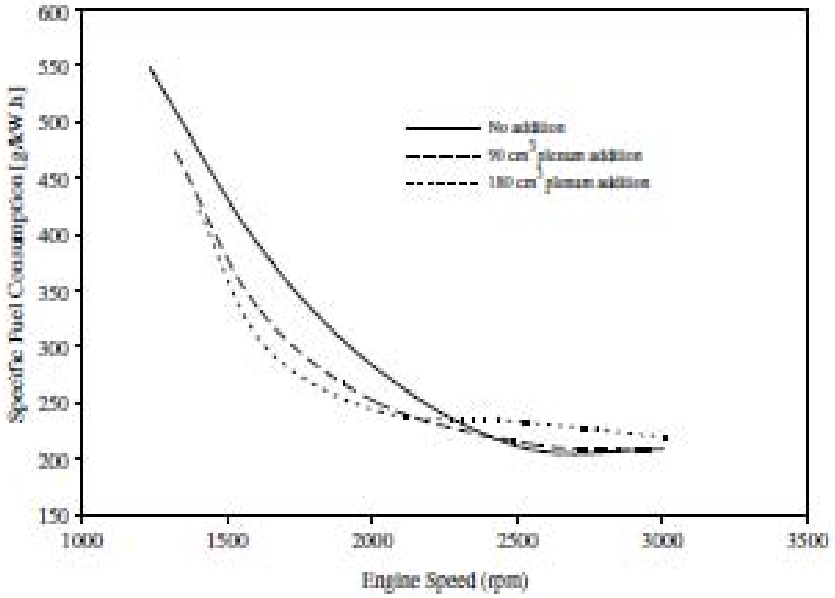

Figure 14: Variation of specific fuel consumption with engine speed for three different intake plenum volumes (21).

Ceviz (21) also showed the impact of plenum volume on the coefficient of variation of indicated mean effective pressure, COV_{imep}. COV_{imep} directly impacts engine design and is an indication of the amount of cyclic variation in the engine. Lowering the COV_{imep} is desirable because it allows the engine to run closer to its limits without encountering abnormal combustion events like knock. Figure 15 documents that the COV_{imep} was about 14% to 39% lower across the range of engine speeds tested for the engine run with increased plenum volumes. These results lead to the conclusion that the decrease in coefficient of variation in indicated mean effective pressure can be attributed to an increase in mixture homogeneities. The decrease in COV_{imep} leads to an increase in

power output since the losses attributed to cyclic variations within the engine are decreased.

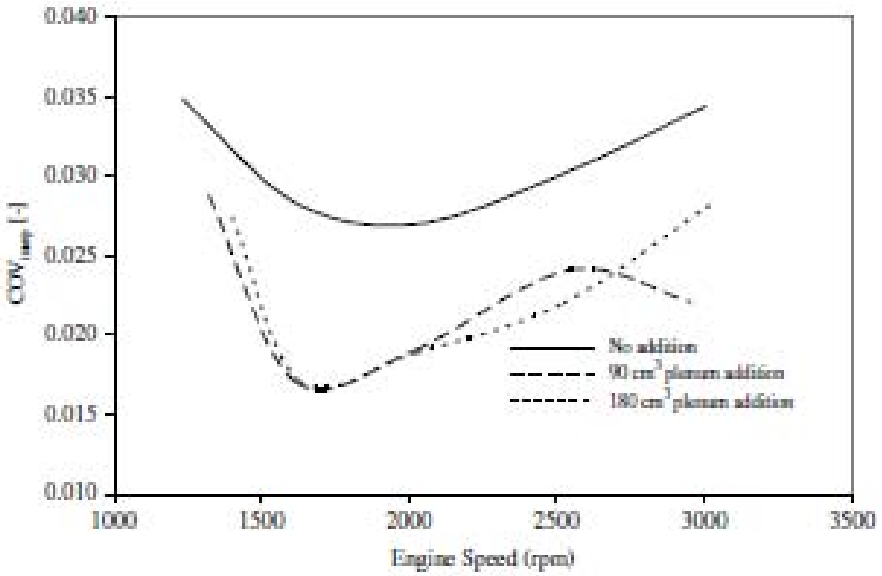

Figure 15: Variation of coefficient of variation of indicated mean effective pressure with engine speed for three different intake plenum volumes (21).

Celik (22) studied the effect of compression ratio, ignition energy, and spark timing on engine performance and emissions. The tests used a Lombardini LA 250 four stroke single cylinder carbureted engine which was first tested in an unmodified condition. The engine was then modified to increase the compression ratio from 5:1 to 10:1, variable spark timing was added, and the magneto ignition system was replaced with a higher energy transistorized coil system. The modified engine also had a water cooling system instead of the standard air cooled design which maintained a cylinder head and block temperature of 90 °C where the air cooled engine had an engine temperature of 120 °C. Celik (22) tested the two engines over a range of excess air ratio values, λ, with a fixed engine speed of 2000 RPM and a fixed engine load of ¾ throttle to determine the lean burn limits of each engine. Excess air ratio is the ratio between the measured air to fuel

ratio and the stoichiometric air to fuel ratio, Eq. (22). Excess air ratio is related to the equivalence ratio, Eq. (23), ϕ, by the use of the fuel to air ratio instead of the air to fuel ratio. The excess air ratio that produced the lowest amount HC emissions was used to set a fixed excess air ratio while the engine speed was varied at wide open throttle (full load). Maximum brake torque timing was used for all testing of the modified engine but the standard engine used a fixed timing.

$$\lambda = \frac{A/F}{(A/F)_{St}} \tag{22}$$

$$\phi = \frac{F/A}{(F/A)_{St}} \tag{23}$$

In Figure 16 Celik (22) showed that the power of the modified engine was on average ~35% higher than the standard engine. This result shows that as excess air ratio increases power output decreases and specific fuel consumption increases. Figure 16 shows the well known result that minimum specific fuel consumption occurs at excess air ratios slightly greater than stoichiometric conditions (4, 22, 23). BSFC was on average 39% lower for the modified engine over the range of excess air ratios tested. Reduction in BSFC for the modified engine was higher at excess air ratio values greater than 1.3 due to fewer misfires and partial burns in the modified engine as compared to the standard engine. The decrease in misfires and partial burns is attributed to the variable spark timing on the modified engine which allowed leaner operations of the engine without abnormal combustion events. The engine timing can be seen in Figure 17 for the modified and standard engines over the range of λ values. The impact of variable spark timing can be seen in Figure 18 which shows cylinder pressure versus crank angle

degrees for two different engine speeds for the standard and modified engines. The pressure traces reveal that the fixed timing of the standard engine results in the peak pressure at the higher RPM occurring after the ideal 16 °ATDC which results in power losses while the variable timing results in peak pressure occurring for both speeds near the ideal crank angle degree. At the optimum excess air ratio for minimum HC emissions the engine power was shown to be ~32% higher for the modified engine across the range of engine speeds tested and BSFC was 36% lower on average for the modified engine. The sum of these results show that increasing the compression ratio and ignition energy combined with variable spark timing will lead to significant gains in power output and specific fuel consumption. These changes also allow the engine to run much further into the lean burn range without suffering from abnormal combustion events like misfires and partial burns.

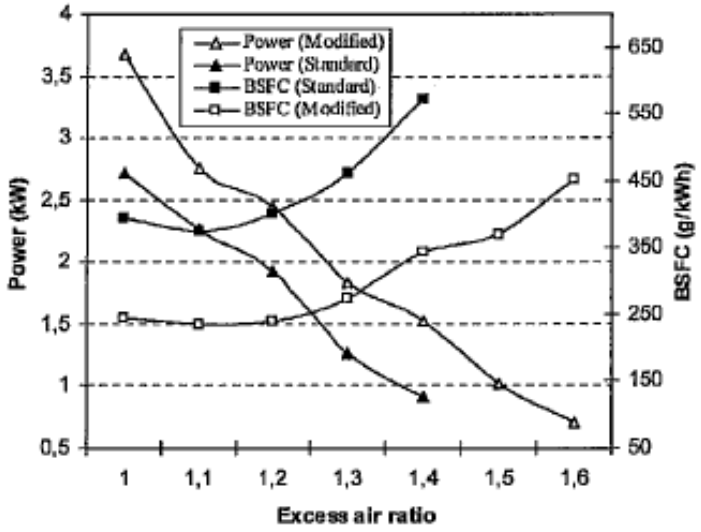

Figure 16: Engine power and brake specific fuel consumption as a function of excess air ratio for modified and standard engines at ¾ throttle opening and 2000 RPM (22).

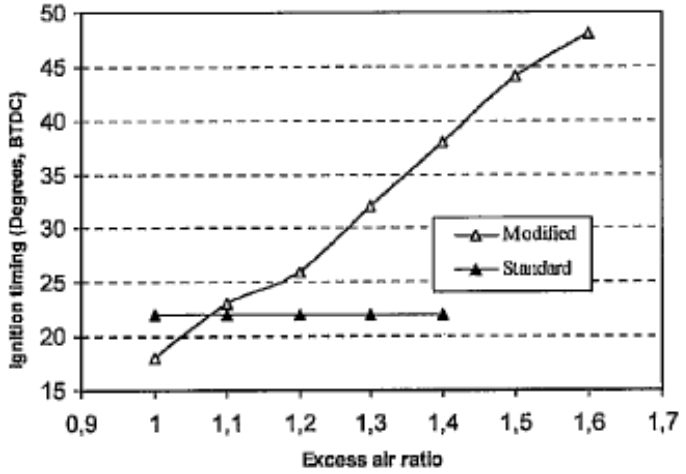

Figure 17: Spark timing as a function of excess air ratio for modified and standard engines at ¾ throttle opening and 2000 RPM (22).

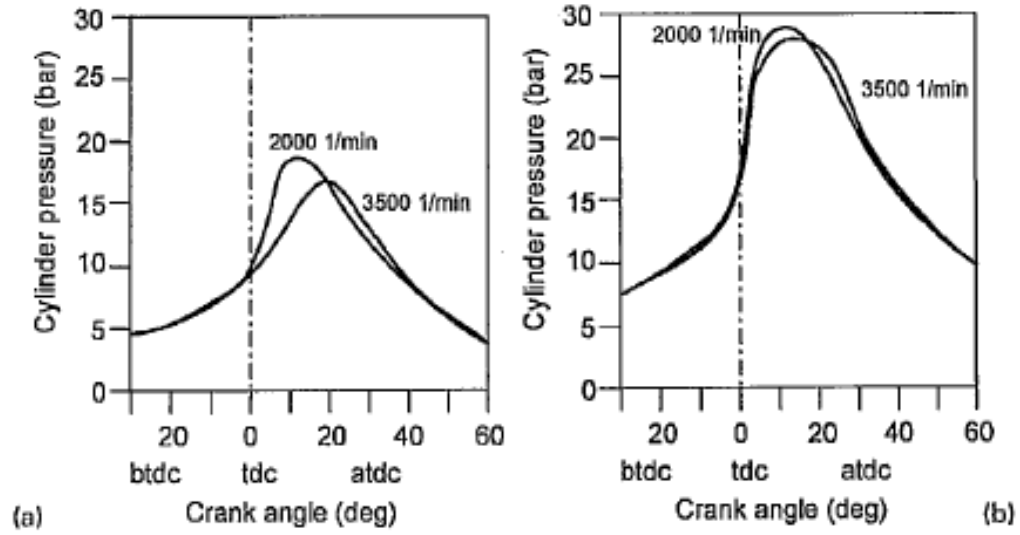

Figure 18: Pressure-time curves of standard, (a), and modified, (b), engines at full throttle and two different speeds (22).

II.8 Combustion and Fuel Impacts

The chemical reaction that occurs in an engine can be impacted by many things including fuel to air ratio, temperature, pressure, turbulence, and other molecules not required for the reaction. The general chemical reaction is given as Eq. (24)

$$C_m H_n O_p N_q S_r + X\left(R\left(O_2\right) + S\left(N_2\right) + T\left(CO_2\right) + h\left(H_2O\right)\right) \rightleftarrows$$
$$P_1\left(CO_2\right) + P_2\left(N_2\right) + P_3\left(O_2\right) + P_4\left(H_2O\right) + P_5\left(CO\right) \quad (24)$$
$$+P_6\left(C_x H_y\right) + P_7\left(NO_2\right) + P_8\left(NO\right) + P_9\left(SO_2\right)$$

where the coefficients in Eq. (24) can be determined in several ways. The recommended practice was originally discussed by Kilpatrick (24) and was further refined as SAE Aerospace Recommended Practice 1533 (25). While Eq. (24) is the general form of a hydrocarbon reaction with air, there are many intermediate reactions that occur. These intermediate reactions are the main reason behind the generation and destruction of product species. There can be hundreds of intermediate reactions and for each intermediate reaction there is an associated reaction rate. The reaction rates for many reactions are not well understood and can be dominated by a variety of variables during the reaction process, such as residence time, temperature, pressure, turbulence, and diluents. Previous research has attempted to correlate the production of different products as a function of equivalence ratio, temperature, and engine loading.

The combustion characteristics of different engine types can make it hard to relate the results of different research. One way in which to relate the overall effects of a given engine on the chemical reaction is to calculate combustion efficiency for the engine. Combustion efficiency, η_C, is defined as the heat of combustion based upon the measured product concentrations, H_C, divided by the stoichiometric heat of combustion, $(H_C)_{St}$, for a particular set of reactants, Eq. (25).

$$\eta_C = \frac{H_C}{\left(H_C\right)_{St}} \quad (25)$$

Another way to compare combustion characteristics is to calculate an emissions index, EI, Eq. (26), for each of the product species. The EI is the ratio of the mass of a product species *Z* to 1000 mass units of fuel consumed (25).

$$EI_Z = \left(\frac{moles\ of\ \ Z}{moles\ of\ \ fuel} \right) \left(\frac{MW_Z}{MW_{fuel}} \right) 1000 \tag{26}$$

The EI of a species can be compared for different engines because it is simply a ratio of the emission per amount of fuel used. Some researchers choose to report product species emissions levels directly in parts per million or by percent volume. Reduction of several important product species such as unburned hydrocarbons, UBHC, and carbon monoxide, CO, lead to increases in combustion efficiency.

In addition to directly comparing how efficient an engine is at converting the fuel and air mixture into product species, the quality of the combustion event must be considered. Qualitatively combustion events can be described as normal or abnormal. Normal combustion occurs as a deflagration where the reaction is controlled by an ignition source and the flame front propagates through the combustion chamber at a fixed rate converting the fuel and air mixture into burned gas products. Abnormal combustion events occur when the fuel and air mixture is ignited in a manner that is uncontrolled and includes knocking, surface ignition, run on, misfires, and partial burns (4). Misfires occur when the fuel and air mixture fails to ignite during a particular cycle and results in the fuel air mixture being exhausted without reacting. Partial burns occur when the fuel and air mixture does not have enough time to completely burn the fuel and air mixture due to slow combustion or late ignition timing. Surface ignition is the result of the fuel air mixture being ignited by a hot surface within the engine and can occur either before or

after the spark ignites the rest of the mixture. Surface ignition may result in a related phenomenon known as run on where the engine continues to run even after the spark stops firing as the surface ignition event occurs earlier and earlier in the cycle.

By far the most important abnormal combustion event is engine knock. Engine knock is the result of a detonation of a small part of the fuel air mixture which sends shock waves through the chamber causing an audible “pinging”. Engine knock is important because it can cause severe damage to engine components. Engine knock is avoided by the correct design of an engine which includes choosing the right fuel, compression ratio, and fuel air mixture ratio. Each fuel has an octane number rating which is a measure of its anti-knock characteristics in relation to a specific blend of research fuels under given conditions. The higher the compression ratio the more likely the engine is to knock all other things being equal as discussed in the previous section. The impact of the fuel to air ratio, or its related quantities such as λ and ϕ, on knock and engine performance will be discussed in more detail below.

The octane rating system is designed to compare a fuels anti knock characteristics to a blend of reference fuels normal heptanes, *n*-C_7H_{16}, with a rating of zero and isooctane, C_8H_{18} or 2,2,4-trimethylpentane, with a rating of 100. The octane rating is the percent of isooctane in the blend of research fuels which corresponds to the same knock performance characteristics as the test fuel (26). There are two current methods for testing octane rating, the research octane number, RON, covered under ASTM D-2699, and the motor octane number, MON, covered under ASTM D-2700. In the U.S. the octane rating is taken as the average of the RON and MON where the test conditions for RON and MON are summarized in Table 2. The conditions for the motor octane number

test are more severe and usually result in a lower octane number than the research method.

Table 2: Operating conditions for research and motor octane rating methods (4)

	Research method	Motor method
Inlet temperature	52 °C (125 °F)	149 °C (300 °F)
Inlet pressure	Atmospheric	
Humidity	0.0036-0.0072 kg/kg dry air	
Coolant temperature	100 °C (212 °F)	
Engine speed	600 RPM	900 RPM
Spark advance	13° BTC (constant)	19-26° BTC (varies with compression ratio)
Air/fuel ratio	Adjusted for maximum knock	

II.8.1 Impact of Fuel-Air Ratio

The impact of equivalence ratio, ϕ, on the generation of combustion products has been studied for a variety of engine and fuel types. There has been an effort in recent years to improve fuel consumption by making the combustion process happen in an increasingly leaner environment. The effect that this lean combustion has on emissions and combustion efficiency is an important way to determine the overall impact to the system. Menon et al (8) studied the impact of using the carburetor to adjust the fuel air mixture from the factory setting to a richer mixture on the engine performance. The test was conducted by opening the needle valve to about 1.5 turns for the factory setting and 2.0 turns for the rich setting. The authors note that due to factory setting instructions it was hard to compare results from this set of tests to other runs completed to compare engine to engine performance differences. The rich setting resulted in higher fuel to air ratios across all engine speeds as expected but resulted in lower power and torque across

the range of engine speeds. Figure 19 shows the range of fuel air ratios recorded over the range of engine speeds and the corresponding power and torque of the engine.

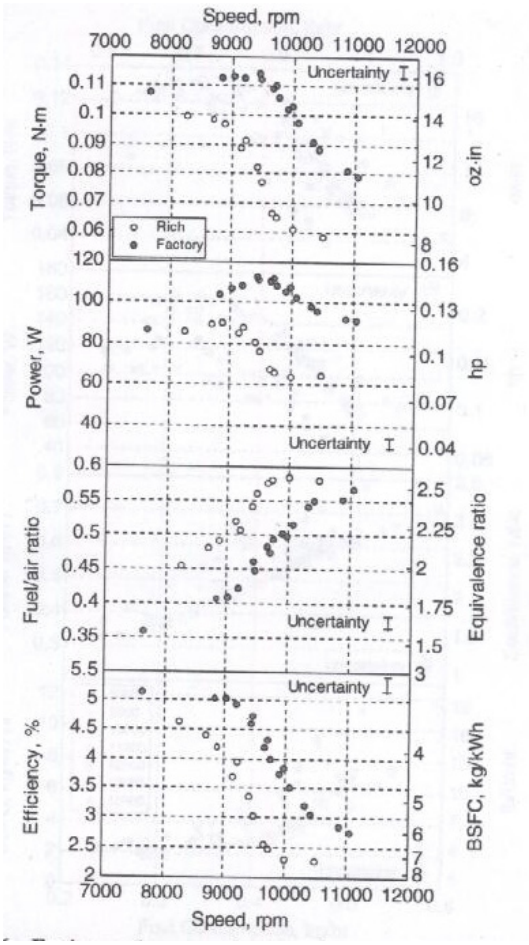

Figure 19: Engine performance for two mixture settings at WOT (8).

Celik (22) investigated the impact of the excess air ratio on engine performance and emissions. Celik showed that as the excess air ratio increases, meaning a leaning of the mixture, a minimum of fuel consumption and a maximum power, Figure 16, is achieved at a value slightly greater than stoichiometric. In the case of the test engine the excess air ratio that produced the lowest emissions of unburned hydrocarbons, UBHC, was 1.2. Figure 20 shows the exhaust emissions for the standard and test engines as a function of excess air ratio for carbon monoxide, CO, and UBHC. CO drops to a nearly

constant value at excess air ratios above 1.1 while UBHC reaches a minimum and then begins to increase. The increase in UBHC above an excess air ratio of 1.2 is due to misfires and partial burn cycles.

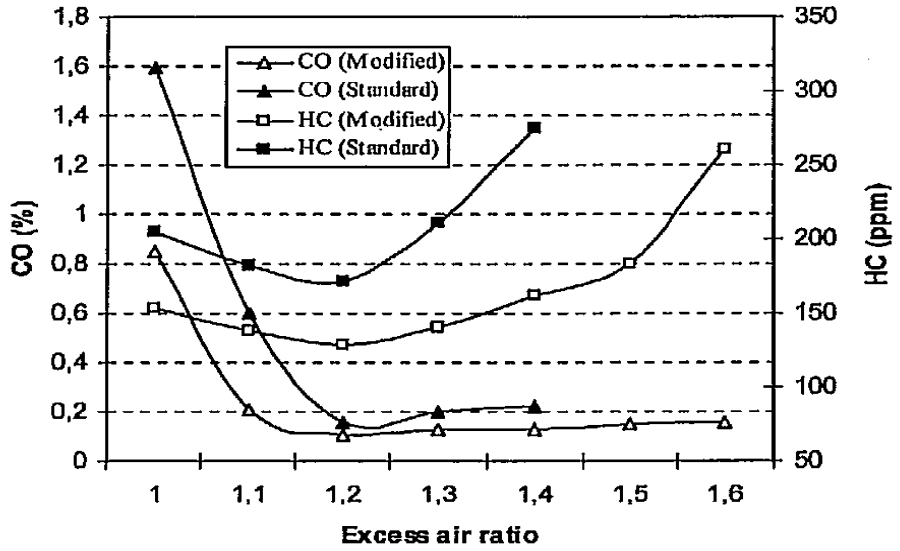

Figure 20: HC and CO emissions as a function of excess air ratio for modified and standard engines at ¾ throttle opening and 2000 RPM (22).

Equivalence ratio will also have an impact on UBHC. As ϕ goes from values below one to values greater than one it creates a peak in the flame temperature. Equivalence ratios less than one indicate that there is excess air available in the reaction. Equivalence ratios greater than one indicate that there is excess fuel available in the reaction. Both conditions lead to heat losses in the reaction. These heat losses lead to an incomplete reaction of the fuel with the air such that some of the hydrocarbons do not dissociate into individual hydrogen and carbon atoms that can be recombined into CO_2 and H_2O, leaving some hydrocarbon compounds in the exhaust emissions.

II.9 Fuel Impact

II.9.1 Categories of Fuels

Fuels fall into several categories including synthetic, petroleum based, and bio-fuels. Table 3 lists properties for a variety of commonly used fuels. Petroleum based fuels include things like JP-8, Jet-A, etc which are used extensively by both the military and civilian aviation communities. Bio-fuels include things like recycled waste oil, methyl ester compounds from plants, and animal-matter based fuels. Bio-fuels are beginning to be used more and more by researchers hoping to find an alternative to petroleum based products that offer similar performance with benefits like lower emission or cheaper production costs. Synthetic fuels are those refined from coal or other minerals like Fischer-Tropsch blends. Synthetic fuels have been around since the 1940's but have begun to find favor due to a cleaner combustion reaction and lower dependence on foreign petroleum based fuels (29). One of the main thrusts in the Department of Defense in recent years is to move towards a single fuel (30) source in order to streamline the logistics train and save a significant amount of money. The main components that are important in the chemical makeup of a fuel include the range of carbon numbers found in the fuel, the arrangement of carbon and hydrogen bonds in each hydrocarbon compound, and the amount of other additives found in the fuel such as sulfur, oxygen, and nitrogen.

Table 3: Typical fuel properties (4, 23, 25, 27, 28)

Fuel	Formula	Molecular Weight, kg/kmole	LHV, MJ/kg	Octane rating (RON/MON)
JP-8	$C_{10.9}H_{20.9}$	152.0	43.37	
Jet-A	$C_{11.6}H_{22}$	161.5	43.08	
Isooctane	C_8H_{18}	114.23	44.3	100/100
n-heptane	C_7H_{16}	100.2	48.17	0/0
Avgas	$C_{7.68}H_{16.8}$	112.0	43.50	100
Heavy Diesel	$C_nH_{1.7n}$	~200	42.8	
Gasoline	$C_nH_{1.87n}$	~110	44.0	91-99/82-89

II.9.2 Impact of Fuel Type

The type of fuel used in an engine can have a large impact on the performance of an engine under test. Using a suitable reference fuel is important so that the test accurately represents expected performance in the field. Antonovski et al (31) studied the effect of fuel properties in synthetic fuels and provides a listing of other research that has been conducted in this area. Antonovski et al focused on learning more about the chemical kinetics of synthetic fuels through the ignition delay time and determining appropriate surrogate fuels such as isooctane, n-decane, and n-heptane in representing the different hydrocarbon compounds found in synthetic fuels. The studies were carried out using shock-tube kinetics using gas phase mixtures, shock-tube spray using liquid phase fuel in the test region, and using a high recirculation combustion rig at the University of Florida. The tests resulted in an initial value for the activation energy 43.3 kcal/mol and a curve of ignition times versus temperature. The ignition times across the range of temperatures for the syntroleum fuel was about 50% longer than the reference fuel of kerosene.

Arpa and Yumrutas (32) studied the effect of a fuel derived from waste lubrication oil on engine performance and emissions in a spark ignition ICE. The basic chemical

properties of the test fuel such as density, flash point, LHV, and distillation range were determined using standard ASTM tests and compared to standard unleaded gasoline. The derived fuel has a similar lower heating value of 43.00 MJ/kg as compared to standard gasoline which had a value in this test of 43.89 MJ/kg. The test engine was a four cylinder four stroke carbureted Fiat water cooled engine with a 76 mm bore and 71.5 mm stroke per cylinder. The test engine is rated at 52.2 kW at 5500 RPM. The engine was run for five minutes in order to reach steady state conditions before data was taken. The derived fuel in this study resulted in a 5% increase in power, torque, and brake thermal efficiency over a range of engine speeds from 1500-3500 RPM. Arpa and Yumrutas (32) showed that the derived test fuel resulted in a 3% decrease in CO emissions over the range of engine speeds with a corresponding increase in CO_2 emissions of about 10%. UBHC emissions for the test fuel decreased to a minimum value and then began to increase across the range of engine speeds while the reference fuel, gasoline, had a nearly linear increase in UBHC over the range of engine speeds tested. The drastic increase in CO_2 emissions shown in this study with the associated reduction in UBHC and CO would lead to the assumption that this fuel provides better combustion efficiency. Since CO_2 is part of the stoichiometric reaction and included in the stoichiometric heat of combustion the closer the CO_2 emissions is to the expected value the greater the combustion efficiency. Similar reasoning can be used to conclude that CO and UBHC are not part of the stoichiometric reaction and thus reduce the combustion efficiency. This effect can be partially seen in the BSFC curve, Figure 21, where the derived fuel has a slightly lower BSFC than gasoline, though LHV of the fuel can have a significant impact on BSFC as well.

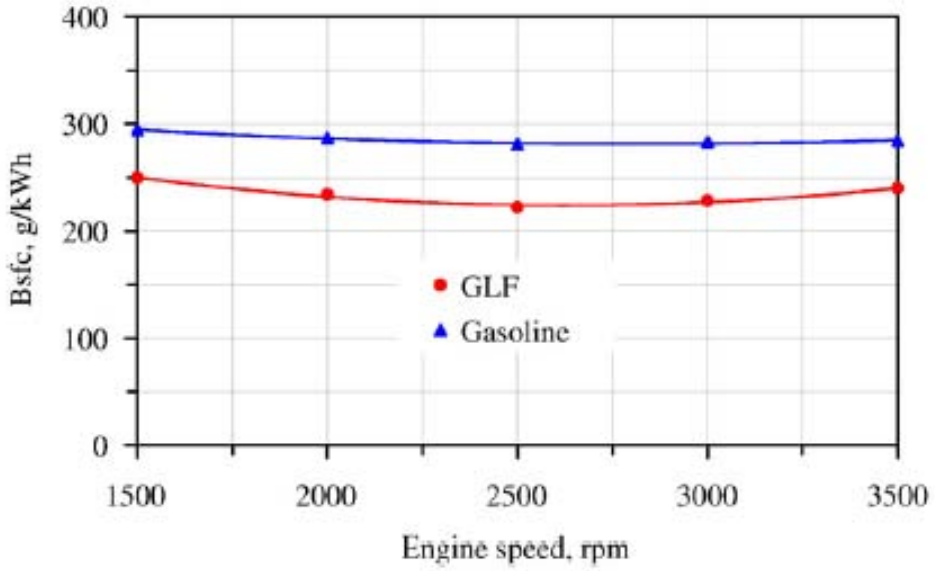

Figure 21: Variation of brake specific fuel consumption versus engine speed (32).

These studies showed the importance of understanding all of the major factors that impact engine performance. These factors include spark timing, fuel composition, inlet temperature and pressure, engine compression ratios, and residence time. The primary focus of this research is to study the impact of inlet conditions on engine performance. The inlet conditions will be varied to simulate atmospheric conditions encountered at different flight altitudes.

III. Test Setup and Apparatus

The design and construction of a small engine test stand capable of measuring basic engine performance characteristics at simulated altitude conditions was the main focus of this research. The goal of the test stand was to simulate atmospheric conditions from sea level up to 30000 feet above sea level on standard day conditions (33). At a minimum the test stand must be capable of recording air and fuel mass flow rates, pressures, temperatures, engine speed, engine torque, and engine power. In addition to the basic measurements listed above, measurements of spark timing, in-cylinder pressure, and exhaust gas compositions were desired. A schematic of the final test stand design is shown in Figure 22.

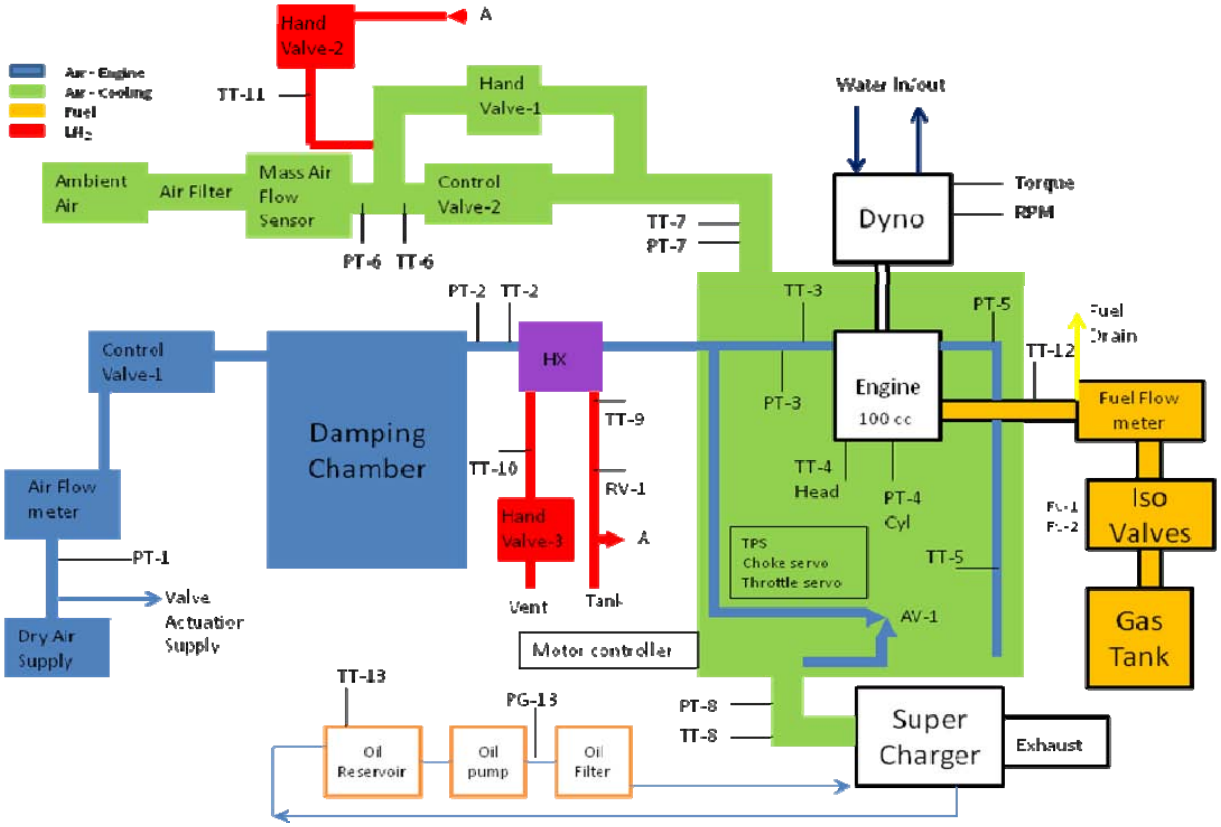

Figure 22: Mobile small engine altitude test system schematic.

The design of the mobile test capability began by understanding how the basic components of the stand would interact with each other. Several preliminary layouts were considered and were variations of the final design shown in Figure 22. One layout included a single air flow path which would cool the engine and provide combustion air. One advantage for this single path layout was the reduction in the number of components. This layout was discarded due to the complexity of measuring the portion of air being used for combustion by the engine. A second major drawback for this design layout was the need for a large heat exchanger capable of cooling a much larger mass flow. Another layout that was considered was a design where the dynamometer was fully enclosed inside the altitude chamber. This design's main advantage was that it would not require a pressure seal around the rotating shaft connecting the engine to the dynamometer. In addition only one coupling between the engine and the dynamometer would be needed. This design was not chosen because of the cooling requirements of the dynamometer and the sensitivity of the measurement equipment within the dynamometer. The cooling water would face temperatures below freezing which may have led to the dynamometer overheating. Furthermore, the electronics used to measure torque and speed and control the dynamometer were sensitive to extreme temperatures. The final design was chosen based on the ability to directly measure air flow into the engine for combustion, protect the sensitive electronics of the dynamometer, and limit the coolant flow rates.

The desired temperature range for the test stand was determined to be from 216.5 K to 320 K and was based upon the 1976 standard atmosphere model (33). The pressure range for the test stand was also determined from the standard atmosphere conditions and ranged from 101325 Pa at sea level to 24014.1 Pa at 30000 ft above sea level.

Temperature versus altitude is plotted in Figure 23 and pressure versus altitude is plotted in Figure 24. In order to attain an inlet pressure equal to that encountered from sea level up to 30000 ft above sea level, the driving device must be capable of pressure ratios in the range of 1.0 to 4.2. Based upon the temperature design goals coupled with the cooling requirements of the engine and the air used for combustion a maximum air mass flow rate for both paths of 0.3 kg/s would be needed. With this air mass flow rate and the assumed temperature differences for each test point approximately 5 to 40 g/s of coolant would be needed to reach the desired operating points.

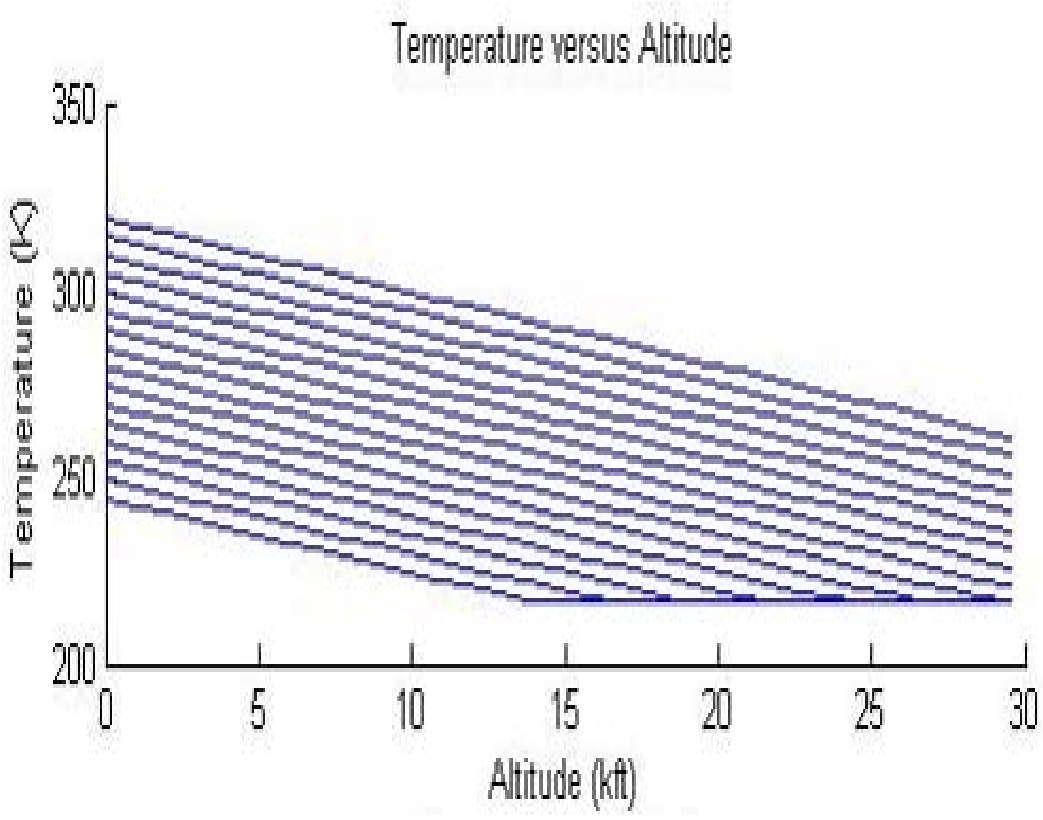

Figure 23: Temperature versus altitude design goal test conditions.

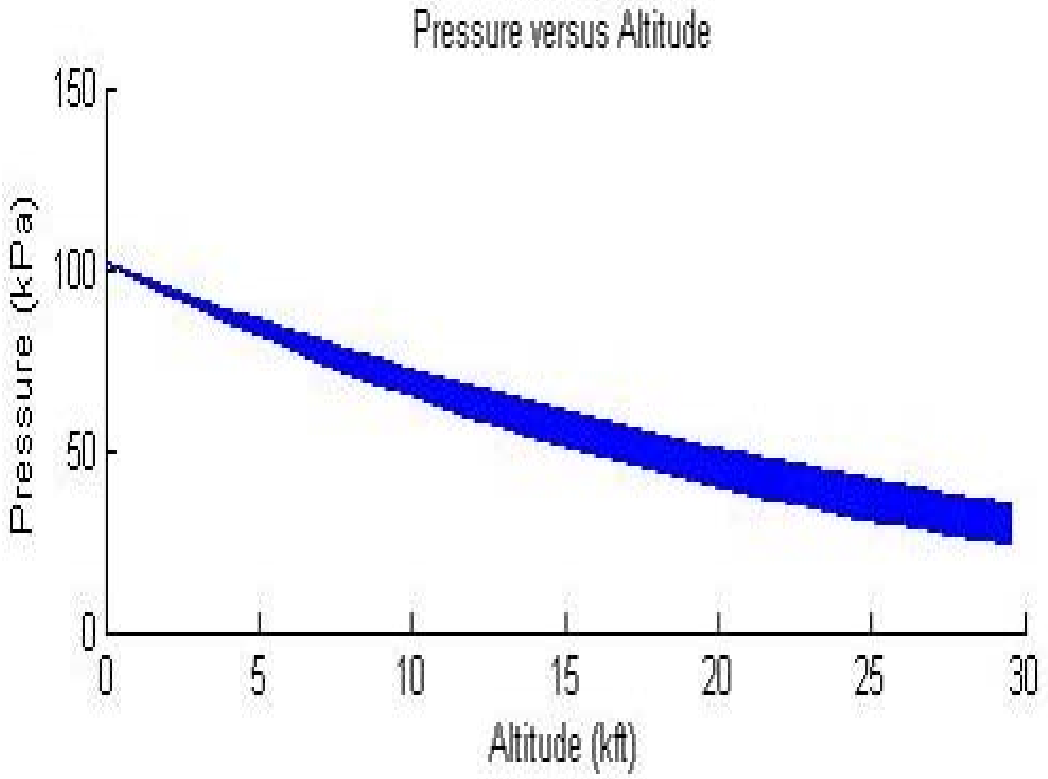

Figure 24: Pressure versus altitude design goal test conditions

Having chosen the flow path layout, the test engine, and the range of desired pressures and temperatures, component selection was completed for the remaining systems. A dynamometer was selected to measure engine performance data based on test engine size and speed. The dynamometer cooling system was designed to remove the heat absorbed during testing based upon maximum expected engine load. The test engine required a fuel and air supply system with a means of measuring flow rates and controlling the flow. The fuel system flow was controlled through a system of supply isolation valves and was measured with a rotary piston flowmeter. In order to accurately control the air pressure into the engine intake and around the engine the air flow system required a driving device, a throttle mechanism, and a supply source. The air system was coupled with a coolant method to match the desired temperature condition with the

desired pressure condition. The coolant system was designed to provide the correct flow rate of coolant without changing the thermo-physical properties or content of the air stream entering the engine intake. An additional requirement on the coolant system design was that it closely matches the thermodynamic properties of air at altitude for the flow stream passing over the engine cooling fins. The test stand was designed to control engine speed, and engine throttle position. A data acquisition system was selected in order to collect all required data during testing. These requirements established the design criteria for the test stand and served as the parameters to evaluate component choices against.

III.1 Engines

The Brison 5.8 cubic inch, 95 cc, single cylinder internal combustion engine was chosen for this project for several reasons. The primary reason was interest by the sponsoring agency, AFRL/RZTC to test a near 10 horsepower single cylinder engine. The Brison 5.8 has been in use in giant scale (generally 80 inch wingspan or greater) remote controlled aircraft models for many years and has potential applications as a small UAV propulsion system. In the giant scale model application the Brison 5.8 is capable of providing thrust to models weighing in excess of 178 N. The Brison 5.8, Figure 25, is a two stroke crank-case scavenged spark ignited engine with a bore of 54.98 mm and a stroke of 40.64 mm. The inlet and exhaust ports are controlled by the motion of the piston. The Brison 5.8 has two inlet ports arranged at 180° from each other with a single exhaust port at 90° from the two inlet ports. The intake ports open and close at 59.7° before and after BDC while the exhaust port open and close at 81.3° before and after

BDC. The test engine utilizes a Walbro SDC80 pump style carburetor with high and low speed needle valves for tuning the fuel air mixture. Test engine properties are summarized in Table 4.

Table 4: Brison 5.8 engine properties

Property	Value
Displacement*	95 cm^3
Swept Volume Displacement+	96.5 cm^3
Bore+	5.498 cm
Stroke++	4.064 cm
Connecting Rod Length+	7.112 cm
Crank Radius+	2.032 cm
Compression Ratio++	19.4:1
Type	2-stroke, crankcase scavenged
Intake Port Area+	2.00 cm^2 / port
Intake Port Arrangement	2 ports 180° offset
Exhaust Port Area+	4.04 cm^2

*Manufacturer advertised value
+Measured Value
++Calculated Value

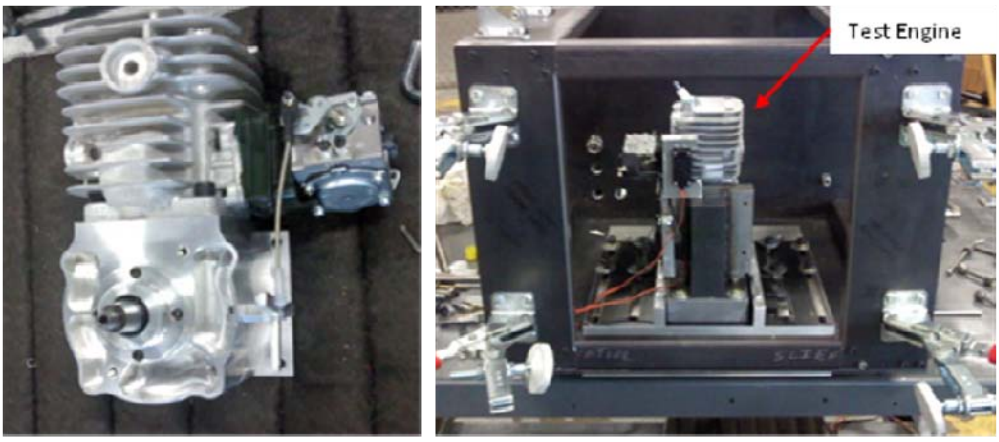

Figure 25: Brison 5.8 in^3 test engine (a) off the stand, and (b) mounted on test stand.

III.2 Flow Path Design and Components

The air flow path to and from the engine was designed based upon the required measurements to calculate engine performance as well as the need to simulate the desired

altitude settings. The initial design stage included a discussion of how to measure the air mass flow rate into the engine, how to cool the engine and reject the heat added to the air flow, and where to place some of the major measurement devices. The decision was made to split the flow path into two separate streams. This split made it possible to accurately measure the mass air flow into the engine directly without having to differentiate between the air flow cooling the engine and that being used for combustion. Splitting the air flow into two streams has the drawback of adding system complexity in the form of additional valves, pressure transducers, and thermocouples. However, the split has the benefit that it allowed the test stand to independently control the cooling of the two air streams so that both are matched to the desired altitude condition. Figure 26 shows how the all of the major components were connected in the two separate air flow paths, while Figure 22 shows how the two flow paths interacted with each other along with all of the other major subsystems on the test stand.

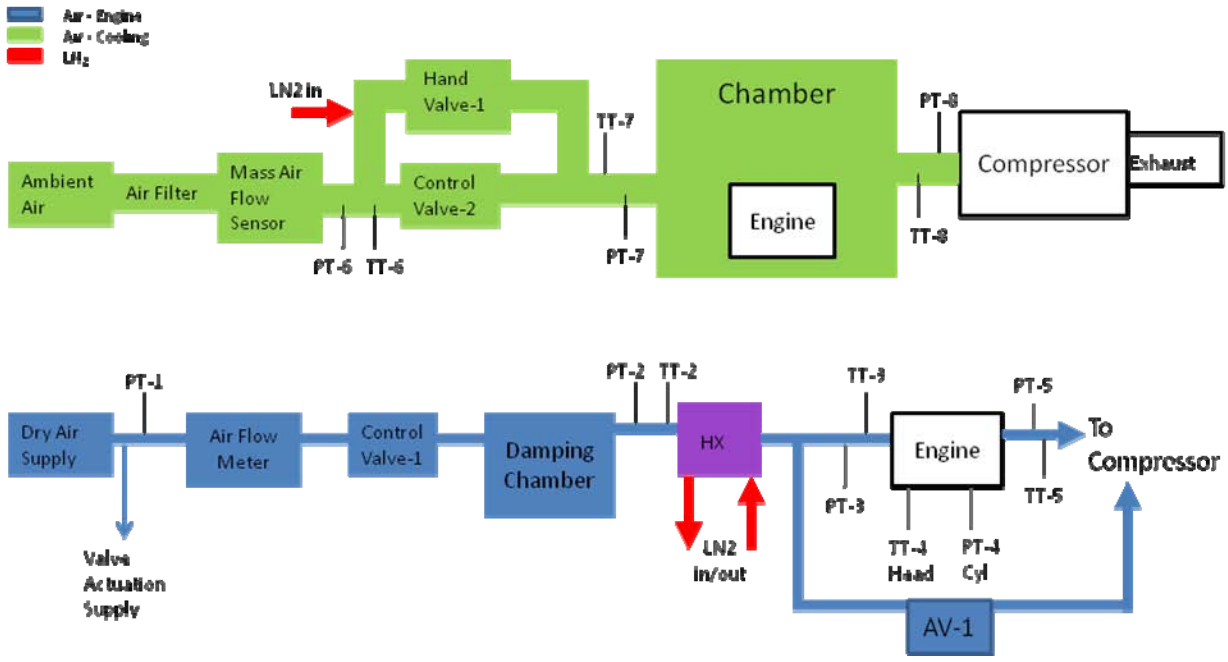

Figure 26: Mobile altitude test stand air flow paths.

The flow paths were designed by first determining how to drive the air flows. The second step was to determine how to control the air pressure in the two flow paths. The last step was to determine how to control the air temperature in the two flow paths. Other design considerations included how to damp the pressure pulsations in the flow path so that accurate flow rate measurements can be made. Lastly coolant flow rates were considered in the design in order to minimize the size of the coolant tank needed in order to run tests of sufficient duration to gather quality data. The LN_2 tank has a capacity of 180 L. The minimum desired run time was 60 minutes which lead to a maximum flow rate of approximately 40 g/s of coolant. The expected flow rates were at or below this maximum flow rate. Testing that required a coolant flow rate higher than 40 g/s would lower the run time available.

The heat exchanger shown in Figure 26 was placed as close to the engine as possible. This was done to reduce increases in air temperature between the heat exchanger and the engine inlet. The engine air flow gained heat from the surrounding atmosphere through the metal walls of the tubing as well as through the walls of the flow path but there were additional heat loads for this flow due to the engine. By separating the two flow paths the test stand was able to simulate very closely the temperature and pressure of the air being used for combustion by the engine. The cooling air flow path around the outside of the engine was not as crucial to the overall test measurements but still had an impact on the performance of the engine.

III.2.1 Compressor

The search for a suitable device to drive the air flow through the chamber started by determining the amount of airflow required to cool the 10 horsepower engine. The assumption was made that approximately the same amount of energy transferred into shaft work would be exiting the engine as heat through the walls with an equivalent amount leaving in the exhaust products. Using the basic thermodynamic equation for energy, Eq. (27), lead to a maximum cooling flow rate of approximately 0.1 kg/sec.

$$\dot{m} = \frac{Q}{c_p \Delta T} \tag{27}$$

where c_p is the specific heat at the average temperature and ΔT is the difference in temperature before the flow reaches the engine and after it has passed the engine. Several assumptions were made in order to simplify the calculation and size the flow rate. The first is that the flow has constant properties taken at the average temperature. The outlet flow temperature was assumed to be fixed at 250 °F so that the flow temperature would be sufficiently below the maximum engine head temperature to avoid overheating the engine. The sizing of this component was done by correcting the mass flow rate back to standard temperature and pressure values from the designed operating conditions. This lead to a maximum required cooling flow rate of 5080 standard Liters per minute, L/min. The pressure rise or drop across the device is an important consideration. The pressure rise or drop was determined based upon the design operating assumption that the air outside the chamber was at standard sea level conditions while the air in the chamber would be at conditions simulating 30000 ft altitude. The required pressure ratio between sea level pressure and the design goal altitude 30000 ft is 4.2. Four types of devices were

considered for this task and the advantages and disadvantages of each are described below.

The first type of device considered was the only one capable of providing the flow rate and pressure ratio needed for the proposed design goals. The steam ejector was capable of producing a pressure ratio in excess of 4.2 while still being able to provide a mass flow rate of 0.1 kg/s or greater. The steam ejector considered for this design was a 4 inch diameter steam ejector from Fox Valve Development Corporation. Steam ejectors are used to drive a wide range of altitude test facilities around the world and are well suited to the task. The drawback to this device is the need to provide a sufficient supply of quality steam to the ejector and then remove the steam to a safe exhaust point. The mobility of the design would be somewhat compromised by the use of a steam ejector as permanent lines would be required from the main steam supply header to the test location. The advantage of the steam ejector was that it is capable of providing a pressure ratio up to and exceeding the original 4.2 design value. Discussion with the AFRL/RZTC representatives lead to the determination that a steam ejector may be used in the future to provide simulated altitude conditions above 15000 ft but would not be used on the current design. A new design goal of a maximum altitude of 15000 ft above sea level was chosen as a reasonable goal and resulted in a new design pressure ratio of 2.0.

Two other types of devices were considered in order to provide the desired flow rate and pressure for the chamber but were discarded for a variety of reasons. The first device that was considered and rejected was a vacuum pump. Vacuum pumps were determined unfeasible for one of two reasons. The first reason was that most of the off

the shelf vacuum pumps were simply not capable of providing the required mass flow rate needed to keep the engine below the maximum temperature. The second reason that vacuum pumps were rejected was for size. Several vacuum pumps capable of providing the required flow rate were found during the search but were considered too large for the mobile test stand being constructed. Some of the vacuum pumps were capable of flow rates in the range from 50 to greater than 5000 L/min, however the pressure ratio for these devices were generally below 1.2.

The second type of device that was considered and rejected was an industrial air blower or shop air compressor. While the industrial air blowers were able to easily handle the required air flow rate they were not capable of the required pressure ratio. Most of the air blowers encountered during the search were only able to provide a pressure rise of one to two pounds per square inch absolute, psia, at best and most were only able to provide a pressure rise below one psia. The industrial blowers considered were also quite large for the proposed application. Shop air compressors are commonly used to provide higher pressure air for pneumatic tools and other equipment and were considered as an alternative to the industrial blower. Shop air compressor suffered from the same problems as the vacuum pump in that they were either incapable of providing the required air flow rate or were far too large to be used in the small mobile design.

The radial compressor was the final device considered and was ultimately selected due to its compact size and ability to meet the pressure ratio and flow rate requirements. The search for a radial compressor began by looking at aftermarket automobile supercharger compressors. It was calculated, using Eq. (28) that a 20 horsepower motor would be required to run the compressor.

$$P = \dot{m}\overline{C_p}T_{inlet}\left(\left(\frac{P_{amb}}{P_{inlet}}\right)^{R/\overline{C_P}} - 1\right) \quad (28)$$

where T_{inlet} is the temperature at the inlet to the compressor and is equal to the chamber temperature, P_{amb} is the pressure at the exit of the compressor and is assumed to be at ambient conditions, P_{inlet} is the pressure at the inlet of the compressor and is equal to the chamber pressure, $\overline{C_p}$ is the average specific heat at constant pressure across the compressor, is the air mass flow rate through the compressor, and R is the specific gas constant for air which is assumed to be 287 J/kg-K.

A search for the compressor was conducted and it was found that a large range of superchargers were capable of providing the required pressure ratio. Most of the supercharger compressors that were found required far larger motors due to the amount of flow being moved to achieve the desired pressure ratio. A company was located that could provide a motor, compressor, and variable frequency drive as a single unit to meet the requirements of the design. The unit purchased from Vortron was equipped with a 20 hp Emerson Motor Corp. electric motor model AF18, a V-5 K-trim Vortech supercharger, a Delta VFD-F variable frequency drive part number VFD185F43A, an automatic belt tensioner, a mounting plate, and pulley. A guard for the drive belt was constructed to prevent injury in the case of belt failure. The motor pulley to compressor pulley has a measured ratio of 3.362:1 and the motor maximum speed is 3550 RPM. The compressor has an internal step up ratio of 3.45:1. The variable frequency drive required a power source capable of 480 VAC 3 phase power at 38 A and 60 Hz. The building the mobile test stand was located in could only provide 480 VAC 3 phase power at a

maximum of 30 A. A temporary line was run in the facility which was capable of 480 VAC at a maximum of 50 A. The VFD is connected to the DAQ and is controlled with a 0-10 VDC analog input signal that sets the motor frequency between 0 Hz and 60Hz. The compressor speed versus motor input frequency curve was calculated with a simple linear relationship between the commanded frequency input, the total step up ratio, and the actual motor speed, Figure 27. The compressor map for the V-5 K trim Vortech radial compressor, adapted from the manufacturer's data (37), is shown in Figure 28. The expected operating points are noted on the compressor map with values listed in Table 5.

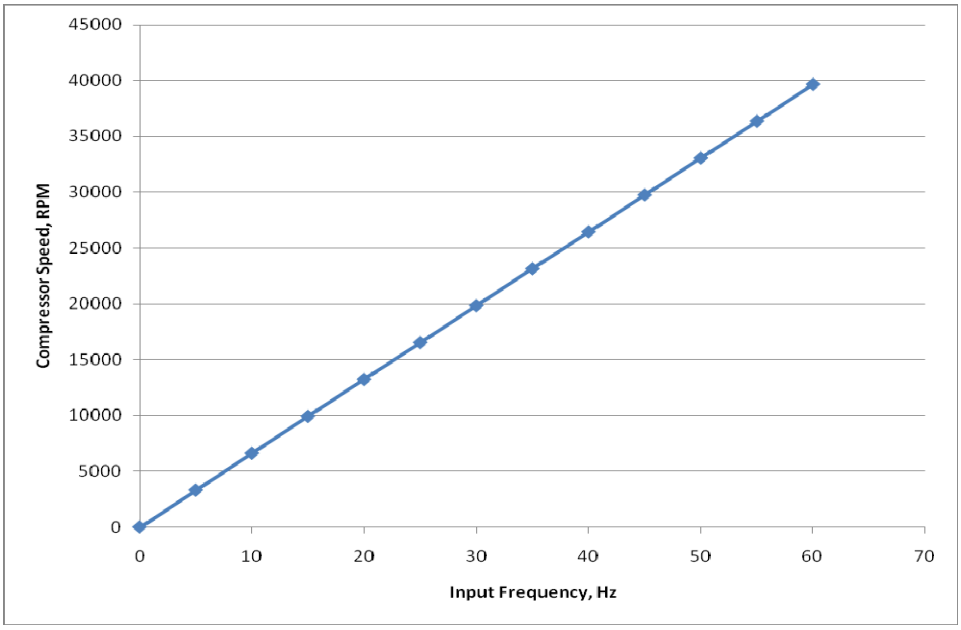

Figure 27: Compressor speed versus commanded frequency.

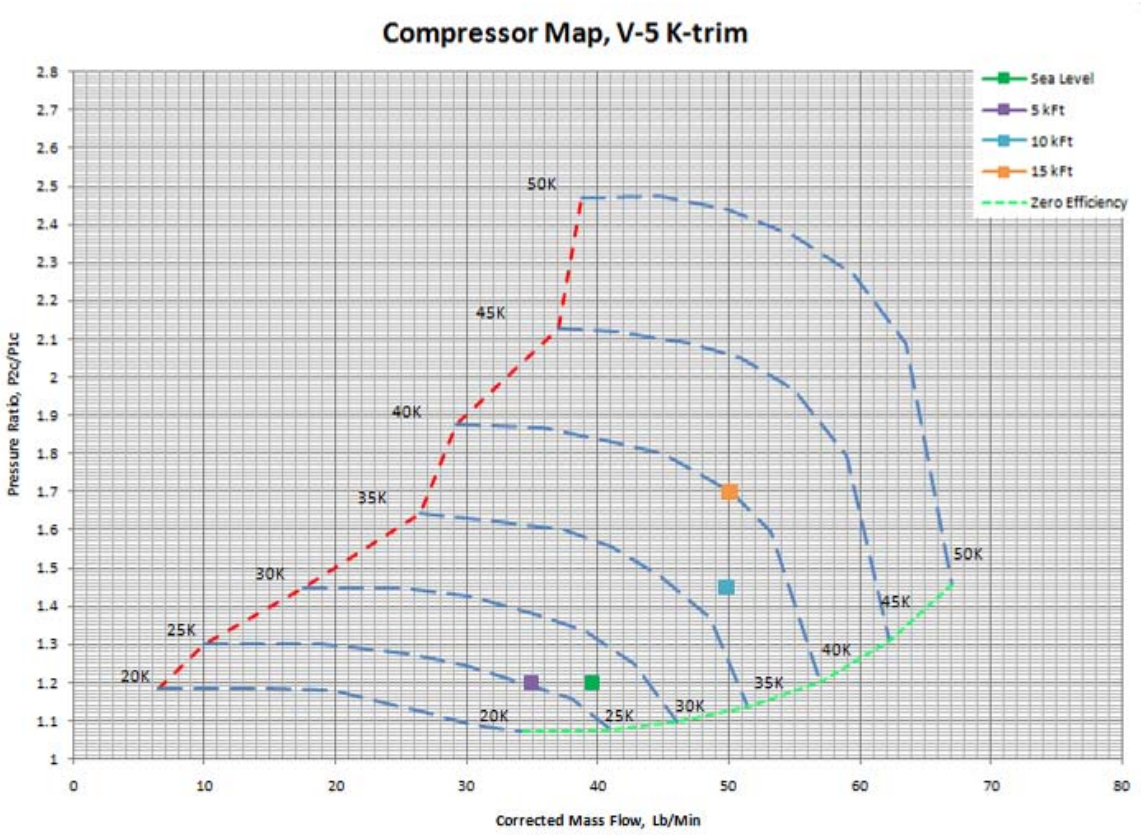

Figure 28: Compressor map of pressure ratio versus corrected air mass flow rate (adapted from 37).

Table 5: Compressor expected operating points.

Point	Altitude	Pressure, Pa	Temperature, K	$\dot{m}_C$, Lbs/min	π_C Required
1	Sea Level*	98600	294.3	39.5	1.00
2	5000 ft	84870	284.5	35.0	1.16
3	10000 ft	70650	274.8	49.5	1.40
4	15000 ft	58430	265.0	50.0	1.69

*Ambient condition in test lab is the highest inlet pressure that the compressor will see

III.2.2 Control Valves

The test stand was designed so that the air pressure to the inlet of the engine, the exit of the exhaust tube, and the air around the engine were controlled during the test. The air pressure is controlled through the use of a compressor and valves. The valves were chosen based on the ability to throttle the incoming flow to the desired level. The

main flow path into the engine cylinder uses a TRIAC ½ inch 30 degree vee port control valve with a WEM-500 electric actuator and positioned as shown in Figure 29. One major reason for selecting this valve combination was the fully electric actuator that did not require a separate air supply. The TRIAC ½ vee port control valve is sized to handle a maximum flow coefficient of 2.6 at 100% open. The flow coefficient is a function of the percent opening of the valve and closely approximates Eq. (29), as shown in Appendix B, where X is in percent open.

$$C_V = 1E-6 * X^3 + 1..0E-4 * X^2 + 7.0E-4 * X \quad (29)$$

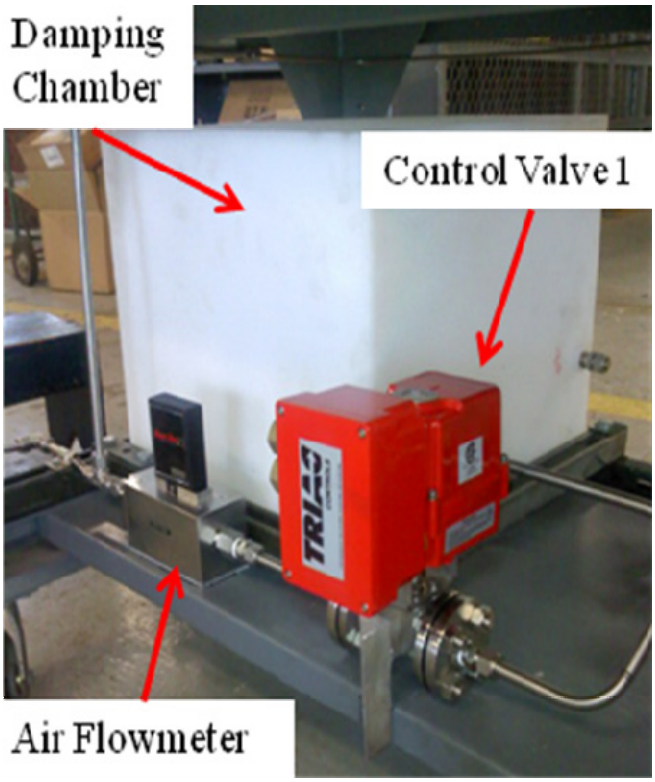

Figure 29: Control valve 1 on the engine intake line just downstream of the air mass flowmeter and upstream of damping chamber.

This valve was chosen based on the inlet pressure and the desired flow rate to the engine. The flow rate was calculated based upon engine speed, an assumed cylinder volume of 100 cubic centimeters, and an assumed volumetric efficiency of 85%.

Volumetric efficiency does not really apply to two stroke engines and a more appropriate value would have been to assume a delivery ratio in order to calculate the flow rate. The inlet pressure to the valve was assumed to be 65 psig and is based upon the available shop air supply. This flow rate was then corrected back to standard day conditions to determine the range of flow rates that the control valve must accurately meter. The flow rate for the small control valve ranged from 85 to 396.5 SLPM, which were translated into flow coefficient values using Eq. (30) where q is the flow rate in scfm, Sg is the specific gravity of air, T_{alt} is the temperature of the simulated altitude, P_{in} is the inlet pressure in psia, and P_{alt} is the desired simulated altitude pressure in psia. The flow coefficient required for this smaller control valve ranges from 0.1 to 0.5.

$$C_v = \frac{q\left[Sg\left(T_{alt}+460\right)\right]^{1/2}}{\left[1360\left(P_{in}-P_{alt}\right)P_{alt}\right]^{1/2}} \tag{30}$$

For the larger engine cooling flow path it was determined that two valves were needed to cover the range of design pressures. The large flow path must be fed by ambient air due to the volume of air required. The desire was to use high pressure air to feed this cooling loop but it was determined that the shop air compressor did not have the capability to supply the required volumetric flow rate. The next step was to determine the flow coefficient for a single valve over the entire range of flow conditions. The result was that at conditions near ambient pressures the flow coefficient was excessively large. A simple full port manual ball valve was chosen to provide the required flow at these near sea level pressure conditions. As the pressure drops below the ambient air pressure the flow coefficient drops dramatically so that the use of a vee port control valve is acceptable. The large control valve is a 2.5 inch vee port TRIAC ball valve with a

WEM-690 electric actuator and positioner. The bypass valve is a 3 inch full port manual ball valve from TRIAC. The manual actuation of the bypass valve allows the main control valve to operate farther from its full open position so that the pressure can be controlled with finer resolution. Figure 30 shows the large control valve and the cooling flow bypass valve mounted on the test stand.

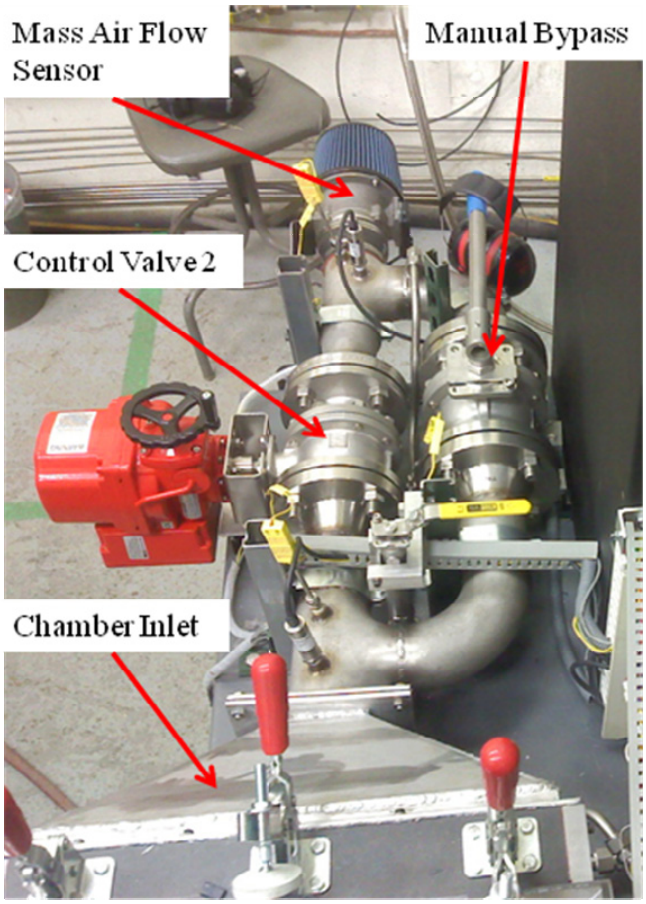

Figure 30: Cooling air flow path with control valve 2, manual bypass valve, mass air flow sensor, and chamber inlet.

III.2.3 Heat Exchanger

The temperature control for both flow paths was originally going to be accomplished through heat exchangers. The search for heat exchangers capable of producing the required temperatures at the simulated altitude conditions proved

somewhat difficult. The first challenge in locating appropriate heat exchangers was the choice of coolant for the devices. Liquid nitrogen was chosen because of the extreme temperature range that was required for the higher altitude test points as well as its readily available supply. For the main engine flow a simple tube in tube counter flow heat exchanger was chosen due to the much lower volumetric flow rates needed to supply the engine. The sizing of the small heat exchanger is documented in Appendix A and began by assuming an approximate volumetric air flow rate required by the engine. Assuming the engine operates at 8000 RPM with a volumetric efficiency of 85% the maximum amount of air used for combustion was calculated by multiplying the volumetric air flow rate times the air density at altitude divided by the reference density to correct the value back to standard conditions to get the volumetric air flow rate in scfm using Eq. (31).

$$\dot{V}_C = \frac{RPM}{2} * \eta * Vol * \frac{\rho}{\rho_{ref}} \tag{31}$$

where *RPM* is the engine speed, η is the volumetric efficiency, *Vol* is the volume of the cylinder, and ρ is the density. Substituting the values assumed above into Eq. (31) and using 100 cm^3 as the cylinder volume leads to a maximum volumetric air flow rate of 14.167 scfm. The uncorrected mass flow rate can be calculated at each altitude using the standard atmosphere density at altitude times the maximum volumetric flow rate given by Eq. (32).

$$\dot{m} = \dot{V}_C * \rho \tag{32}$$

The heat that must be removed from the air stream can be calculated from the energy equation, Eq. (33), using the assumption of an ideal gas with the specific heat at constant

pressure, C_p, a function only of temperature. The value used for the specific heat was calculated at an average temperature where the inlet temperature was assumed to be 300 K.

$$Q = \dot{m} * C_p * \left(T_{alt} - T_{in}\right) \tag{33}$$

Using Eq. (33) the maximum amount of heat that the small heat exchanger must remove from the flow was calculated as 458 W. In addition to heat removal from the inlet air stream if hot day conditions at sea level are to be reached then a heater capable of adding 121 W to the air stream would be needed. Based on the chosen coolant it was desired to find a heat exchanger which would have a small enough flow rate to allow the stand to operate for a given amount of time. The assumption was made that one hour of run time was adequate to collect relevant data before refilling the LN_2 supply tank. Based on the need to sue the coolant for both the engine inlet flow and the engine cooling flow paths it was determined that 6 g/s of LN_2 would be used as the coolant mass flow rate for determining heat exchanger size. Researching several possible small heat exchangers lead to the selection of an Exergy LLC tube-in-tube counter flow heat exchanger model 670. The number of loops needed in the Exergy model 670 was calculated in Appendix A. The calculations in Appendix A showed that in order to provide addition cooling capacity in the heat exchanger that a seven loop coil, part number 00670-3, would be purchased and is shown in Figure 31 installed on the test stand.

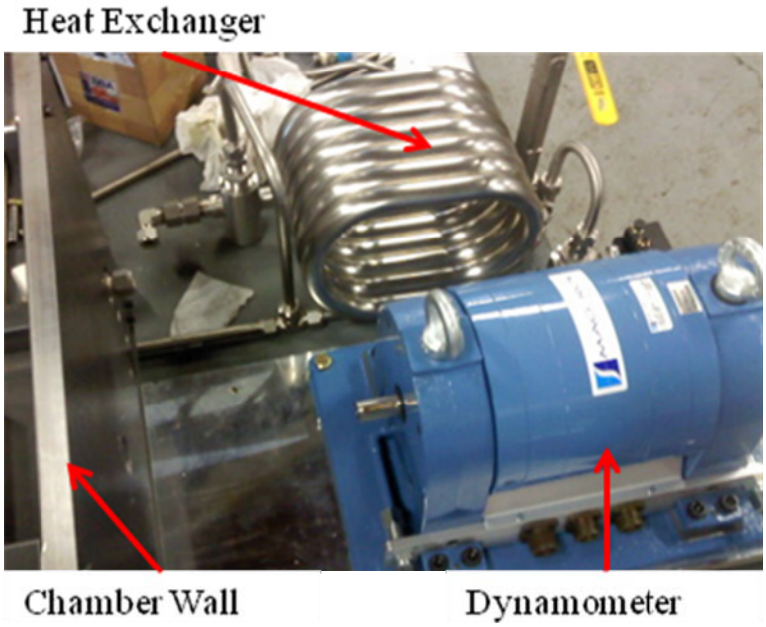

Figure 31: Engine inlet flow path heat exchanger installed on test stand.

A commercially available heat exchanger that would work for the engine cooling flow path was harder to locate. After contacting several companies a design by Super Radiator Coils™ was chosen to meet the requirements. This heat exchanger design was not ordered as it was decided that simply injecting the coolant into the flow stream would reduce the amount of coolant usage and allow the test stand to run for longer periods of time. It was understood that direct injection of LN2 into the cooling stream would lead to slight variations in pressure and mass flow rate. In addition, it was known that exactly matching the temperature of the cooling flow path stream to the engine inlet stream would be very difficult. Controlling these variations in the engine cooling flow path were not deemed critical and no attempt was made to reduce their magnitude. The direct injection of liquid nitrogen, LN2, into the flow stream will not impact the engine performance as this stream was not being used in the combustion process and nitrogen will closely replicate the thermo-physical properties of air. The Super Radiator Coils™

design was a tube and fin design utilizing aluminum fins and copper tubes listed as coil model 8x8-4R-38/60. No attempt was made to review the manufacturers calculated heat removal capacity, however the manufactured did give enough data on the proposed design in order to perform an analysis in the future.

One additional item of interest for the heat transfer in the engine cooling path was the need to provide a velocity across the engine in order to generate a high enough local convective heat transfer coefficient from the engine cooling fins to keep the engine below the maximum engine head temperature. The calculations done to determine the required mass flow rate to meet the engine cooling requirement did not take into account the local velocity or local heat transfer coefficient. There was some concern that there would not be sufficient air flow velocity across the engine cooling fins to keep the engine from overheating. In the event that additional flow velocity was required provisions for installing a fan inside the box were made though not completed. Initial tests of the engine running with the compressor on showed that a fan was not required. During initial testing the engine head temperature did not exceed 200 °C and the melting temperature of aluminum is approximately 660 °C leaving a wide margin of safety.

III.2.4 Damping Chamber

In order to accurately measure the mass air flow into the engine for combustion calculations a damping chamber was needed in the engine supply air flow path. The purpose of this damping chamber was to provide sufficient volume to damp out pressure pulsations from the engine so that they do not impact the mass air flow sensor measurements. The cyclic nature of internal combustion engines generate pressure pulses

in the intake system as the intake ports or valves open and close during each cycle. The removal of pressure pulses also allows the control valve on the engine supply stream to operate more smoothly without having to react to constant pressure fluctuations in the system. The control valve is set based upon downstream pressure measurements and constant pressure changes in the line would cause the valve to continually modulate which could cause even larger pressure fluctuations in the intake system preventing the test from reaching the desired pressure set point.

The size of the damping chamber was determined by examining relevant research and looking for guidelines to follow. The study conducted by Watanabe and Kuroda (12) used a damping chamber 690 times, equal to 0.04 m^3, the size of the test engine cylinder volume. Cadou et al (8) used a damping chamber 3000 times, equal to 0.007 m^3, the size of the test engine cylinder volume. These volume ratios were used as an upper and lower limit on the size of the damping chamber. The size of the chamber was limited by the space available on the test stand and so a damping chamber that was a little over 1200 times the size of the test engine cylinder volume. The chamber was ordered from Plastic-Mart.com with part number B273 and has an internal capacity of 0.1154 m^3. The physical volume was much larger than those used by previous researchers but the ratio of the damping volume to cylinder volume falls towards the lower end of the scale.

III.2.5 Flow Meters

In order to calculate useful engine performance parameters for comparison to other similar engines accurate measurements of the air mass flow and fuel mass flow rates must be taken. Based upon the calculated air mass flow rate from the earlier control valve

selection it was determined that the air flow meter required a range of 0 to 500 standard liters per minute, SLPM. The air flow meter selected for the test stand was a Sierra Instruments Smart-Track series 100 thermal mass flow sensor, with part number M100H-NR-15-O1/1-PV2-V1-C3. The M100H has a ± 1.0% of full scale accuracy with a ± 0.2% of full scale repeatability and shown mounted to the test stand in Figure 29.

The fuel flow rate range was determined from the engine owner's manual given flow rate. The owner's manual states that the fuel flow rate will be between 1-2 ounces per minute which is equivalent to 30-60 cm^3/min. The fuel flow meter was ordered from Max Machinery and is a model 213 piston flow meter with a Max 294 transmitter and is shown in Figure 32. The model 213 has a range of 0-1800 cc/min with and accuracy of ± 0.2% of reading. The Max Machinery flow meter and transmitter were chosen mainly due to the familiarity and commonality between it and other fuel flow meters used in other AFRL/RZTC small engine stands.

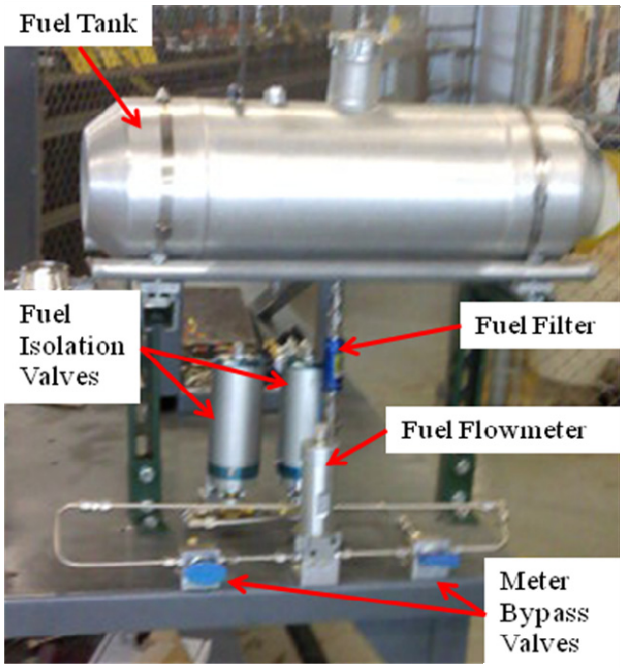

Figure 32: Fuel system with fuel flow meter installed on test stand.

III.2.6 Chamber

The main chamber was designed to allow the test stand to run at conditions simulating 30000 ft above sea level flight conditions. The size of the chamber was chosen to allow for the testing of larger engines as well as to enhance the ability of engineers to make changes if required without having to disassemble the entire chamber. Two large polycarbonate view ports were included in the design to allow the test article to be visually monitored for indications of damage and irregular operation. The view ports were made of ½ inch thick polycarbonate which was determined to be suitable for pressures down to about 7 psia simulating 15000 ft above sea level flight conditions. It was determined that ¾ inch polycarbonate would be needed to operate the chamber at pressures from 3 psia to 7 psia which represent flight conditions from 15000 ft to 30000 ft above sea level, ASL. The stress analysis used as the basis for this determination is included as Appendix C.

Several design iterations were completed for the chamber before a final design was chosen which allowed for relatively easy removal of components with the required sealing capacity. Stress analysis was also performed on the bottom face of the box which is constructed out of 3/16 inch thick A36 low carbon steel. The stress analysis of the bottom surface revealed that the original design which utilized 1/8” thick steel would not provide an adequate safety margin for pressure differences created by running the test stand at conditions simulating 30000 ft ASL. The chamber was designed to be bolted together in sections with gaskets and sealant material placed between the pieces to provide a seal, as shown in Figure 33. The clamps, McMaster Carr part number 5126A47, visible in Figure 33 were used to hold the polycarbonate windows in place and

have a holding capacity of 290 lbs. Larger diameter, 2 inch, neoprene feet were purchased for use with the clamps to increase the distribution are of the holding force and alleviate possible high stress points created by the original feet, with 7/8 inch diameter. Assembly drawings and models for the main chamber and motor mount design can be found in Appendix E.

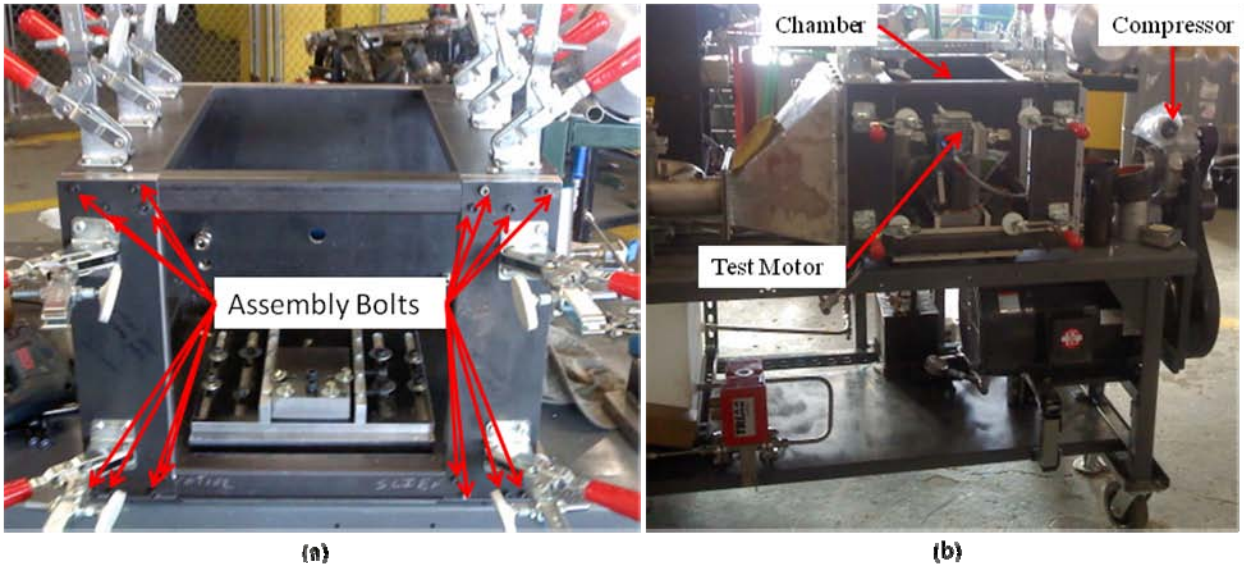

Figure 33: Test chamber construction (a) and placement (b) on test stand.

Some leakage of fuel was noticed near the bottom corner nearest to the dynamometer of the main chamber walls and exit nozzle interface during initial testing and troubleshooting. The observation of fuel leakage at this location in the system was assumed to be allowing air to leak into the chamber. Additionally the shaft seal was damaged, Figure 34, after initial testing and no longer formed a tight seal against the shaft. The seals inner sealing surface that was supposed to stay snug against the shaft has been pushed back and was no longer able to return to its original shape. This plastic deformation of the seal provided another leak path into the chamber. The cause of the deformation was unknown but it was suspected that during one of the initial tests when

the motor and shaft visibly wobbled the seal was pushed past the manufactures limits of motion. Lastly, the gasket material used for the upper window tore in several places, Figure 35, during the repeated openings of the chamber to troubleshoot problems during activation of the test stand. This seal while torn was used as a partial seal though it was known that air would leak through at each tear location. From these observations it was assumed that some additional air was leaking into the box during low pressure runs due to the pressure differential. This leakage was not addressed as initial test runs of the compressor were able to create sustained chamber pressures around 10.0 psia. This pressure differential was not 100% of the design goal of around 7 psia but it was sufficient to begin altitude testing up to conditions simulating approximately 10000 ft above sea level.

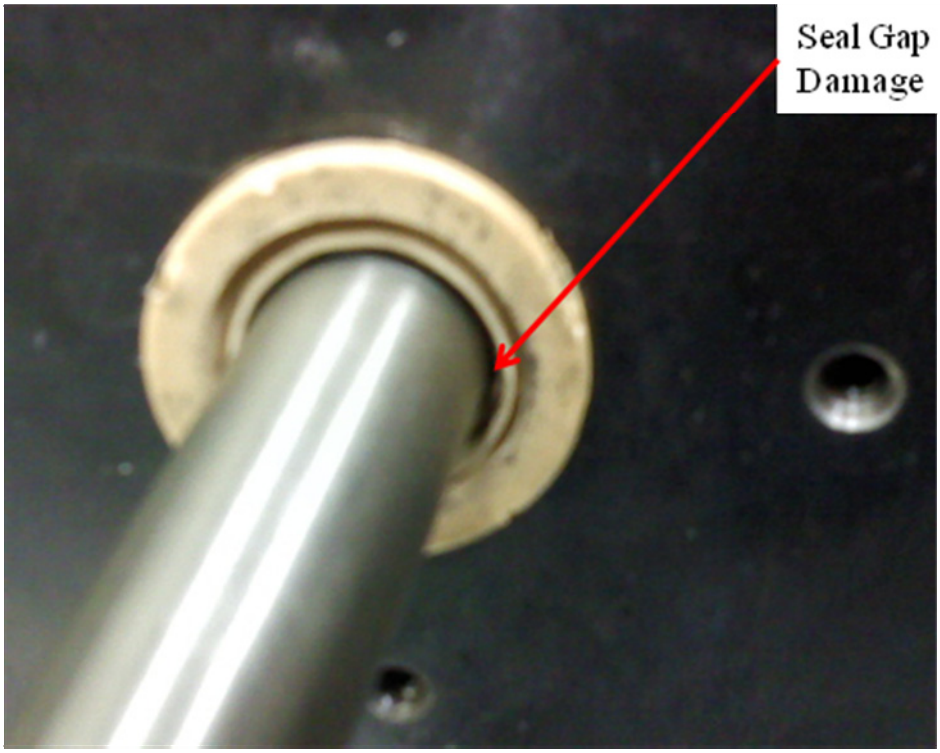

Figure 34: Shaft seal damage observed after initial testing and troubleshooting.

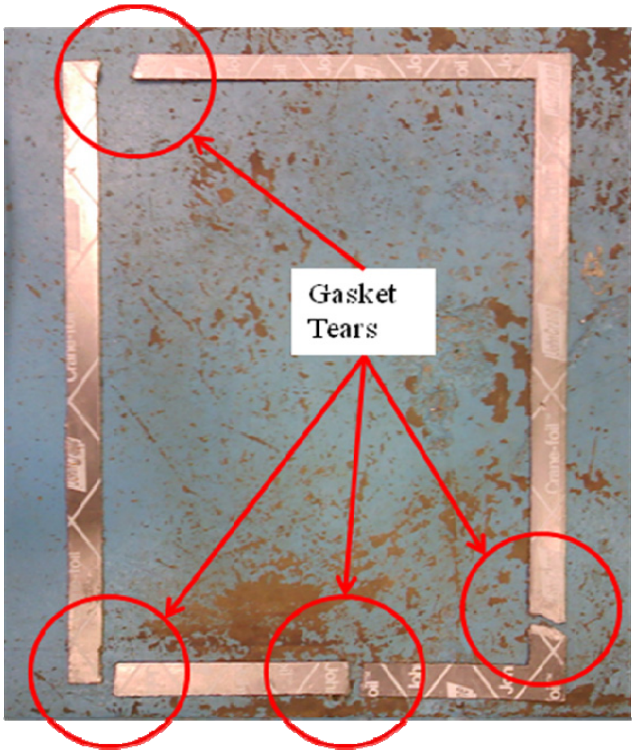

Figure 35: Upper window gasket damage after several removals of the upper viewing window.

III.2.7 Pressure and Temperature

Pressure measurements for the engine intake and cooling flow paths were made using Omega piezoresistive absolute pressure transducers with part number PX409-030A5V. The Omega model PX409 has a compensated temperature range of -29 to 85 °C with a pressure measurement error of +/-0.5% of span within the temperature range. Omega type K model KMQSS thermocouples were used throughout the system to obtain temperature measurements. Omega type K thermocouples have a range of -200 °C to 1250 °C with an error above 0 °C of 2.2 °C or 0.75% of full scale whichever is greater and an error of 2.2 °C or 2.0% of full scale whichever is greater. Exposed junction thermocouples were used where immersion in a gas phase flow was needed. Exposed junction thermocouples were utilized in the gas flow paths because they have a faster

response time to changes in the gas temperature than shielded junctions. Ungrounded shielded thermocouples were used in the fuel system and liquid nitrogen cooling system lines to ensure that the junction was not damaged by the liquid flows. The choice of thermocouples and absolute pressure transducers was influenced by common usage within the engine tests stands of AFRL/RZTC.

In cylinder pressure was measured with a Kistler 6118BFD16Q02A41 measuring spark plug piezoelectric sensor. The model 6118 has an interference suppression resistor a BOSCH 6 heat rating which closely matches the original OEM spark plug. The OEM spark plug has a M14x1.25 mm thread with a depth of 9.5 mm. The Kistler model 6118B was chosen after discussion with Capt. Cary Wilson (15), Adam Brown of ISSI, and Dr. John Hoke of ISSI on previous experiences with a range of other piezoelectric spark plug type sensors. Several other models from other companies had been used in the past but suffered from poor performance and or damage in the knocking combustion region. The piezoelectric sensor was connected to a Kistler 5064B11 dual channel charge amplifier module mounted in a Kistler 2852A12 Slim Signal Conditioning Platform, SCP, with the use of low resistance insulated cables. The charge amplifier 0 to 10 VDC output was connected to the data acquisition system. The Kistler 6118 measuring spark plug sensor has a range from 0 to 200 bar with a natural frequency of about 65 kHz and a sensitivity at 200 °C of about -10 pC/bar. The model 6118 has a linearity of less than or equal to ± 0.5% of full scale. The accuracy of the cylinder pressure measurement will depend on the pegging method used as discussed in the previous chapter.

III.3 Other Important Components

III.3.1 Dynamometer

One of the main goals of the test stand is to provide accurate measurements of power, speed, and torque that can be used to create engine performance maps. The dynamometer must be capable of withstanding large torque variations produced by a single cylinder internal combustion engine while providing accurate measurements. The dynamometer chosen for the test stand was the Magtrol Inc. model 2WB65/S006 eddy current dynamometer with part number 312-201-S006. This particular part number has more robust bearings for the internal combustion engine test application than the standard 2WB65 model. The 2WB65 is capable of testing engines up to 12 kW or 16.1 hp of power and can provide a loading torque, T_L, of up to 20 N-m with a maximum speed of 30000 RPM. The loading torque is equivalent to the aerodynamic load placed on the engine by the propeller of a UAV and can vary based on engine speed, propeller size, and flight operating conditions.

The eddy current dynamometer is controlled by a Magtrol DSP6001 high speed programmable controller with part number 004604. The system includes a dynamometer excitation power supply, part number 234-311-123, a torque and speed conditioner, part number 234-401-122, and the associated interface cables. The Magtrol dynamometer and controller were chosen primarily due to commonality between other small dynamometers used with the AFRL/RZTC small engine researchers (15) and due to its cost as compared to other options that were investigated. Figure 36 shows the dynamometer installed on the test stand main base plate which is mounted on vibration dampers. The vibration

dampers, McMaster Carr part number 64875K9, were used to damp out the vibrations caused by the single cylinder test engine and isolate the engine from the rest of the test stand. The isolation of the main base plate was done to reduce possible noise in the data acquisition system as well as reduce vibration loads on the dynamometer shaft and bearings.

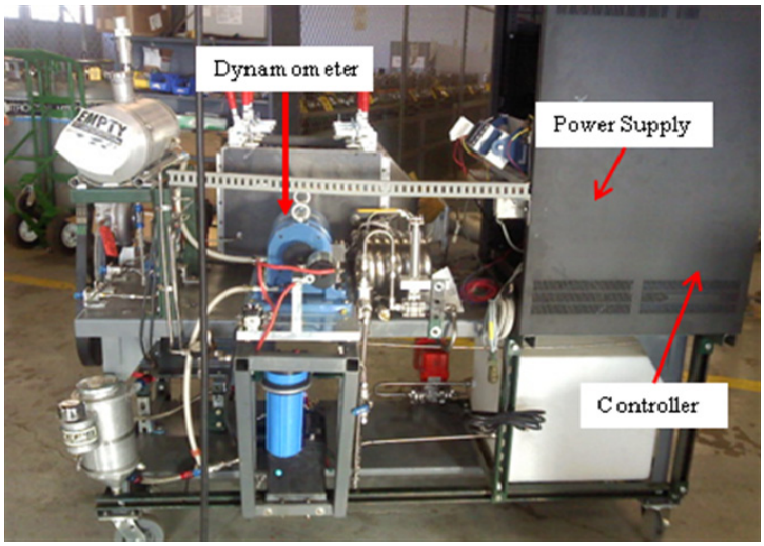

Figure 36: Magtrol 2WB65 mounted on engine test stand with power supply and programmable controller.

III.3.2 Couplings

The dynamometer and motor are connected with two shaft couplings and an intermediate shaft that passes through the wall of the chamber. This arrangement allows the dynamometer to be located outside the simulated altitude environment while the engine is fully contained within the chamber. Minimizing the chamber volume was done in order to reduce the mass flow rate requirement for the compressor as will be explained further in the next section. Locating the dynamometer outside of the simulated environment avoided having to take precautions to prevent freezing the inlet side of the dynamometer water cooling system. The intermediate shaft is sealed with an SB40

profile rotary seal from American High Performance Seals. This seal was originally designed to seal high pressure liquid inside an enclosure. After discussion with the manufacturer it was determined that this seal should easily support the differential gas pressure created by reducing the pressure inside the chamber. The observation listed previously of the damaged seal and shown in Figure 34 will be discussed further in chapter IV.

The intermediate shaft is connected to the dynamometer and engine with Lovejoy GS28/38 curved jaw couplings with elastomeric spider inserts. Lovejoy curved jaw couplings were chosen after a considerable search for couplings capable of handling the torque and speed of the application. Several high torque couplings were researched but were not capable of the expected maximum speed of the test engine of 10000 RPM. After considerable discussion with Capt Cary Wilson of AFRL/RZTC on his use of elastomeric couplings and the issues associated with their use it was determined that the Lovejoy curved jaw coupling would work the best. The spider inserts used in the coupling have a shore hardness rating of 92A. Each coupling was made up of two hubs and the spider insert. The hub connected to the engine was machined to replace the propeller mount that comes with the test engine and fits on the tapered drive shaft. The engine side hub, shown in Figure 37, had to fit inside a collar that holds a magnetic proximity sensor that is used by the engine to sense engine speed and set ignition timing based upon the speed. The engine side hub has a magnet set at 45° before top dead center, BTDC, and the ignition box sets the delay time based upon speed and this signal.

The dynamometer side hub is a standard Lovejoy GS28/38 with two keyways that fits directly onto the dynamometer shaft. The couplings on the intermediate shaft are

Lovejoy GS28/38 couplings with a ¾ in diameter shaft and a locking device to clamp the hub to the shaft. The hubs and spiders that form the two shaft couplings are designed to withstand 95.00 N-m of torque in normal operation with a maximum peak torque load of 198.93 N-m. The locking device hubs are rated for a maximum speed of 11700 RPM while the double keyway hub on the dynamometer and the machined hub on the engine are not given a rating. Tests will be maintained at speeds below 10000 RPM to reduce concerns of hub failure. The 92A shore spider is made from urethane and is rated for temperatures down to -50 °F. The minimum temperature expected within the chamber is down to -70 °F which is lower than the rating of the spider but heat from the load imparted into the coupling along with heat release from the engine should keep the coupling above the minimum temperature rating. Tests performed at or below the minimum temperature rating will be monitored closely for indications of spider failure. Curved jaw couplings are designed so that failure of the elastomeric spider does not result in immediate failure of the coupling which is part of the reason they were chosen to connect the dynamometer to the engine. Figure 38 shows the two couplings installed on the test table connecting the dynamometer to the test engine.

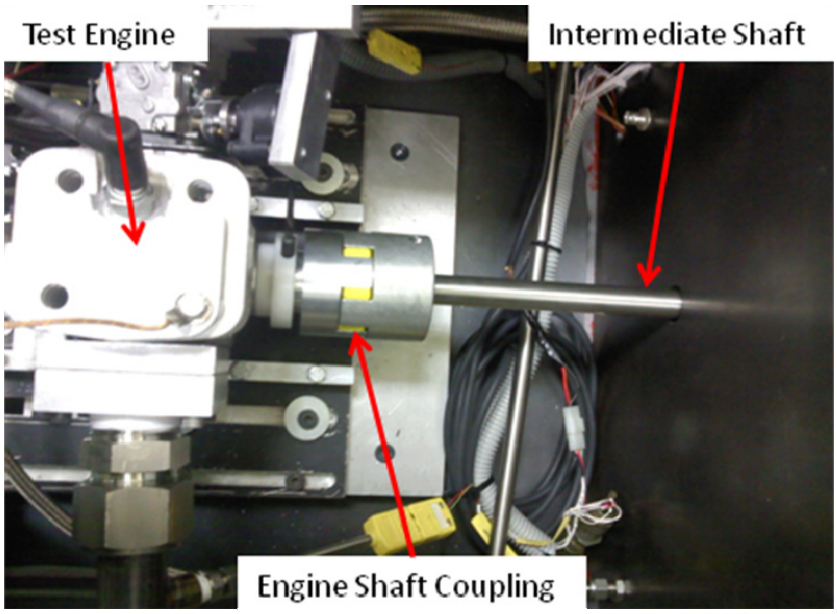

Figure 37: Engine side hub, Lovejoy GS28/38.

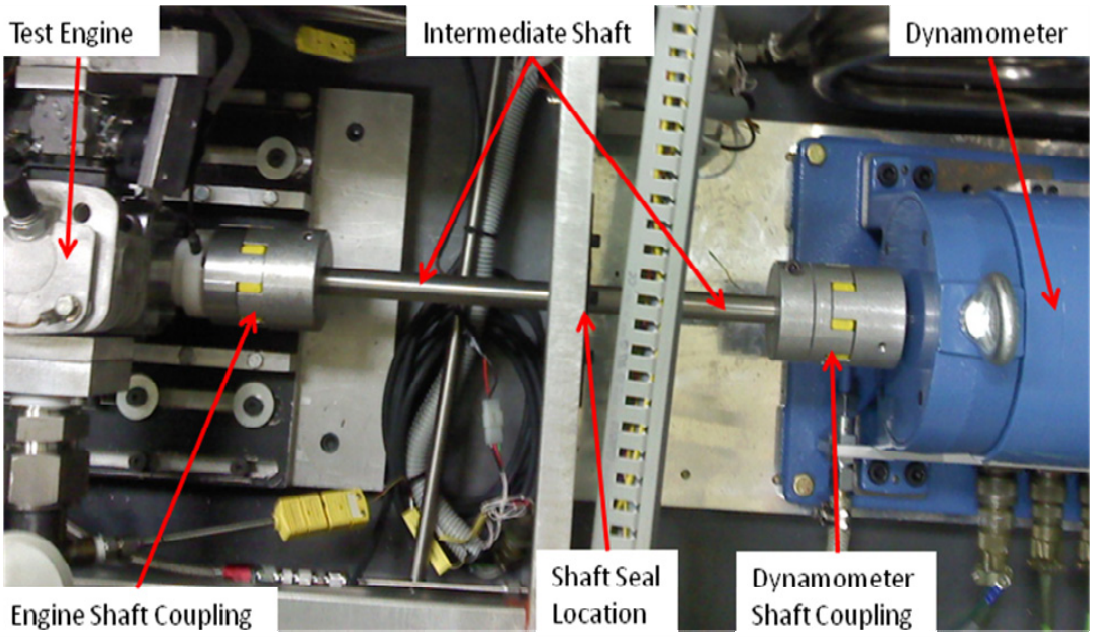

Figure 38: Engine, coupling one, intermediate shaft, coupling two, and dynamometer installed on test stand.

Coupling alignment was very important in reducing loads imparted to the intermediate shaft and dynamometer as well as the elastomeric spider insert. Coupling alignment was done by measuring spacing between the two hubs of each coupling at four

points 90° apart to determine angular, parallel, and horizontal misalignment. The engine is connected to a three axis mount which is adjusted by way of screws and shims in order to create the proper alignment of the shafts and couplings.

III.3.3 Data Acquisition

Data acquisition was accomplished with a National Instruments CompactDAQ system with a NI9213 thermocouple module, a NI9401 digital TTL module, a NI9205 ±10 VDC analog input module, a NI9264 ±10 VDC analog output module, a NI 9219 ±5 A analog input module, and a NI9485 ± 60 VDC solid state relay. The CompactDAQ was connected to a PC based computer which recorded all values and was run using an in house developed Labview software code written by Mr. Dave Burris of ISSI. Low speed data was recorded throughout the tests at a speed of 1 Hz and high speed bursts of data were recorded at each set point at a rate of 50 kHz. The CompactDAQ chassis and computer were mounted in a small 19" electronics rack, shown in Figure 39. In addition to the data acquisition system and computer, the power supplies, dynamometer controller, emergency shutoff system, and charge amplifier were mounted in the electronics rack in order to save space on the test stand and better organize equipment.

(a) (b)

Figure 39: Equipment rack (a) front and (b) back.

III.4 Error Uncertainty Analysis

Each measured value has an uncertainty associated with the particular measurement device. These measurement uncertainties are compounded when measured values are used to calculate performance parameters. Using the methods of Moffat (34-35), and Kline and McClintock (36) the uncertainty in four important calculated performance parameters was accomplished. Brake mean effective pressure, BMEP, is calculated using Eq. (6) where the measured values of torque, T_b, displacement volume, V_d, and engine speed, N are used in the calculation. Brake specific fuel consumption, BSFC, is calculated from Eq. (3) where the measured values of power, P_b, and fuel mass flow rate, $\dot{m}_f$ are used in the calculation. Similarly delivery ratio and power are calculated using the same process. Table 6 gives the manufacturers listed instrument uncertainty values. The values in Table 6 are used in Eq. (34) to calculate the overall uncertainty of each of the important engine performance parameters, BSFC and BMEP. Table 7 gives the

calculated parameter uncertainties based on the instrument uncertainty values given in Table 6. The perturbation method, Eq. (35) was used to determine the largest contributor to the error for the parameters listed in Table 7.

$$\delta R = \left[\left(\frac{\partial R}{\partial x_1} \delta x_1 \right)^2 + \left(\frac{\partial R}{\partial x_2} \delta x_2 \right)^2 + \Lambda + \left(\frac{\partial R}{\partial x_N} \delta x_N \right)^2 \right]^{1/2} \tag{34}$$

$$\delta R = \left[\left(R_0 - R_{x1+\delta x1} \right)^2 + \left(R_0 - R_{x2+\delta x2} \right)^2 + \Lambda + \left(R_0 - R_{xN+\delta xN} \right)^2 \right]^{1/2} \tag{35}$$

Table 6: Instrument measurement uncertainty values.

Instrument	Range/Value	Uncertainty
Speed	10-100000 RPM	0.01% of reading
Torque Controller	0-20 Nm (0-10 VDC)	0.02% of range (±2mV)
Torque Dynamometer	0-20 Nm	0.5% of full scale
Engine Volume	96.5 cm^3	±2.05E-6 mm^3
Fuel Mass Flow	0-1800 cc/min 0.89cc/rev	±0.2% of reading
Air Mass Flow	0-500 SLPM	±1.0% of full scale
Pressure	0-30 PSIA	±0.5% of full scale
Temperature	0 to 1250 °C	2.2 °C or 0.75% of reading
Temperature	-200 to 0 °C	2.2 °C or 2.0% of reading

Table 7: Calculated parameter uncertainty values.

Parameter	Uncertainty, UC, %	Largest Contributor
Power	2.0 < UC < 5.0	Torque, direct relation
BMEP	2.0 < UC < 5.0	Torque, direct relation
BSFC	2.0 < UC < 5.0	$\dot{m}_f$, direct relation
Delivery Ratio	0.8 < UC < 4.2	V_d, 1.18% error per % change

The uncertainty in all of the major parameters is the greatest at the lowest end of the instruments measurement range. This supports the manufacturer's recommendation to operate the instrument at least 10% above its minimum value. From the error analysis the largest impact to important performance parameters is torque measurements and fuel flow rate measurements.

IV. Results

IV.1 Initial Test Stand Checkout

During the initial troubleshooting and checkout phase of activating the altitude test stand several problems were encountered. Most of the problems encountered were fixed with minor adjustments to or in some cases replacements of components. An example of this was the need to change out an actuator on one of the fuel valves due to an incorrect stop setting which allowed the valve to turn 180° instead of only 90°. During this stage of testing several changes and enhancements were made to the Labview test program to allow the stand operator finer control of the throttle, choke, and main valve position settings. The need for finer valve position control was determined during the second day of engine testing when it was discovered that after the engine started it would immediately being to reduce the intake line pressure. If the small control valve was not opened fast enough to offset this pressure reduction then the engine would flood with fuel and cease to operate. This effect can be seen in Figure 40 where the control valve position must be continually adjusted to keep up with the engine demand. In addition the sharp drop in inlet pressure at 45 seconds and 371 seconds correlate to the engine start times. The sharp drop in control valve position at 207 seconds and 500 seconds correlate to engine stop times and the valve closure is to avoid over pressurizing the inlet lines. The first engine run in Figure 40 started at 45 seconds and engine operation stopped at 187 seconds. In the 10 seconds it took to send the closure command signal the inlet pressure increased from 15.64 psia to 17.31 psia. This test was done with extremely lean carburetor needle settings which is why the engine speed did not exceed 2000 RPM

during this time frame. The same test is shown in Figure 41 with inlet pressure and dynamometer speed versus elapsed time. Figure 41 shows how dynamometer and thus engine speed varied as the inlet pressure oscillated during each engine run. Each spike in the dynamometer speed data correlates to an attempt to start the engine by turning on the starter motor briefly. Engine run time can be determined by looking at the dynamometer speed data and finding time periods where the speed does not return back to zero after the initial spike.

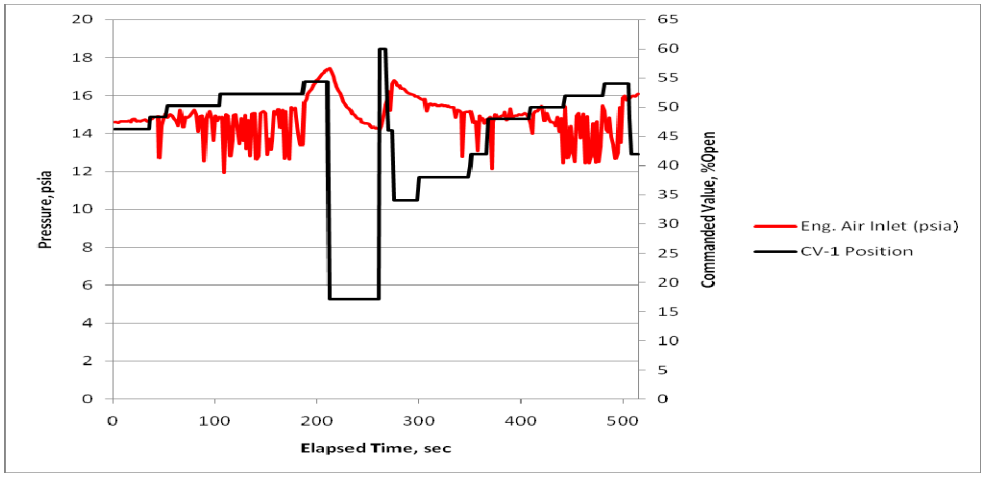

Figure 40: Control valve position and inlet pressure as a function of time during initial engine start tests.

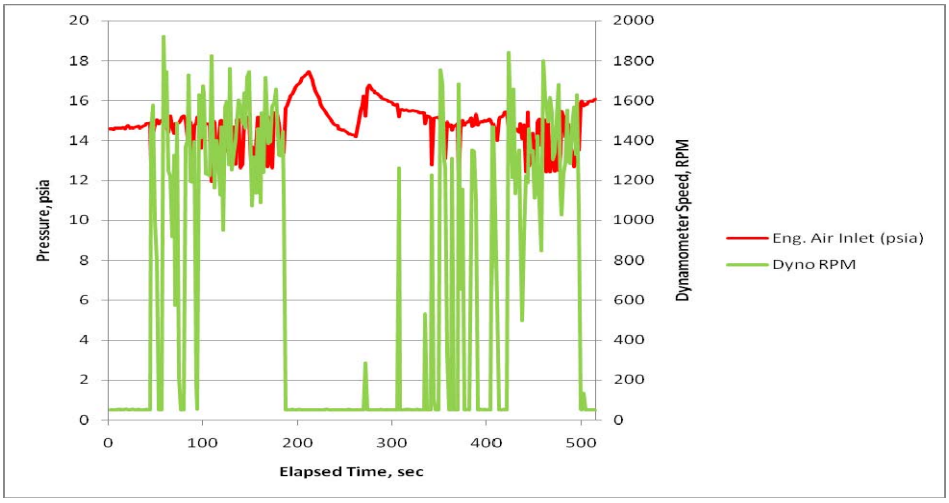

Figure 41: Engine speed and inlet pressure as a function of time during initial engine start tests.

It was noted during initial testing with the compressor running that the oil temperature began increasing over time. The maximum lubrication oil temperature recommended by the manufacturer is 200 °F. The tests were terminated when the oil temperature reached 200 °F and the oil pump was left on to circulate the oil through the system. Once the oil temperature returned to around 90 °F compressor operation was resumed. The outside door to the test facility was opened slightly after the initial tests to help cool the oil. The oil tank was located about one foot from the open door and the outside air temperature was approximately 30 °F. This additional cold air helped cool the bulk oil temperature with 30 minutes.

IV.2 Testing

IV.2.1 Altitude Experiments

The main experiment was to determine the impact of altitude on engine power, fuel consumption, and mean effective pressure. The first priority was to determine the range of conditions that the test stand was capable of achieving. The test stand was designed to simulate conditions up to 15000 ft above sea level. The test stand should be capable of achieving temperatures below 270.3 K and pressures below 58521 Pa. In order to determine the limits of the test stands abilities several check outs were performed. The first test was to determine the minimum pressure that the compressor was capable of achieving inside the chamber. This test was completed by varying the main control valves with the compressor operating. A combination of bypass valve position, main control valve position, and compressor speeds were used in order to determine the

optimal settings to generate minimum pressure within the chamber. Raw data for three separate attempts is shown in Appendix D. After several attempts it was determined that the compressor motor and variable frequency drive were limiting the ability to further reduce chamber pressure. The first attempt to bring the chamber pressure down is shown in Figure 42 where the rapid recovery after only a second or two is due to the rapid commanding of the control valve and the compressor speed. The second and third test are shown in the raw data of Appendix D and resulted in a minimum chamber pressures at or below 10 psia. The second and third test were achieved with much closer observation of the compressor map along with a more methodical approach to changes in valve position and compressor speed.

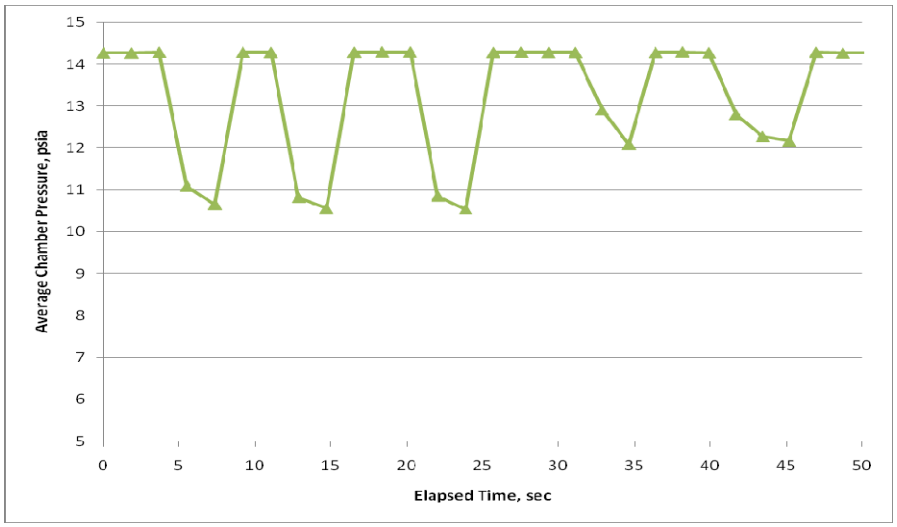

Figure 42: Chamber pressure versus time for first test.

The second test was to determine how well the compressor and coolant system were able to work together. By varying the liquid nitrogen valve positions as well as the main tank isolation valve position the test stand was able to achieve temperatures around 10 °F. This temperature variation was accomplished in coordination with a reduction in chamber pressure as shown in Figure 43. The limits shown in Figure 43 are a minimum pressure

of 10.1 psia and a minimum temperature of 13.0 °F. The upper range shown is 14.4 psia and 61.0 °F. The upper limits were set by the atmospheric conditions in the test cell during the testing. Temperatures above the maximum and below the minimum shown by the limits are achievable if the temperature in the test cell is sufficiently high, or the main LN_2 tank isolation valve is opened further to allow a higher coolant flow rate. The pressure limits as discussed previously could be increased by reducing the amount of air leaking into the chamber and possibly by adjusting the drive settings. The over current condition that limits the compressor is a safety mechanism within the variable frequency drive. This safety can be adjusted and completely removed if desired, however current testing does not require adjusting or removing the limit currently set at 23.5 A at full motor loading.

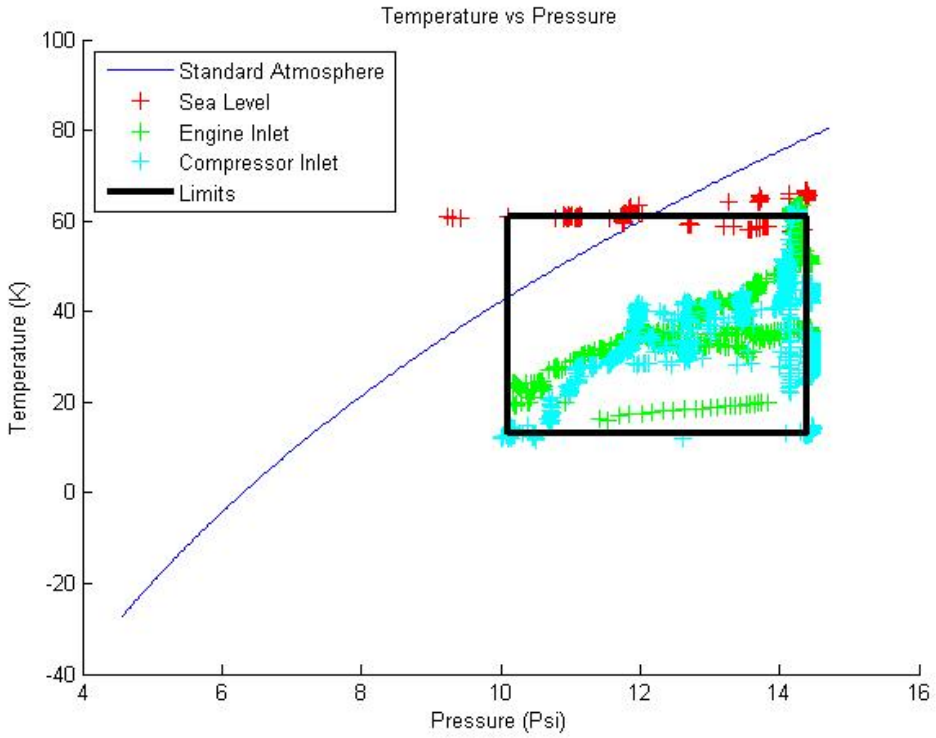

Figure 43: Chamber temperature versus chamber pressure.

Attempts were made to complete engine performance maps at 1500 m and 3000 m conditions, however sufficient data was not collected at these conditions. The series of test points needed to determine the impact of altitude on engine performance parameters was generated by varying engine speed over the range of 2000 RPM to 8500 RPM in increments of 1000 RPM and varying throttle position from wide open throttle, WOT, down to 25% throttle in increments of 25% at a given altitude condition. At each test point corresponding to a throttle setting and engine speed, volumetric fuel flow, temperature, pressure, speed, and torque values would be recorded at a rate of 1 Hz for 10 seconds. High speed data of in cylinder pressure, and spark timing should be taken in bursts at a rate of 50 kHz to record representative cycles for each test point. The set of test engine speeds and throttle settings would then be repeated for at each altitude condition. The pressure and temperature for the three altitude settings are shown in Table 8 and correspond to sea level, 1500 m, and 3000 m above sea level.

Table 8: Altitude test points

Altitude, m	Pressure, Pa	Temperature, K	Pressure Ratio
Sea Level	101325	300	1.00
1500	85000	285	1.16
3000	70650	275	1.40

Each test point should be averaged over a minimum of 10 seconds and any sample that was greater than 2 standard deviations away from the mean should be discarded. In addition samples with negative values or zero values were discarded. Engine performance maps could be created by putting the averaged data into a matrix form in order to create plots of BMEP versus engine speed with contours of constant BSFC.

IV.2.2 Engine Load Tests

The test engine was tested under sea level pressure and temperature conditions in order to create a baseline engine performance map. The average inlet pressure for all sea level tests was measured as 13.82 ± 0.20 psia. The average inlet temperature for all sea level tests was measured as 73.16 ± 11.93 °F. Initial sea level testing using the separate engine inlet line began by slightly increasing the engine inlet pressure from the average ambient 14.4 psia to approximately 15.5 psia. Once the inlet pressure was increased the engine was started and the engine flow control valve was adjusted to keep up with engine air flow demand. This process as stated previously took many tries and was very sensitive to inlet pressure increases. The engine was loaded by setting a desired engine speed on the dynamometer controller and setting the engine throttle at a fixed percentage of full throttle. Engine load test speeds were attempted at 2000 to 8500 RPM in increments of 1000 RPM with the throttle position was set to between 25% and 100% of full throttle in increments of 25%. Figure 44 shows the engine BMEP versus engine speed for several attempted tests at sea level conditions. The data presented in Figure 44 shows some of the issues encountered during initial testing. The engine had trouble reaching the desired speed set point due to the intake air flow previously described. Because the engine failed to reach the set point the dynamometer did not impart a load to the engine. This can be seen in the torque versus engine speed data in Figure 45. The expected response was an increase in torque as the engine speed increased up to a maximum value and then a decrease as engine speed continued to increase. Assuming that the Brison 5.8 test engine was capable of a power output of 6.5 hp at 6500 RPM the expected torque should be around 5.25 ft-lbs and the BMEP should be around 66.4 psi.

The values in Figure 44 and Figure 45 are far below the expected values were not used to determine engine performance characteristics.

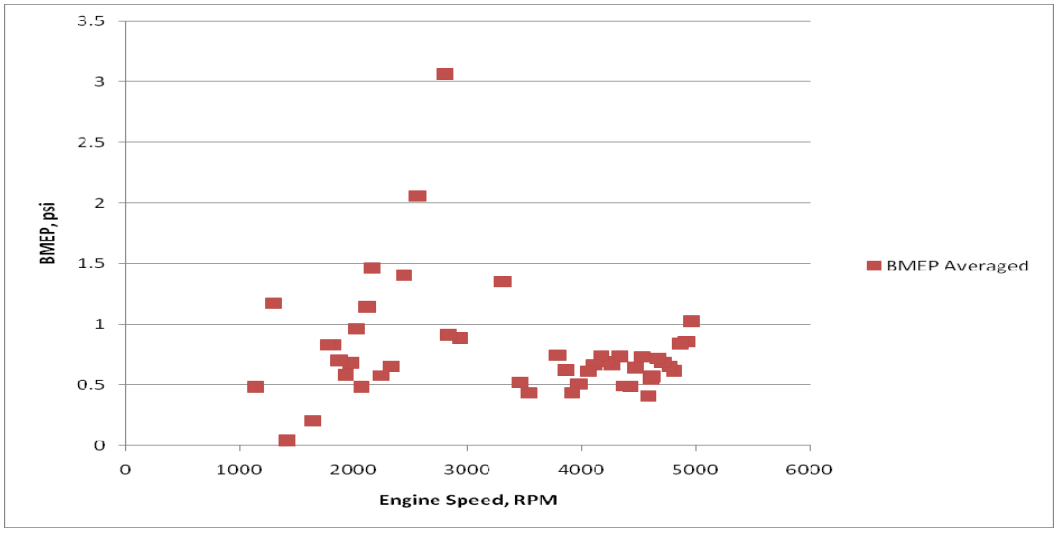

Figure 44: BMEP versus engine speed for sea level conditions.

The fuel to air ratio was very important to the operation of the test engine. Several adjustments were made to the carburetor settings during the initial attempts to start the test engine. The impact of these adjustments will be discussed in more detail in section IV.2.3. Additional difficulties were encountered in measuring the air and fuel flow rates. These issues affected the ability to determine delivery ratio of the test engine. Delivery ratio is a measure of how efficiently the engine is at expelling the burned gases and inducting a fresh fuel/air charge during each cycle. An engine running at a delivery ratio close to 100% is desirable because the engine is able to intake the largest amount of fresh charge per cycle and in theory run at a higher power output.

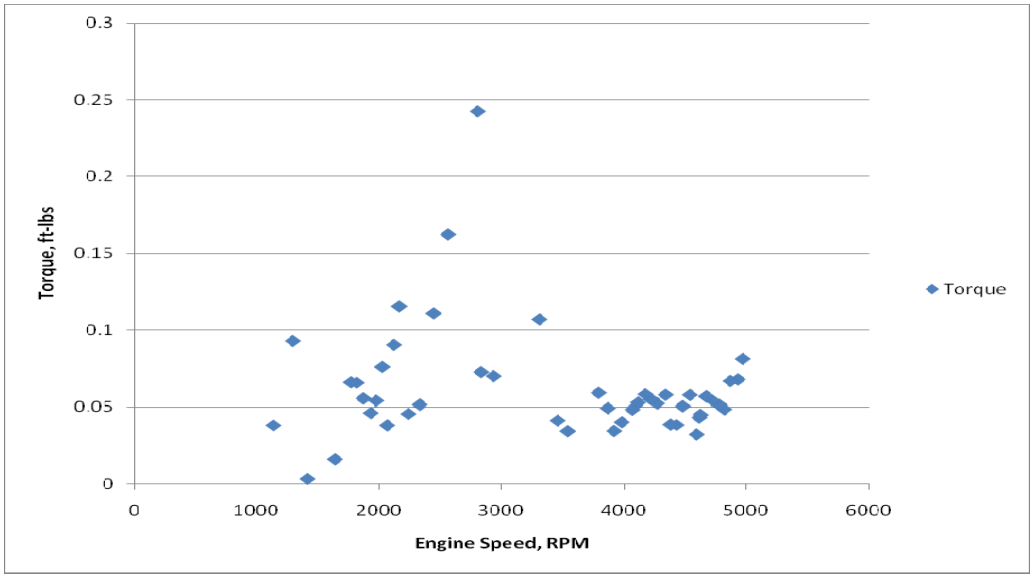

Figure 45: Torque versus engine speed for sea level conditions.

In order to correctly calculate the delivery ratio an accurate measurement of fuel and air mass flows, pressures, and temperatures is required. Fuel pressure was assumed to be at ambient conditions and fuel temperature was measured with a thermocouple located outside of the altitude chamber. Fuel flow rates were measured with a Max Machinery rotary piston flow meter and several issues were encountered. The first issue was that during testing the data acquisition system would occasionally record flow rates greater than 340000 cc/sec and was assumed to be a faulty value. All other recorded fuel flow rates were suspected to be faulty as well and the over estimation was caused by the method that the data acquisition system originally used to calculate fuel flow rate. The system was using instantaneous frequency generated by the pulses from the flow meter at the time of recording the value. A sample of raw data collected with the original programming is shown in Appendix C. The data was used only for preliminary analysis by removing obvious outliers from the sample set and using a ten consecutive sample average. Figure 46 shows how the fuel flow rate varied during two engine test runs at

WOT under sea level conditions at approximately 2000 RPM. An adjustment was made to the Labview program which counted the total number of pulses between time samples. The number of pulses was multiplied by the volume per pulse and divided by the time between samples to determine the fuel flow rate. After each time sample the count was reset to zero. This enabled a more direct and accurate measure of fuel mass flow rate during engine testing and was used for all future testing. In addition to the fuel flow rate, total fuel consumed during each test was recorded to verify the fuel flow rate values.

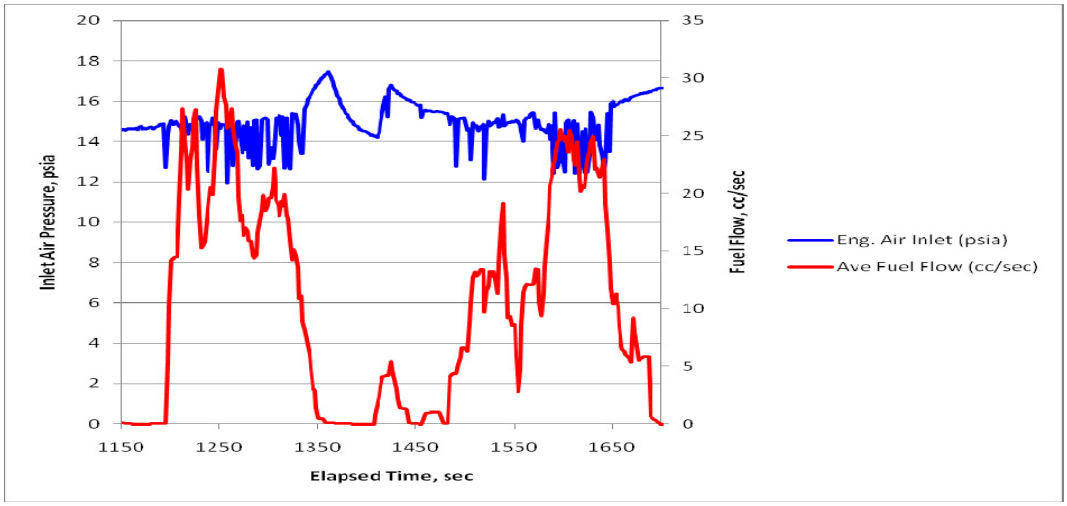

Figure 46: Fuel flow rate and inlet pressure versus elapsed time for test engine at 2000 rpm, WOT, and sea level conditions.

The second issue was the air flow meter which failed to produce reliable results for all of the initial engine tests. A significant amount of time was spent trouble shooting the cause of the problem and it was ultimately determined that an internal failure in the flow meter was the cause. The failure resulted in having to return the flow meter to the manufacturer for repair. No air flow rate data was collected due to this malfunction and as a result air to fuel ratio and delivery ratio's could not be calculated. It was expected that the data would show the delivery ratio decreases with engine speed. The decrease in delivery ratio is caused by the shorter time period of port opening due to higher piston

velocities. The decreased port open time leads to a higher percentage of the burned mass being trapped in the cylinder and also to higher short circuiting of the fresh charge.

After resolving the fuel flow meter issue and removing the inlet line to the test engine to resolve the inlet pressure issue sea level performance map tests were completed. The main reason for removing the inlet line was due to the ability to operate the engine reliably. Tuning of the carburetor and dynamometer controller settings were completed in order to achieve reliable engine operation across the range of engine speeds from 2000 to 8500 RPM. The throttle was set to 100%, 75%, 50%, and 25% open at each engine speed and data was collected for ten seconds. Each constant speed and throttle setting data point was averaged over the ten second sample to create a range of engine mean effective pressures and specific fuel consumption rates. The data was then put in matrix format and used in a Matlab code which interpolated between the data points to create Figure 47.

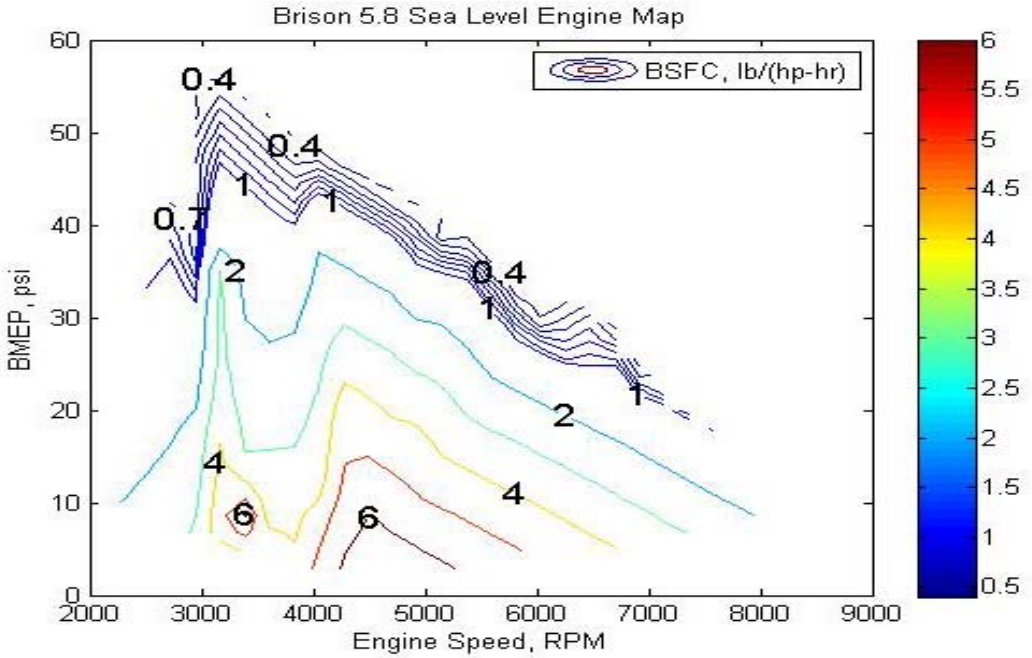

Figure 47: Sea level Brison 5.8 cubic inch performance map.

Engine power and torque for sea level conditions follow the expected trends. Figure 49 shows engine torque versus engine speed for sea level conditions. The peak torque for the Brison 5.8 occurs at 4000 RPM while peak power, shown in Figure 48, occurs at 6500 RPM. Additional testing is needed at smaller engine speed increments to determine the exact speeds for which peak power and peak torque occur. The large drop in power output seen in Figure 48 for 25% throttle conditions is due to equivalence ratio. The Brison 5.8 carburetor was seen to work well at medium to high throttle conditions but did not perform well under low throttle settings. The carburetor was not able to meter the correct amount of fuel for the lower air demand causing the engine to operate poorly.

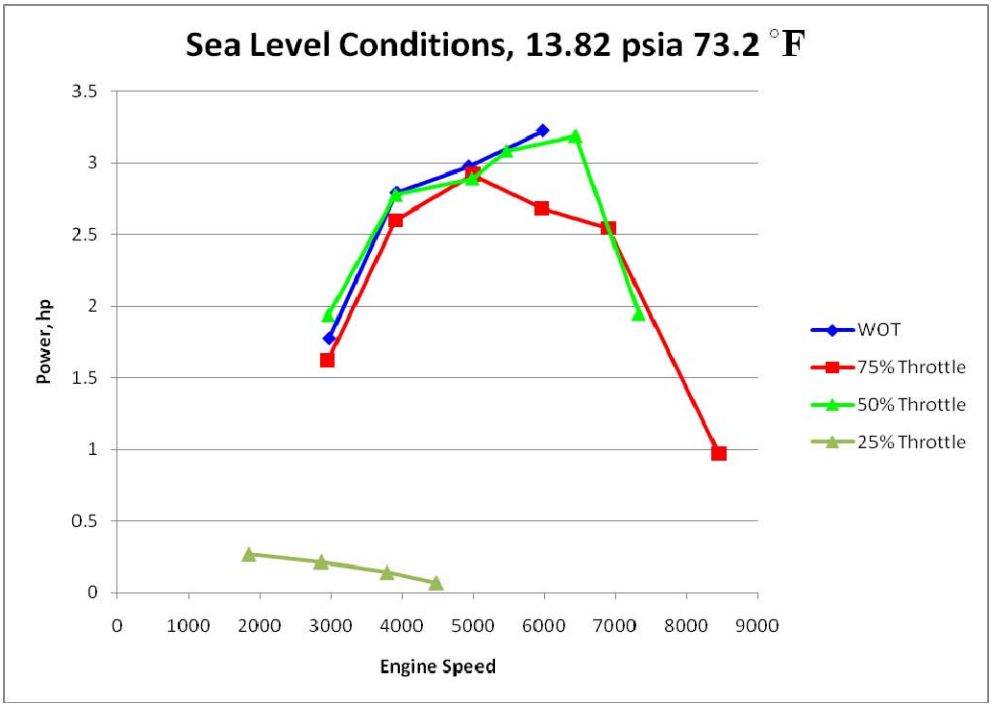

Figure 48: Engine power versus engine speed at sea level conditions.

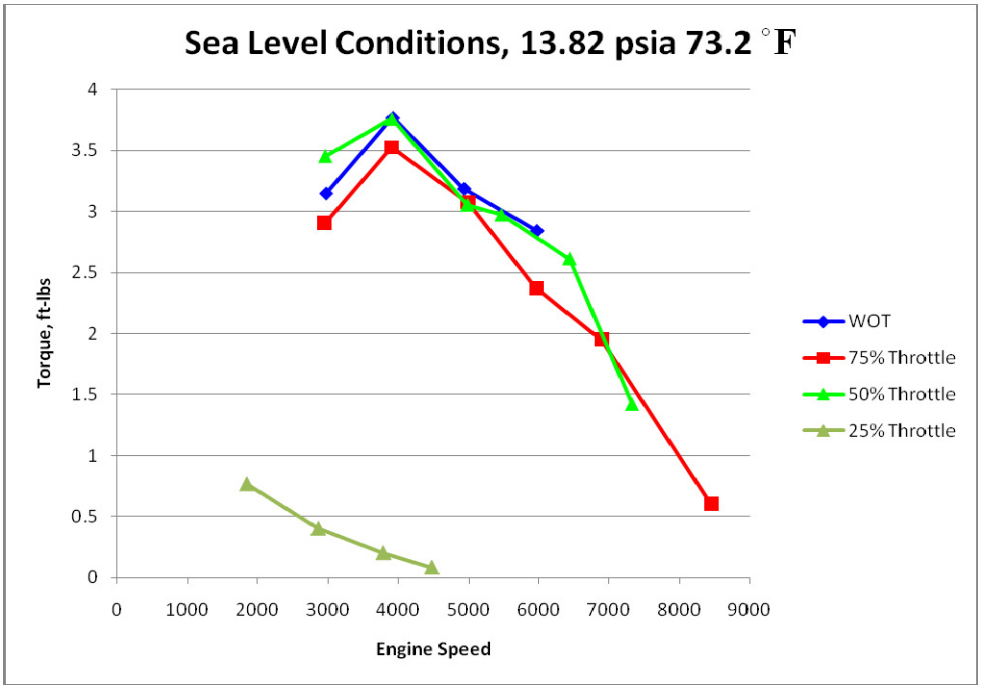

Figure 49: Engine torque versus engine speed at sea level.

Engine performance testing under lower pressure conditions was accomplished to determine the impact that inlet pressure has on engine performance. The lower pressure tests were performed with the inlet line disconnected from the engine for the reasons stated previously. The test was performed by running the test engine at a fixed throttle position and speed while reducing the inlet pressure. This test was repeated at for two speeds and three throttle positions. The first test was run at 3500 RPM and is shown in Figure 50 where the throttle position was set at WOT and 75% throttle. The inlet pressure was varied from 13.982 psia to 13.865 psia for the WOT setting and 13.865 psia to 13.455 psia for the 75% throttle setting. Figure 50 shows that for a 0.84% decrease in inlet pressure at WOT the result is a 14.2% decrease in both power and torque. Figure 50 also shows that at 75% throttle a 2.96% decrease in inlet pressure results in a ~54% decrease in power and torque. Similar results are seen in Figure 51 with the engine set at 3000 RPM where the throttle positions were set at WOT and 25%. At 3000 RPM and

WOT a 7.97% decrease in inlet pressure resulted in a 25% decrease in power and torque while at 25% throttle a 14.6% decrease in pressure resulted in a 29% decrease in power and torque. These results compare well with past research and show that inlet pressure will have a significant impact on engine performance.

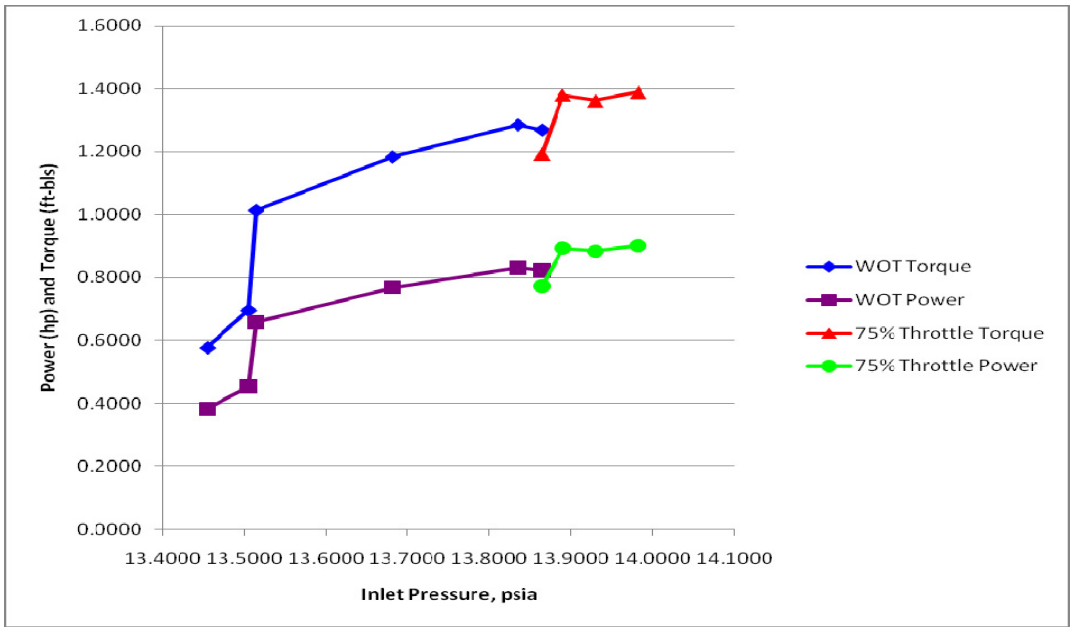

Figure 50: Engine power and torque versus inlet pressure at 3500 RPM.

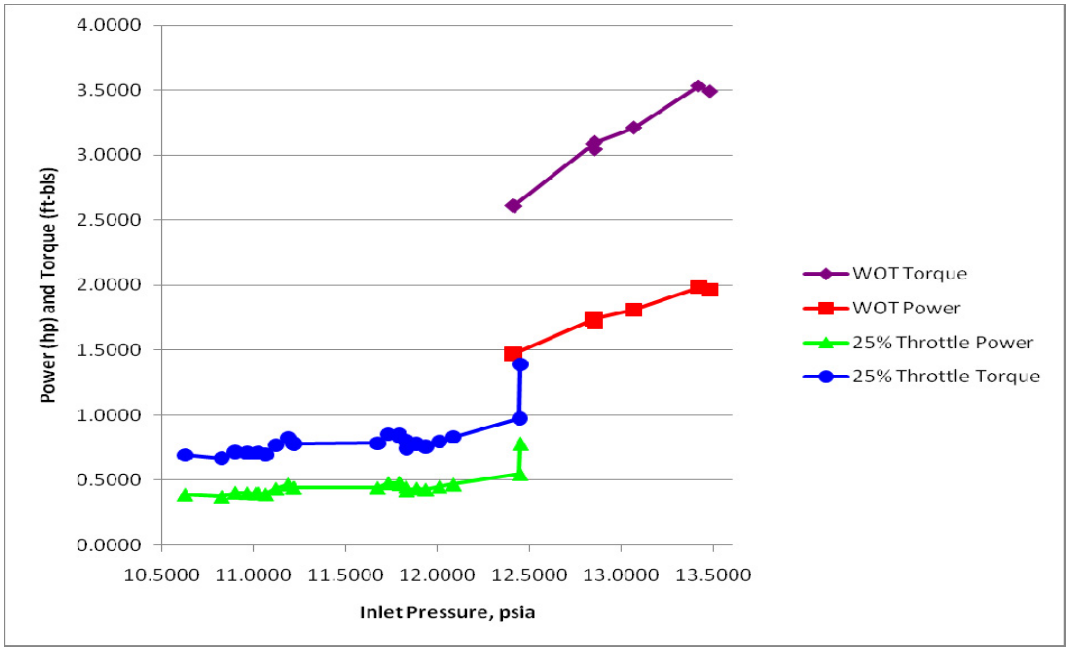

Figure 51: Engine power and torque versus inlet pressure at 3000 RPM.

Due to the issues related to the inlet line tests could not be conducted at lower temperatures. The power and torque decrease shown from the lower pressure tests may be offset by a slight increase in power and torque associated with lower inlet temperatures. The full impact of engine performance due to environmental conditions will not be known until the engine is tested under these coupled environmental conditions. The intended cylinder pressure data used to detect knocking combustion and peak pressure timing was not available. The Kistler spark plug pressure sensor ordered in December of 2010 did not arrive and was not incorporate into the test stand. The data collected by this sensor may have lead to additional insight into the decease of power and torque due to reduced inlet pressures.

IV.2.3 Carburetor Experiments

One of the secondary goals of this research was to determine the impact of carburetor tuning on engine performance. In order to get repeatable results for these tests two mark were placed on the carburetor body at 180° apart for each needle while the needle was at the full in position. The test was set up by setting the high and low speed needles to ¾ turns out from the full in position. The engine would then be run at wide open throttle over the range of engine speeds from 2000 to 8000 RPM in 2000 RPM increments. This data would be used as a baseline for comparing engine performance at other needle settings. The high speed needle would then be turned 0.5 and 1.0 turns out from the baseline position and the test repeated over the range of engine speeds. To determine the impact of carburetor setting with altitude the set of tests would be repeated at 1500 m and 3000 m simulated conditions. For all test point's raw data would be collected on engine speed, torque, pressure, temperature, fuel flow rate, and air flow rate.

The stock timing box should be used for all tests and timing signals recorded. Data should be averaged at each test point for 10 time samples. Plotting of power versus engine speed at the baseline, 0.5 turns, and 1.0 turns can be used to compare how increasing the richness of the mixture impacts engine performance. Similar plots for BSFC versus engine speed, torque versus engine speed, and $BMEP_{max}$ versus engine speed for the different mixture settings and altitudes are also useful in determining the impact on engine performance and how incorrect engine tuning can change performance as the engine increases in altitude.

IV.2.4 Carburetor Tests

Specific tests were not accomplished to understand how the carburetor setting impacts engine performance as the inlet altitude condition changed. Some observations of carburetor settings can be made based upon the engine load testing that was performed. The test engine was very sensitive to the air to fuel ratio in the cylinder and slight changes caused by increasing or decreasing the inlet air pressure caused poor engine performance. In most cases if the inlet air mass flow was restricted the engine would flood with fuel and cease to operate. During conditions where the inlet pressure was allowed to rise quickly the carburetor was unable to keep up and the engine would end up in a condition where almost no fuel was entering the cylinder. This fuel lean condition caused the engine to stop running. It was observed that the engine would continue to operate under fuel lean conditions much more readily than under fuel rich conditions. Fuel rich conditions caused by low inlet pressures lead to almost instantaneous engine operational failure, while fuel lean conditions would slowly lead to misfires and ultimately engine failure.

V. Conclusions and Recommendations

V.1 Conclusions

The goal of the research was to design and build a mobile test facility capable of test small internal combustion engines under 10 hp in size. The facility was tested and proved capable of reaching pressure and temperature conditions representative of atmospheric conditions seen at 10000 ft. A representative test engine was tested in the mobile test stand and performance data was collected under sea level conditions. Initial data showed the impact of inlet pressure on the power, torque, and fuel flow rates of a two stroke spark ignition crank case scavenged engine. The primary goal of designing, building, and testing a mobile test facility for small internal combustion engine performance testing was partially accomplished. The primary limitation of the test stand is the ability to operate the engine under low temperature conditions resulting from poor inlet line design

The secondary goal of testing a representative IC engine to gather performance information was also partial completed. A seal level performance map was created and will give a baseline for future testing. The testing process resulted in a better understanding of the issues involved in operating the altitude test stand. The solution to many of the issues encountered during the testing process were presented. Additionally test methodologies were presented for completing engine performance maps at simulated altitude conditions. Methodologies for investigating carburetor impacts on engine performance as a function of engine speed and altitude were also presented.

The tertiary goal of testing engine to engine performance variations was not completed during this research. Engine to engine performance variations may play a key role in system operation along with carburetor tuning. Results from several identical engines over a range of speed, throttle, and altitude conditions should be compared in order to determine acceptable correlations of engine performance as a function of altitude.

V.2 Recommendations

There are many recommendations that could be made regarding the mobile test capability developed as the major goal for this research. The mobile test stand was only partially successful in attaining the design goals set forth by AFRL/RZTC. In order to make the most use of the developed capability some additional functionality should be added to the test stand. The first step would be to use the facility to take performance data at simulated altitude conditions on the Brison 5.8 test engine as originally intended. The creation of performance maps at 1500 m and 3000 m would allow AFRL to better understand the impact that environmental changes have on the performance of a stock engine. In order to make it easier to operate the test stand the following steps should be taken:

1. Resolve the shaft seal, top window gasket, and exit nozzle interface seal leakage in order to reach and sustain pressure conditions more easily.
2. Methodically test manual bypass, and main control valve position settings as a function of compressor speed to determine where the over current limit is and plot it on the compressor map.

3. Add an actuated isolation valve to LN_2 system in order to quickly shut off the coolant supply in the event of an emergency or when the compressor abruptly stops.
4. Design and fabricate a coupling alignment system to quickly and accurately measure coupling parallel, axial, and angular misalignments.
5. Resolve the inlet line pressure oscillation issue to allow the engine to operate at lower pressure and temperature conditions.

By undertaking these tasks the mobile test stand would have the ability to quickly set up tests and the operator would have a better idea of how to achieve desired conditions quickly and safely. In order to test future engine design modifications that allow small IC engines to operate above 3000 m the test stands capability limits need to be expanded upon. The lower temperature limit is easily reduced with the addition of higher coolant flow rates. The lower pressure limit may be reduced by addressing items number one and two above. By carefully avoiding the current limit and reducing the amount of air leaking into the chamber lower pressures should be possible. In order to test higher temperatures than those shown in Figure 43 the addition of electric heaters on the main coolant flow path would be needed. The engine flow path should utilize the current counter flow heat exchanger by flowing warm fluid through the current LN_2 side. This has two benefits, it removes the need to add additional heaters to the line and it requires no additional wiring or plumbing.

After the baseline and altitude performance maps are complete there are several additional areas of research that would lead to a better understanding of small internal combustion engines. The use of carburetors has been common in internal combustion

engines of all sizes for many years. In recent year's advancements in manufacturing and digital electronics has lead to smaller fuel injectors and engine control systems. Investigating the impact of carburetor settings at a variety of flight conditions would enable future researchers to determine what if any performance improvements are made with the addition of new technologies. The impact manufacturing tolerances on the stock carburetor and engine performance should be researched. The variability of engine performance for identical engines from a single manufacturer is an important figure of merit for the acquisitions and design communities. If there is a large variability in engine performance than the designers of future systems must account for the lowest common denominator. This leads to many systems having significant inefficiencies due simply to the fact that they have more capability than they were designed for.

Research specifically tailored to two stroke engines includes determining an appropriate pegging method for the in cylinder pressure measurements, determining trapping efficiencies, and investigating the impact of intake and exhaust geometry on engine performance. Many of the pegging methods described in chapter II focused on four stroke engines without any type of scavenging. For the test engine presented in this research the fresh fuel and air charge is pre-compressed in the crankcase prior to entering the cylinder. This pre-compression is done in order to increase the inlet pressure helping to force the burned gases out of the cylinder prior to port closing. Pre-compression also increases the enthalpy of the fuel air mixture just prior to injection into the cylinder making it easier to ignite the mixture. The increase pressure and temperature caused by the pre-compression may aid in mixing. The impact of this type of scavenging on engine performance at increasing altitude conditions is of interest. If scavenging efficiencies

increase with altitude then two stroke engines may be a better option even though their fuel consumption is greater than similar four stroke engines.

Two stroke engines use a mixture of fuel and oil and the ratio and type of oil may have an impact on engine performance. The heating value and thus the available energy in the fuel and oil mixture are a function of the fuel and oil types as well as the volumetric or mass ratio of the mix. Tests designed to measure the impact of fuel and oil mixture ratio would be useful in determining the best mixture ratio for specific fuel and oil combinations. It would of interest to test if the fuel to oil mixture ratio is specific to each engine design.

With the mandate for a single fuel supply chain within the DoD it is of great importance to test the impact of using heavy fuels in two stroke engines. Heavy fuels have very different qualities than the standard high octane fuels used in most small two stroke IC engines. Additionally the impact of heavy fuels on engine performance at different altitudes is also crucial for the development of small IC engines capable of running on heavy low octane fuels over a wide range of environmental conditions. These engines will power new man portable UAS's and it is vital to understand how they will perform.

V.3 Future Work

The mobile altitude chamber functioned well during the current test program. In the future automation of the test stand is desired in order to remotely operate the stand from the control room. In order to operate the stand remotely, actuators must be added to all of the manual valves including the two coolant valves, and the main engine cooling flow bypass valve. The addition of PID control loops for the control valve actuators

would be useful in preventing compressor surge or over current conditions. PID control loops would also prevent engine cutout due to inappropriate fuel to air ratio conditions caused by restricting the air flow once the engine starts running. Upgrades to the chamber seals are necessary in order to reach higher pressure ratios as well as making it easier to open and close the chamber without worrying about the lid seals. A more robust and accurate system for aligning the engine and dynamometer couplings is also desired. The addition of an oil cooling system is needed to allow the compressor to operate for sustained periods of time. The last improvement to the test stand would be to allow connection of the fuel system to the test bay fuel distribution system. This upgrade would allow for the testing of multiple fuels without having to empty the fuel tank. Connecting to the facility fuel system would require the addition of a separate oiling system for the mixing of fuel and oil in the proper ratio for two stroke engine operation. The fuel and oil mixing control should be capable of adjustable mixture settings from zero mixing up to about 30:1 mixing ratios in order to operate a wide range of small internal combustion engines. The impact of oil addition to the fuel should be studied in order to quantify the effect that the fuel oil mixture has on engine performance.

Other future work includes continuing to take a larger number of data points to enhance the resolution of the engine performance maps for the Brison 5.8. The stock timing box should be investigated in more detail to determine if an upgrade is needed to reach maximum cylinder pressure at the desired crank angle degree. An investigation of the intake and exhaust system should be conducted to see if tuning the intake and exhaust legs would lead to increases in power and torque and decreases in BSFC. Work by other

researchers has indicated that fuel injection technologies may lead to decreases in BSFC without significantly impacting engine power or engine torque.

Testing of carburetor tuning impacts is an important step that is needed to baseline engine performance. This baseline can then be used to determine the impact of using a fuel injector in the test engine. Implementing fuel injectors into the Brison 5.8 will be a challenge due to the two stroke crankcase scavenged operation of the engine but may lead to a more consistent fuel and air mixture on a cycle to cycle basis. Carburetor tuning impacts should be investigated to determine how slight adjustments in the needle valve settings impact performance at a constant altitude. The impact of carburetor tuning on engine performance based on a fixed needle valve setting over a range of altitude conditions should also be determined. The variability of engine performance based on carburetor tuning is an important design consideration for UAS systems that must be operated in austere conditions with limited tools and limited time.

The Brison 5.8 should be tested to determine how much variability occurs between identical engines by testing multiple Brison 5.8 engines under the same throttle and speed conditions. Engine to engine performance variation is an important design consideration for the DoD as a large number of engines would be needed to power a single type of UAS. UAS system and mission design must account for the lowest average performance of an engine.

Appendix A: Heat Transfer Calculations

The evaluation of the Exergy LLC model 0670 heat exchanger began with the physical dimensions of the heat exchanger. The inner tube diameter is 0.435 inches and the outer tube diameter is 0.935 inches. The calculation of the area required to transfer the correct amount of heat starts by assuming that the temperature of the coolant exiting the heat exchanger is equal to the coldest temperature needed for the inlet combustion air or 216 K. The log mean temperature can be calculated using Eq. (36)

$$\Delta T_{lm} = \frac{\left(T_{hi} - T_{co}\right) - \left(T_{ho} - T_{ci}\right)}{\ln\left(\frac{T_{hi} - T_{co}}{T_{ho} - T_{ci}}\right)} \tag{36}$$

where T_{hi} is assumed to be 300 K, and T_{ho} is required to be 216 K for the coldest condition. The coolant inlet temperature, T_{ci}, is equal to 77 K. This leads to a log mean temperature of

$$\Delta T_{lm} = \frac{\left(300 - 216\right) - \left(216 - 77\right)}{\ln\left(\frac{300 - 216}{216 - 77}\right)} = 109.2013$$

The next step is to determine the Reynolds number, Eqs (37) & (38), and the Prandtl number for both of the flows. The Prandtl number for air at the average temperature is 0.72 and the Prandtl number for nitrogen at the average temperature is 0.768.

$$\mathrm{Re}_{air} = \frac{4\dot{m}_{air}}{\pi D_i \mu_{air}} \tag{37}$$

$$\mathrm{Re}_{air} = \frac{4\left(0.01 kg/s\right)}{\pi\left(0.011 m\right)\left(159.6 x 10^{-7}\, N - s/m^2\right)} = 72202.8$$

$$\mathrm{Re}_{N2} = \frac{4\dot{m}_{N2}}{\pi(D_o + D_i)\mu_{N2}} \tag{38}$$

$$\mathrm{Re}_{air} = \frac{4(0.006kg/s)}{\pi(0.02375m + 0.011m)(68.8x10^{-7}\,N - s/m^2)} = 31909.4$$

Since both of the Reynolds numbers are well above the transition point for flow thru a duct it is assumed that the flow is fully turbulent and the correlation from Reference 39 can be used to calculate the Nusselt number as Eq. (39)

$$Nu_D = 0.023\,\mathrm{Re}^{4/5}\,\mathrm{Pr}^n \qquad n = 0.4\ Heating,\ n = 0.3\ Cooling \tag{39}$$

$$Nu_{Dair} = 0.023(72202.8)^{4/5}(0.72)^{0.3} = 160.61$$
$$Nu_{DN2} = 0.023(31909.4)^{4/5}(0.768)^{0.4} = 82.99$$

Using the standard relation for the convective heat transfer coefficient given by Eq. (40) the overall heat transfer coefficient, U, can be calculated by Eq. (41). The area required can be calculated by using Eq. (42).

$$h = Nu_D \frac{k}{D_h} \tag{40}$$

$$h_h = 160.61\frac{0.0223W/m - K}{0.011m} = 324.155W/m^2 - K$$
$$h_c = 82.99\frac{0.00958W/m - K}{0.0127m} = 62.60W/m^2 - K$$

$$U = \frac{1}{1/h_h + 1/h_c} \tag{41}$$

$$U = \frac{1}{1/324.155 + 1/62.60} = 52.47W/m^2 - K$$

$$A = \frac{Q}{U * \Delta T_{lm}} \tag{42}$$

$$A = \frac{500}{52.47 * 109.2} = 0.087m^2$$

Based on the above area and to provide some factor of additional capacity due to the fact that several somewhat questionable assumptions had to be made the 7 coil heat exchanger with an area of $0.19m^2$ allows for an area of slightly more than twice what is required. No attempt was made to account for the phase change that will occur in the nitrogen which will aid in the exchange of heat.

Appendix B: Flow Coefficient Calculations

The flow coefficient range for each of the two control valves was determined from the required flow rate based on engine demand and based on engine cooling requirements. In order to calculate the range of flow coefficients needed several assumptions were made concerning the conditions upstream of each valve. The inlet pressure for the small control valve was assumed to be 65 psig. The temperature was assumed to be 65 °F. The inlet pressure for the large control valve was assumed to be 14.7 psia and the inlet temperature was assumed to be 65 °F. The flow coefficients are calculated using Eq. (30) when the exit pressure is greater than 53% of the inlet pressure. This equation is valid for the large control valve based on the assumptions but does not hold true for the small control valve. The small control valve flow coefficient can be calculated with Eq. (43).

$$C_v = \frac{q\left[Sg\left(T_{amb} + 460\right)\right]^{1/2}}{\left[1360\left(P_{in} - P_{alt}\right)P_{alt}\right]^{1/2}} \tag{30}$$

$$C_v = \frac{q\left[Sg\left(T_{amb} + 460\right)\right]^{1/2}}{660 * P_{amb}} \tag{43}$$

The specific gravity was assumed to be close to one for all inlet conditions. The volumetric flow rates, *q* (ft^3/hr), in Eq. (30) were calculated based upon assumptions made in Appendix A for evaluation of the heat exchanger designs. The expected flow rates for the small control valve ranged from 200 to 840 SCFH. The expected flow rates for the large control valve ranged from 3780 to 10840 SCFH. Lastly the pressure range required down steam of the small control valve was needed in order to use Eq. (30). The design pressure ranged from 14.7 psia to approximately 7.35 psia. Using these equations

lead to a calculated flow coefficient range for the small control valve of 0.10 to 0.53 while the large control valve required a flow coefficient range of 0.5 to 54.0. Figure 52 shows that the small control valve should be operating between 15% open and 50% open for the flow rates expected during engine testing. Figure 53 shows that the large control valve should be operating between 15% open and 70% open based on the expected flow rates. In actual testing the large control valve operates between 50% open and 100% open in order to meet the mass flow demands of the compressor.

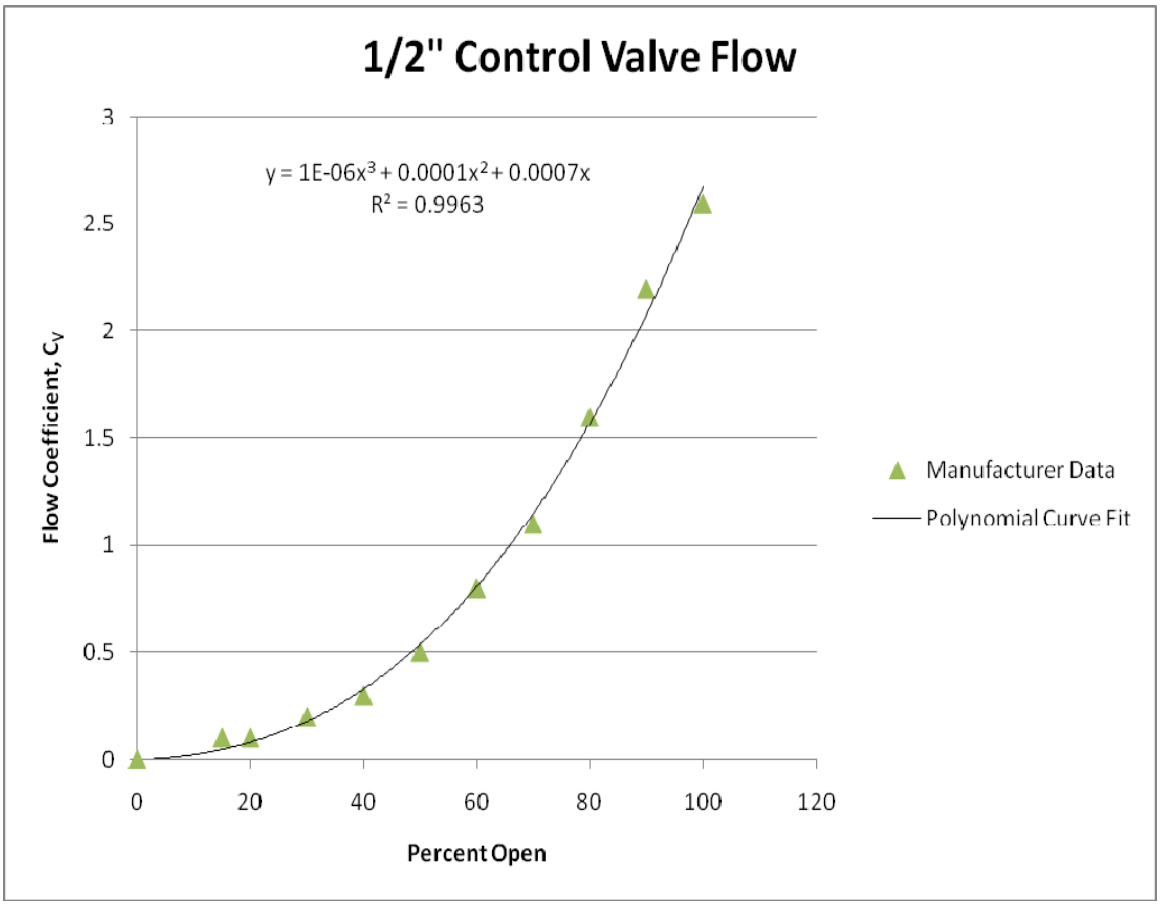

Figure 52: 0.5 inch Triac 30 degree vee port control valve flow coefficient versus percent open.

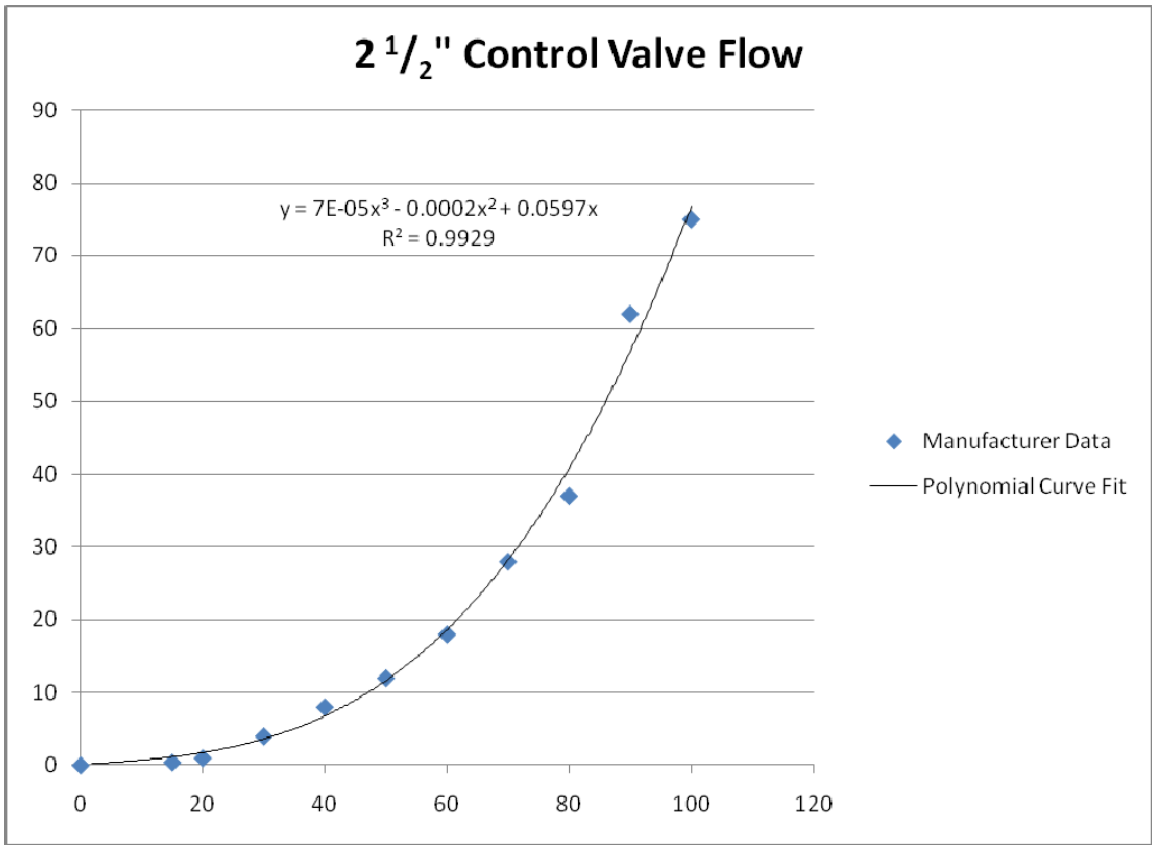

Figure 53: 2.5 inch Triac 30 degree vee port control valve flow coefficient versus percent open.

Table 9: Control Valve C_V versus on percent of valve opening (39).

	0%	15%	20%	30%	40%	50%	60%	70%	80%	90%	100%
0.5" Valve C_V	0	0.1	0.1	0.2	0.3	0.5	0.8	1.1	1.6	2.2	2.6
2.5" Valve C_V	0	0.4	1	4	8	12	18	28	37	62	75

Appendix C: Window and Wall Stress Calculation

Stress calculations were performed during the design phase in order to determine the required thickness of the chamber windows, the inlet and exit nozzles, and the chamber bottom surface. The stress calculations were based upon standard material properties for structural steel, 6061 aluminum, and polycarbonate (40, 41). The material properties used for the stress calculations are shown in Table 10. Each surface was considered to be in a held but not fixed configuration according to the definition in Reference 40.

Table 10: Material properties for aluminum, steel, and polycarbonate (40, 41).

	Yield Strength, MPa	Tensile Strength, MPa	Elastic Modulus, *E*, GPa	Allowable Design Stress*, MPa
Aluminum	270.00	310.00	70.00	67.50
A36 Steel	360.00	580.00	210.00	90.00
Polycarbonate[40]	55.16	65.50	2.24	13.79

*Based on a safety factor of 4 from the yield strength.

The first step in calculating the stress in the material is to determine the unsupported area that will be subjected to a differential pressure force. The upper poly carbonate window opening is 13.5 inches by 19 inches. The front polycarbonate view port has an opening 13.5 inches by 15 inches. The base of the box has two small unsupported areas that are 7 inches by 18 inches. Lastly the largest panel wall area for both the inlet and exit nozzles is approximated as 15 inches by 9 inches. This approximation was made to simplify the calculations for the inlet and exit which was constructed from trapezoid shaped pieces of differing sizes.

The next step in the process is to determine the maximum pressure differential, Δp, that will be generated across the unsupported regions. Based upon the design

assumptions a maximum pressure differential of 745 kPa is assumed to be the maximum for 15000 ft above sea level test runs. For conditions approximating 30000 ft the maximum pressure differential would be approximately 1114.5 kPa. Equation (44) was used to determine the displacement to thickness ratio. This ratio is then used to determine the stress in the center of the unsupported region, Eq. (45). The solution must be solved iteratively by varying the displacement to thickness ratio, Eq. (46) until the left hand side of Eq. (44) matches the right hand side of Eq. (44).

$$\frac{(\Delta p)a^4}{Et^4} = K_1\left(\frac{w}{t}\right) + K_2\left(\frac{w}{t}\right)^3 \tag{44}$$

$$S_{center} = E\left(\frac{t}{a}\right)^2\left[K_3\left(\frac{w}{t}\right) + K_4\left(\frac{w}{t}\right)^2\right] \tag{45}$$

$$\left(\frac{w}{t}\right)_{n+1} = \left(\frac{w}{t}\right)_n - \frac{K_1\left(\frac{w}{t}\right)_n + K_2\left(\frac{w}{t}\right)_n^3 - \frac{(\Delta p)a^4}{Et^4}}{3K_2\left(\frac{w}{t}\right)_n^2 + K_1} \tag{46}$$

The solution to the set of equations depends on the choice of material thickness, *t*. If the converged stress at the center, S_{center}, exceeds the design stress the material thickness must be increased and the process repeated. The constants, K_1 through K_4, are given in Table 11 for thin plate theory and are a function of the maximum dimension of the unsupported region, *b*, divided by the minimum dimension of the unsupported region, *a*. The subscript *n* in Eq. (46) denotes the current iteration and the variable *E* represents the elastic modulus of the material given in Table 10. The equation set given above was given in English units of psi and inches so all further calculations will be done in inches and pounds per square inch for consistency.

Table 11: Constants for stress equation based on *b/a* ratio(40).

b/a	K_1	K_2	K_3	K_4
1	22.5	30.5	6.5	2.7
1.1	18.9	27.6	6.3	2.7
1.2	16.2	25.7	6.1	2.7
1.3	14.3	24.6	5.9	2.7
1.4	13	23.7	5.9	2.7
1.5	11.9	23.1	5.8	2.7
1.6	11	22.7	5.7	2.7
1.8	9.8	22.2	5.6	2.7
2	9	22	5.5	2.7
3	7.5	21.4	5.3	2.7
∞	7	21.4	5.3	2.7

The solution to Eqs. (44), (45), and (46) for each of the given materials and dimensions is given in Table 12. While some of the materials have maximum stresses higher than the design stress at the higher differential pressure they are all well below the yield stress of the material. The only part that is still above the design stress at a differential pressure of 8 psi is the upper viewing window. This was accepted as a risk for two reasons. The first reason was that the window stress is only 1.4% above the design stress limit so the risk of breaking is very low. The second reason for accepting the risk was due to the cost of the material. The cost of ¾" thick polycarbonate was approximately $800 more than the cost of the ½" thick material for the same length and width.

Table 12: Solution to stress equations for each region.

Name	*Material*	*Dimension, b x a, in*	*Thickness, in*	*Max Displacement @ 11psi, in*	*Max Stress @ 11psi, psi*	*Max Stress @ 8psi, psi*
Upper Viewing Window	Polycarbonate	15 x 13.5	0.5000	0.307	2498.6	2028.6
Front Viewing Window	Polycarbonate	19 x 13.5	0.5000	0.358	2177.8	1723.6
Chamber Bottom	A36 Structural Steel	18 x 7	0.1875	0.015	9587.7	6952.3
Chamber Inlet and Exit	6061 Aluminum	15 x 9	0.2500	0.040	7548.9	5514.3

Appendix D: Raw Data

Figure 54: Inlet pressure and engine speed versus time for 16 February 2011 testing.

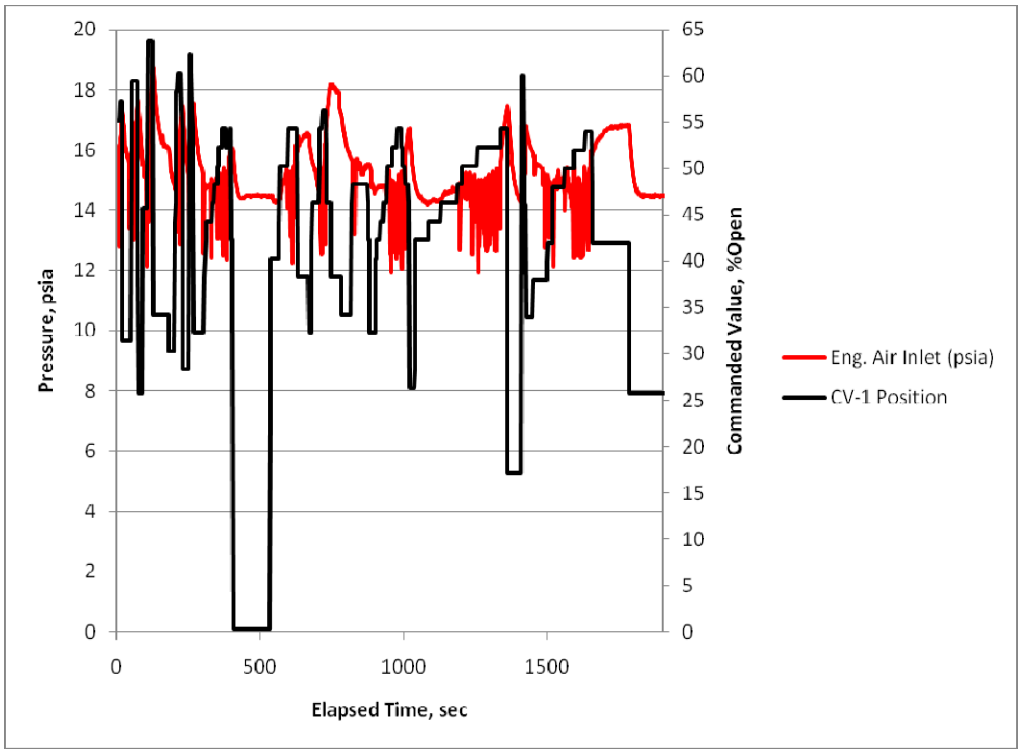

Figure 55: Inlet pressure and control valve position versus elapsed test time for 16 February 2011 testing.

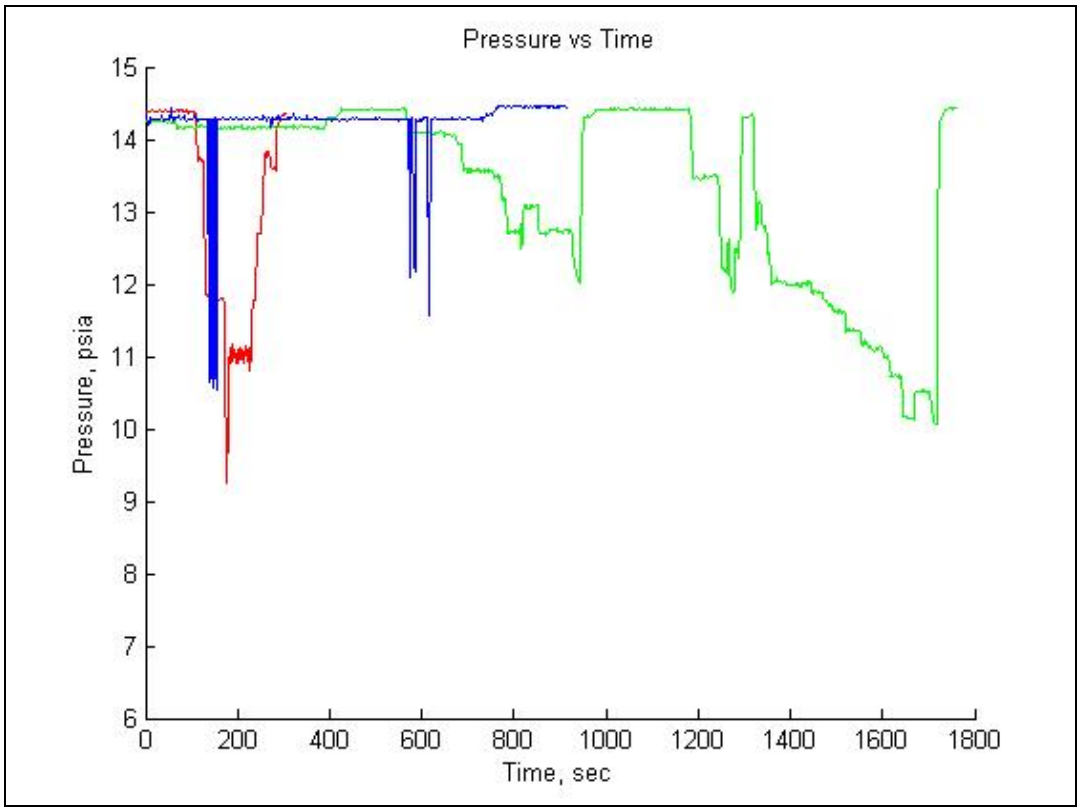

Figure 56: Chamber pressure versus elapsed time for three separate tests.

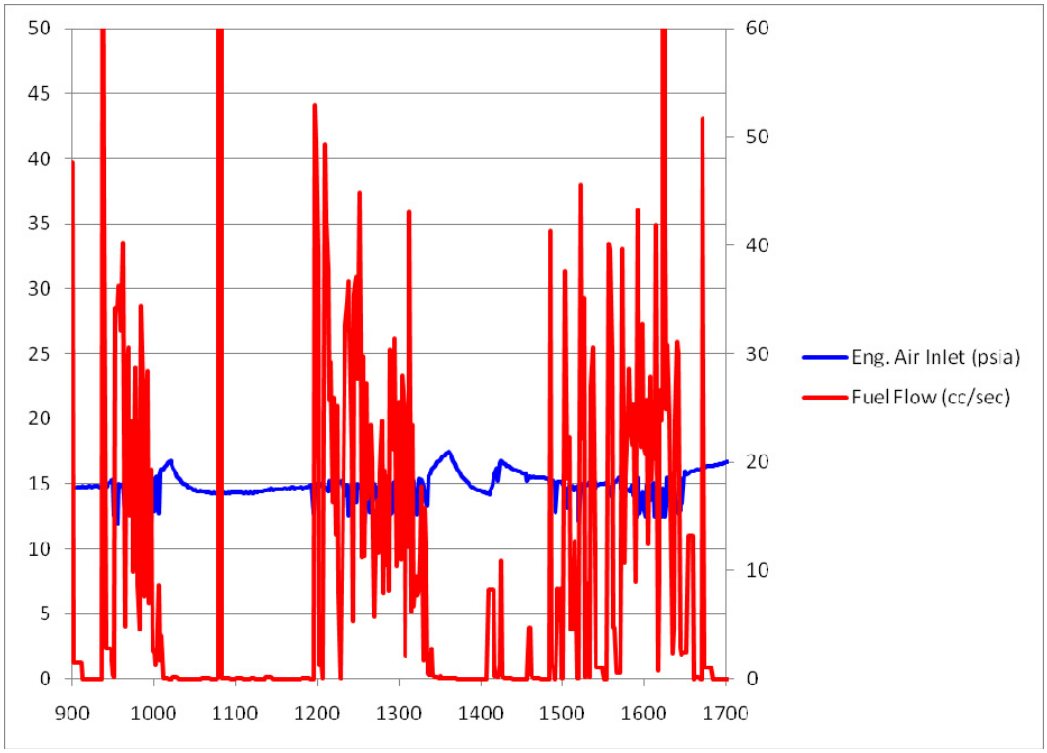

Figure 57: Inlet air pressure and fuel volumetric flow versus elapsed time.

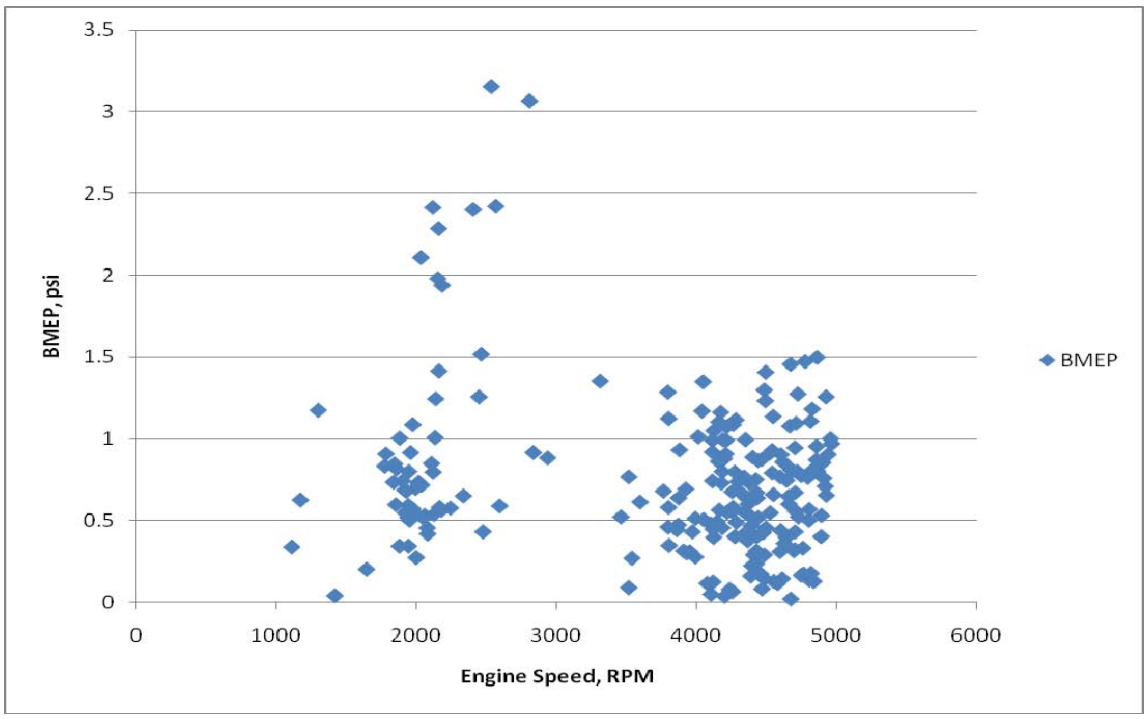

Figure 58: Brake mean effective pressure versus engine speed for test on 15 February 2011.

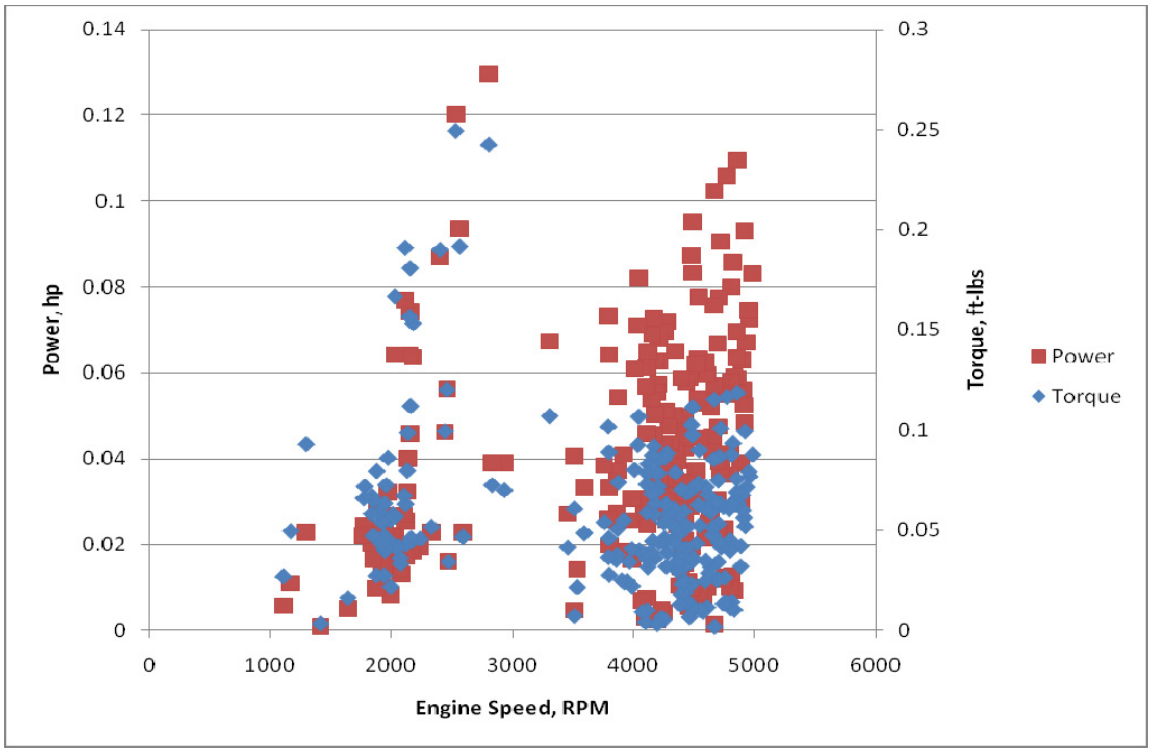

Figure 59: Power and Torque versus engine speed for 15 February 2011 test.

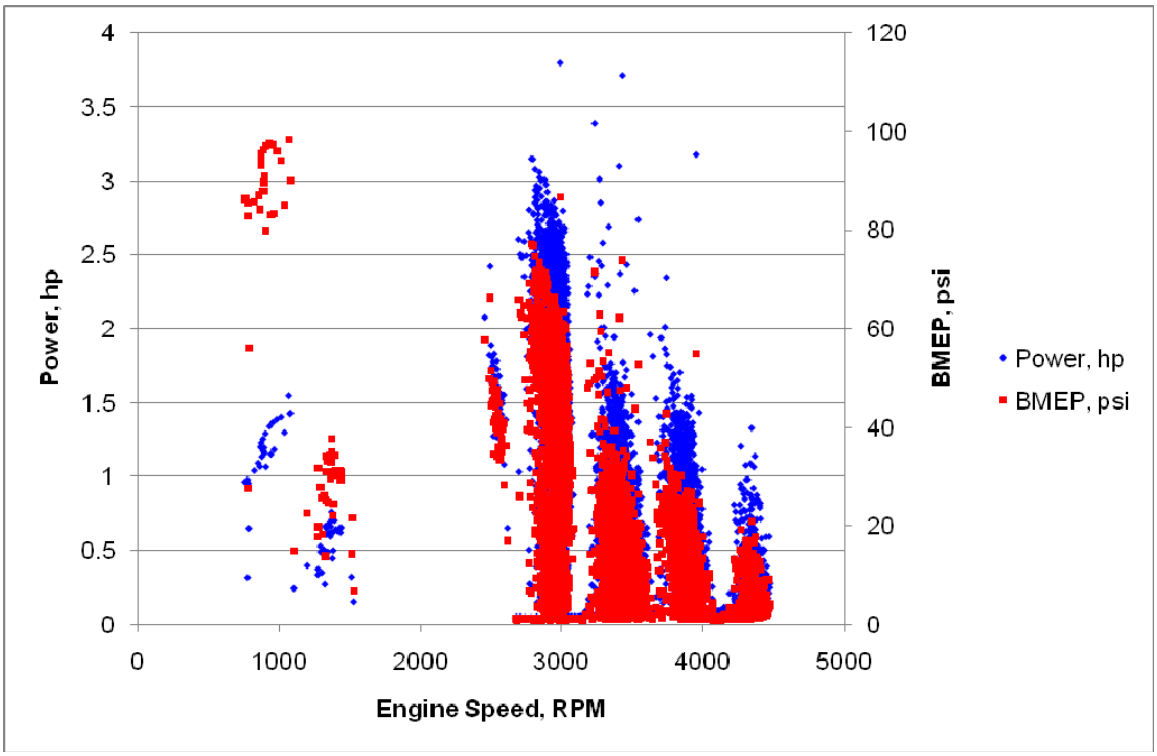

Figure 60: Power and BMEP versus engine speed for 25 February 2011 test.

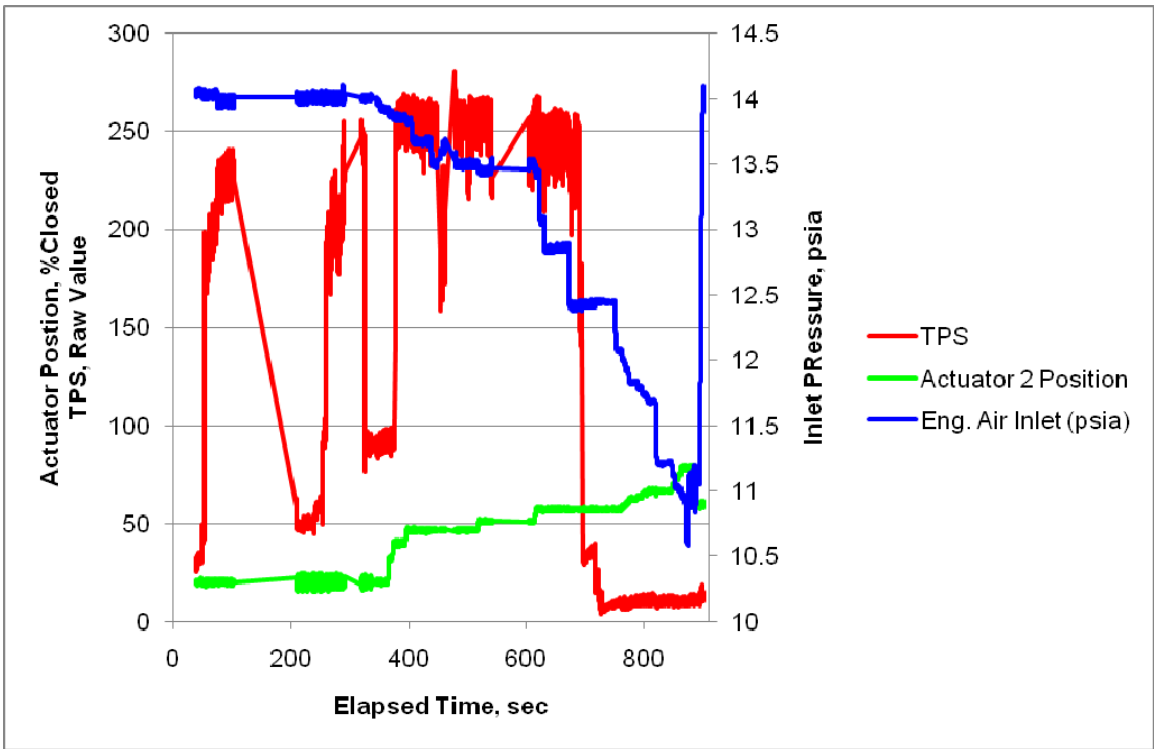

Figure 61: Throttle position sensor, control valve 2 position and inlet pressure versus elapsed time for 25 February 2011 test.

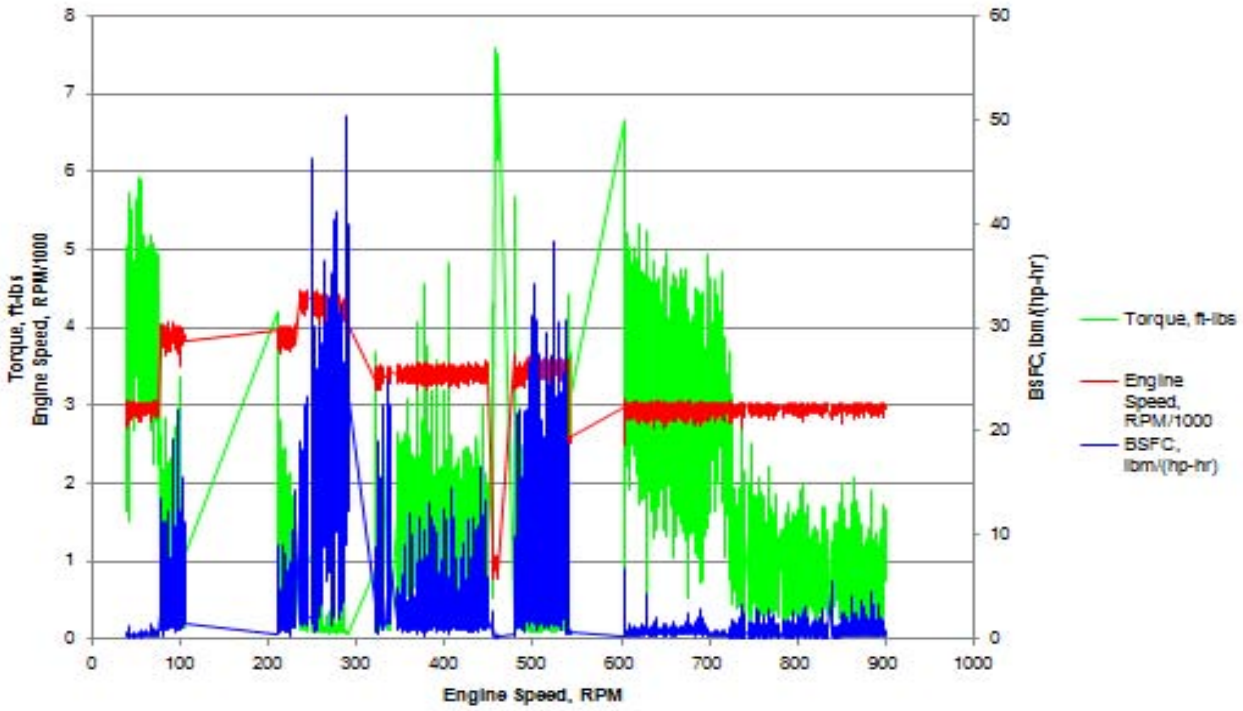

Figure 62: Torque, engine speed, and BSFC versus elapsed time for 25 February 2011 test.

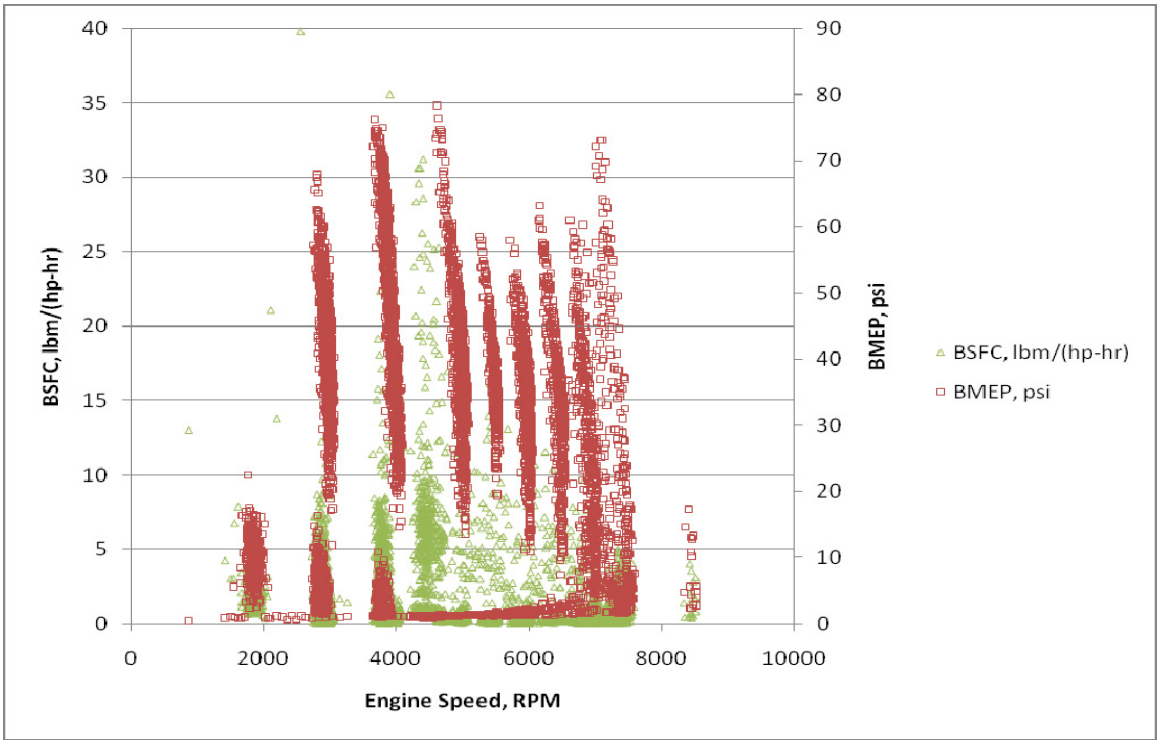

Figure 63: BMEP and BSFC versus engine speed for 28 February 2011 test.

Appendix E: Chamber Mechanical Drawings

The chamber was designed using the NX 7 CAD package from Siemens. The following are some of the drawings and models used to develop the overall chamber design and layout.

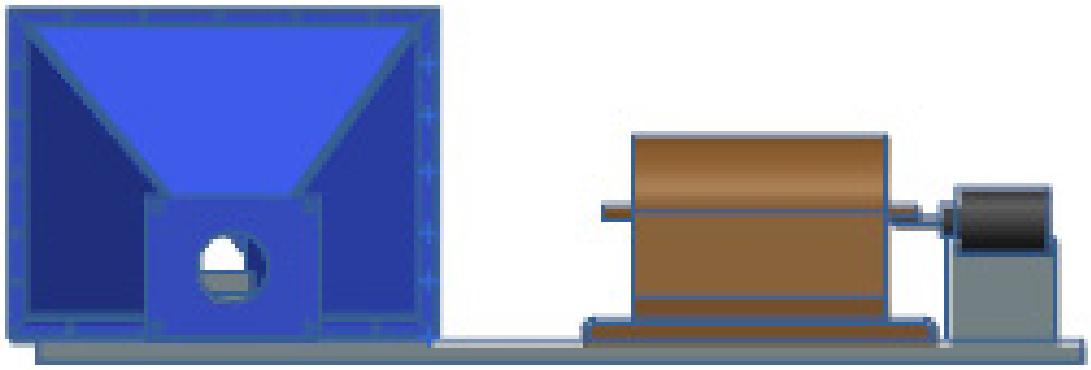

Figure 64: Side view of CAD model showing dynamometer, starter motor, base plate, and exit nozzle.

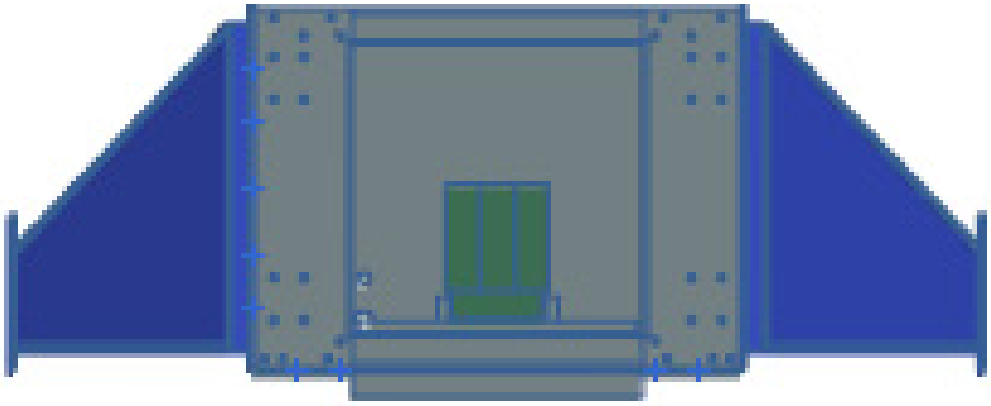

Figure 65: Front view of CAD model showing chamber, motor mount, base plate, entrance diffuser, and exit nozzle.

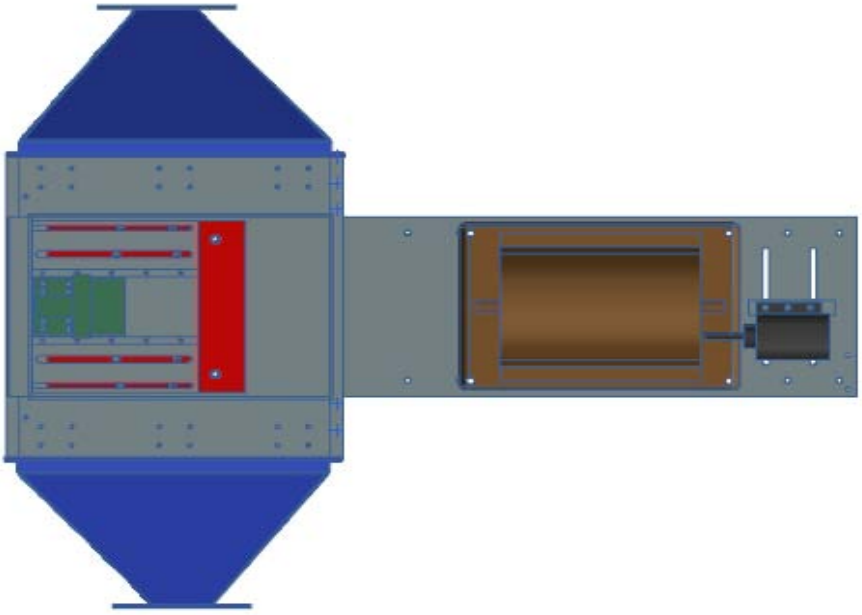

Figure 66: Top view of CAD model showing dynamometer, starter motor, base plate, motor mount, motor mount adjustment plate, entrance diffuser, and exit nozzle.

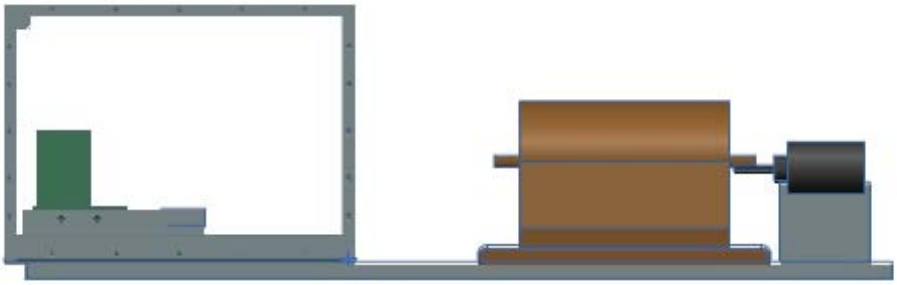

Figure 67: Side view of CAD model showing dynamometer, starter motor, base plate, chamber without inlet and exit diffusers, motor mount, and motor mount adjustment plate.

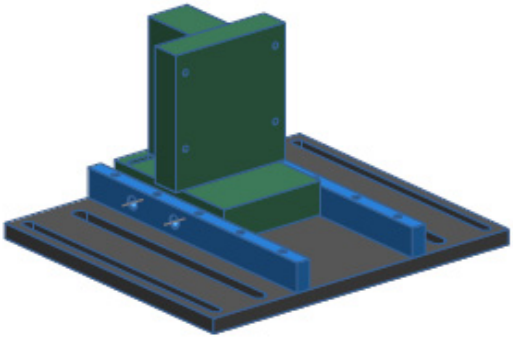

Figure 68: CAD model of motor mount and motor mount adjustment plate.

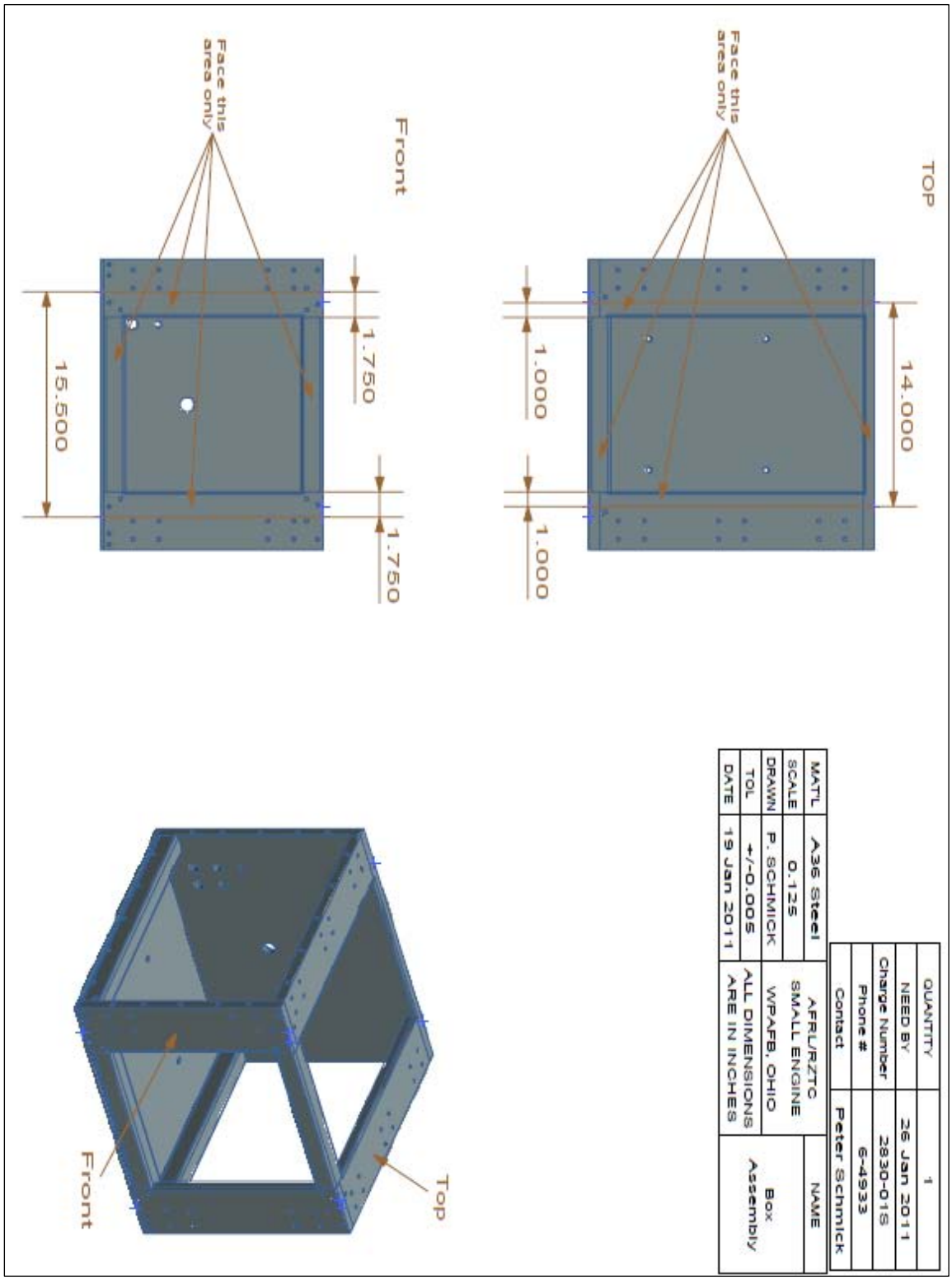

Figure 69: Machine shop drawing of assembled chamber with instructions to create level surface for top and front viewing windows.

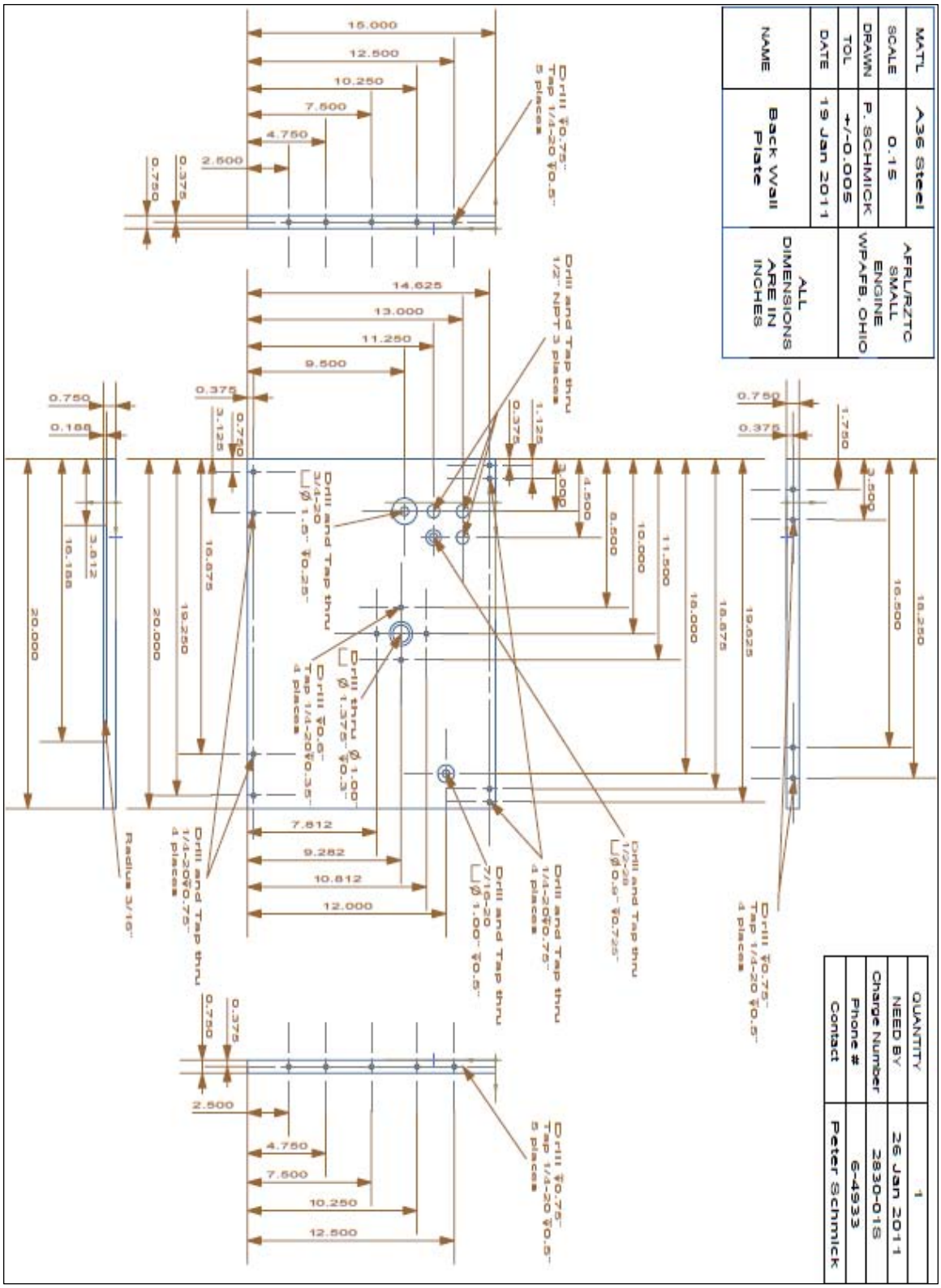

Figure 70: Machine shop drawing for creating the chamber rear wall.

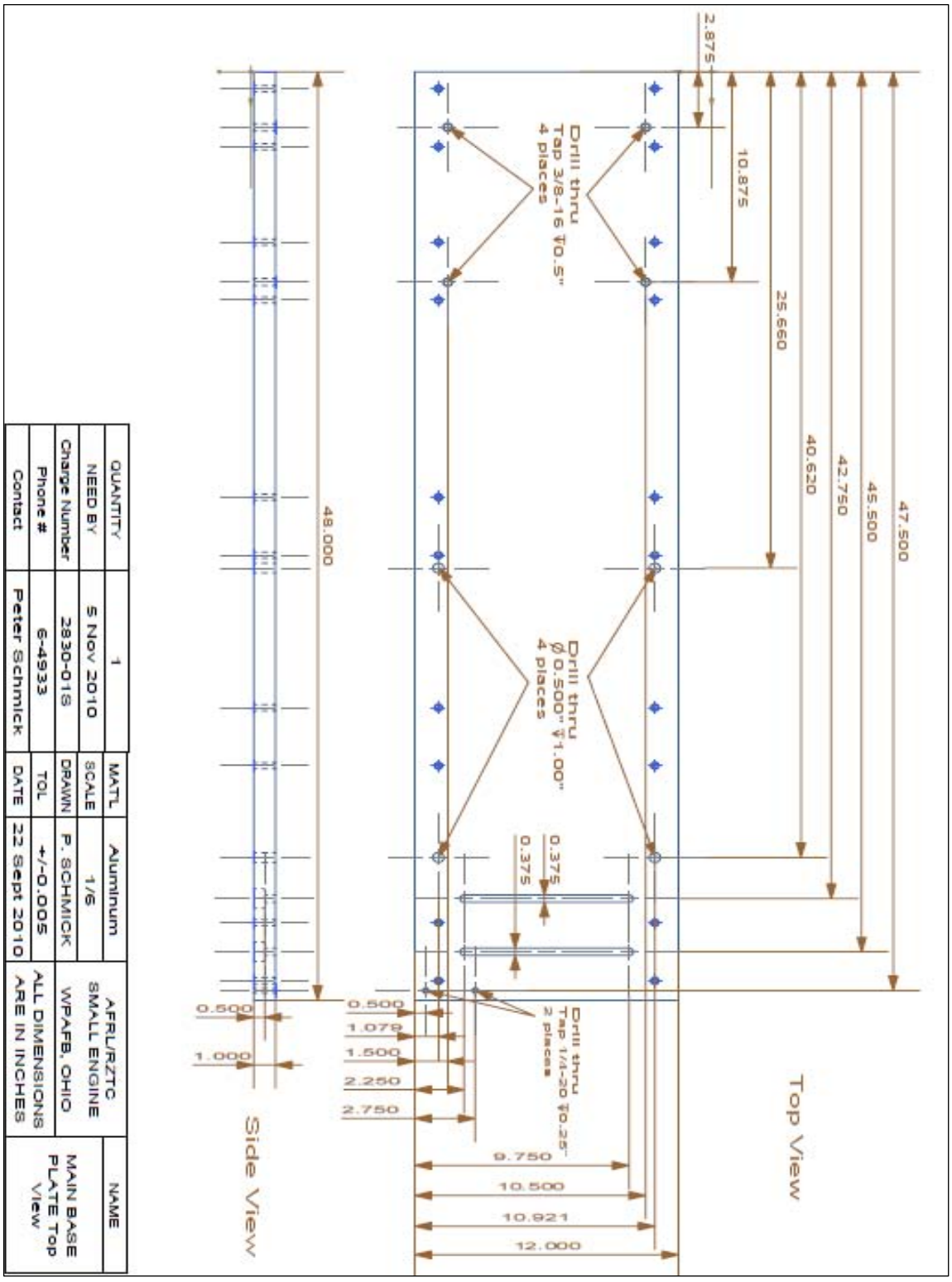

Figure 71: Machine shop drawing for fabrication of main base plate.

Appendix F: Parts List

Table 13: Parts List for Mobile Test Stand

Ref #	Item	Qty	Status	Contact	Part Number	S/N	Price	Notes
1	Engine Starter Motor	1	Installed	Quick Start Automotive Electric	Kohler 5761N (2-2129-UT)	N/A	$99.99	starter motor run off 12v car battery
2	Starter Gear	1	Installed	Motion Systems Inc.	N/A	N/A	$160.00	3.5" diameter gear with 33 teeth and pitch of 10 with 14.5 deg pitch angle
3	Starter Relay	1	Installed	Unknown	N/A	N/A	$0.00	Found in Bldg 21.
4	Dynamometer and controller equipment	1	Installed	Paul Abbott 716-668-5555 ext. 161 Pabb@magtrol.com	2WB-65, DSP-6001, TSC 401, DES Power Supply	Dyno: 3000054 Power: 01153 Torque: 3000054 Controller: OH601155	$28,780.00	includes eddy current dyno sized for 12kW with max 30000rpm, excitation supply, torque/speed conditioner, programmable controller, and cords
5	Fuel Flow Meter	1	Installed	Max Machinery T707-433-2662 F707-433-1818 33A Healdsburg Ave, Healdsburg, CA 95448	213-311-000 flow meter, 294 transmitter, 181-294-060 cable assembly	Flow Meter: Transmitter:	$2,570.00	Flow Meter(213), tranmitter(294), calibration, chords
6	Test Engines	2	One installed, one in storage	Cimmaster Arthur Lueng 905-564-3099	Brison 5.8 engine	N/A	$1,540.00	
7	Thermocouples	12	Installed	Omega	KQSS-14U-6, KQSS-14E-6, KMQSS-062G-6	N/A	$359.00	Omega

Ref #	Item	Qty	Status	Contact	Part Number	S/N	Price	Notes
8	Charge Amplifier and Chassis	1	Installed	Simon Johnson, Kistler T248 489 1090 x 6030 F248 489 1280	5064B11 Amp, 2852A12 Chassis	Amp: 1910377 Chassis: 1931559	$3,910.00	Kistler charge amplifier with analog direct current voltage output of in cylinder PT signal and 19" rack mount chassis
9	Low Noise Cable and Pass Through	1	Installed	Simon Johnson, Kistler T248 489 1090 x 6030 F248 489 1280, Mouser	1601BSP2M, 523-21-3220	N/A	$76.16	Kistler low noise cable to connect in cylinder transducer through the chamber wall and into the charge amplifier
10	In cylinder PT	2	Waiting for Part	Simon Johnson, Kistler T248 489 1090 x 6030 F248 489 1280	6118BFD16Q0 2A41	N/A	$7,770.00	Kistler spark plug sensor
11	Pressure Transducers	7	Installed	Omega	PX409-030A5V	403607, 403809, 413900, 418686, 403595, 403599, 403598	$3,675.00	Omega 0-30 PSIA transducers
12	Pressure Transducer	1	Installed	Honeywell	060-3883-09TJA	1305129	$0.00	Honeywell 0-100 PSIA transducer
13	Throttle and Choke Servo	2	Installed	Polulu	6001HB	N/A	$25.90	
14	Servo Motor Controller	1	Installed	Polulu	mini-Maestro 12 channel USB servo controller	N/A	$32.44	Ability to control up to 12 servo motors, currently only using two channels for throttle and choke positioning
15	Throttle Position Sensor	1	Installed	Sensor Product Manager, CTS Automotive Products, T574-389-2890, F574-295-3580, sensors@ctscorp.com	CTS P/N: 521-99-015 Advanced P/N: EC3026	N/A	$26.09	CTS Corp provided samples but actual TPS was purchased from Advanced Auto

Ref #	Item	Qty	Status	Contact	Part Number	S/N	Price	Notes
16	Compressor	1	Installed	Vortron, Bob Endress, bendress@vortechsuperchargers.com	V-5 K-Trim Supercharger HD	55074	$3,645.95	Votron put together a complete package that included the compressor, the motor, the variable frequency drive, belts, pulleys, and tensioner.
17	Variable Frequency Motor Drive	1	Installed	Vortron, Bob Endress, bendress@vortechsuperchargers.com	Delta 25 hp VFD-F	185F43A6W021 0034	$2,049.50	
18	Compressor belts, tensioner, pulleys, etc.	1	Installed	Vortron, Bob Endress, bendress@vortechsuperchargers.com	N/A	N/A	$2,366.60	SC Mounting plate, Tensioner and hardware, 3.25 10 rib pulley upper, Pulley retainer, 12" Dia drive pulley and drive belt
19	Compressor Motor	1	Installed	Vortron, Bob Endress, bendress@vortechsuperchargers.com	Emerson Motor Company 20 hp Model AF18	R08 7446055-0038 M 0001	$1,545.23	
20	Small Heat Exchanger	1	Installed	Exergy, LLC Warr Mui 320 Endo Blvd., Garden City, NY 11530 T516-832-9300 F516-832-9304	00670-2	N/A	$1,760.00	Tube-in-Tube counter flow heat exchanger
21	Large Heat Exchanger	1	Not Ordered	Super Radiator Coils, Dr. Juin Yu	Coil Model 8x8-4R-38/60	N/A	$0.00	Not ordered based on design philosphy of using LN2 injection into main cooling flow, quoted price of $732.00
22	Manual Bypass Valve	1	Installed	Kenwood Fluid Controls LLC	TRIAC 90-F1-300/2R6S-AA	N/A	$1,960.00	3" full port ball valve for sea level flow

Ref #	Item	Qty	Status	Contact	Part Number	S/N	Price	Notes
23	0.5" Control Valve	1	Installed	Kenwood Fluid Controls LLC	TRIAC V9-FS-050/WEA2-XX-30	0105550-3-1-1	$2,369.00	
24	2.5" Control Valve	1	Installed	Kenwood Fluid Controls LLC	TRIAC V9-FS-250/WEB2-XX-30	0105550-16-1-1	$3,891.00	
25	Damping Chamber	1	Installed	Plastic Mart	B273	N/A	$189.00	Ordered with 1/2" FNPT fittings
26	Test Table	1	Installed	McMaster Carr			$0.00	Used Existing Equipment
27	Fuel Tank	1	Installed	Unknown	N/A	N/A	$0.00	Used Existing Equipment
28	Fuel Filter	1	Installed	Earl's Performance Plumbing	230206ERL	N/A	$0.00	Used Existing Equipment
29	Shaft Seal	2	Installed	American High Performance Seals	SB-40 Profile Rotary Seal - Perchachem 6235	N/A	$75.00	Seal originally designed to seal higher pressure liquids not gases
30	Electrical Pass Throughs	3	Installed	Conax Technologies	TG-24T(CU)-A12-G, TG-24(K)-A12-G	N/A	$1,410.00	Wire pas throughs have 12 wires each, Thermocouple pass through has 6 wire pairs
31	Air Flow Meter	1	Installed	Sierra Instruments, Glen Coblentz, 303-215-9160	Flow Meter: M100H-NR-15-O1/1-PV2-VI-C3 Power Supply: 100-T8F	137040	$2,609.00	Model M100H-NR-15-OV1-PV2-VI-C3, flow meter with 0-500slpm, 1/2"FNPT fitting, no digital readout, 24VDC power, analog output, 3' cable.

Ref #	Item	Qty	Status	Contact	Part Number	S/N	Price	Notes
32	Dynamometer Coupling	1	Installed	Applied Industrial Technologies, Rusty Auxier, P: (937) 276-5340 F : (937) 276-5419 Email: SC0107@APPLIED.COM	Lovejoy GS28/38 B hub 78204, Lovejoy GS28/38 B hub 79718, Lovejoy GS28SOX92Y ELLOW Spider	N/A	$268.56	Dyno side is Lovejoy GS28/38 B hub with 18mm Keyway and Clamping device, with Lovejoy GS28 spider 92 yellow, Shaft side is Lovejoy GS28/38 B hub with 3/4" keyway and Clamping device
33	Engine Coupling	1	Installed	Applied Industrial Technologies, Rusty Auxier, P: (937) 276-5340 F : (937) 276-5419 Email: SC0107@APPLIED.COM	Lovejoy GS28/38 B hub 79718, Lovejoy CJ28 A hub 90102, Lovejoy GS28SOX92Y ELLOW Spider	N/A	$293.60	Engine side is Lovejoy CJ28 A hub solid, with Lovejoy GS28 spider 92 yellow, Shaft side is Lovejoy GS28/38 B hub with 3/4" keyway and Clamping device, plus two extra spiders.
34	Shaft	1	Installed	McMaster Carr	8377T17	N/A	$54.76	3/4" diameter keyed shaft 24" long
35	Control Computer	1	Installed	Super Logics	SL-4U-CL-G41MX-HA	414000064	$1102.00	Ordered by Dave Burris of ISSI
36	Dynamometer Cooling System	N/A	Installed	N/A	N/A	N/A	$0.00	Water system fabricated from existing components
37	LN2 RV	2	Installed	McMaster Carr	49315K732	N/A	$117.12	75 psi set pressure.
38	LN2 Flex Lines	2	One installed, one in storage	Grainger	6MP53	N/A	$332.00	Tank to stand supply line.
39	LN2 Tank Dolly	N/A	Installed	Grainger	5WXG2	N/A	$1,151.00	

Ref #	Item	Qty	Status	Contact	Part Number	S/N	Price	Notes
40	Manual Isolation Valves	5	Installed	N/A	N/A	N/A	$0.00	Fuel flow meter three way valves, fuel tank isolation valve, water supply isolation valve, shop air supply isolation valve all pulled from existing equipment.
41	Steel	N/A	Arrived	Benjamin Steel, Daytona Mills	N/A	N/A	$525.92	Pieces used for chamber construction and motor mount
42	Engine Mount	1	Installed	Benjamin Steel	N/A	N/A	$0.00	Fabricated based on mount drawing from Cimmaster and advice from Wilson.
43	Aluminum	N/A	Arrived	Tri-State Aluminum, Daytona Mills	N/A	N/A	$365.20	Pieces for construction of base plate, motor mount base, chamber entrance and exit, and guards for starter motor and compressor belt.
44	Piping	N/A	Installed	Main Line Supply Company, McMaster Carr	N/A	N/A	$416.44	Piping used to fabricate the cooling flow inlet lines.
45	Window Material	1	Installed	McMaster Carr	8574K66	N/A	$142.06	1/2" thick polycarbonate window material.
46	Window Clamps	10	Installed	McMaster Carr	5147A74, 5147A45, 5004A76	N/A	$477.90	Hold down toggle clamps, larger feet and additional washers.
47	Power Distribution	N/A	Installed	McMaster Carr	7705K22, 9473T173, 9473T191, 9473T187, 9473T19, 9473T144, 9473T145	N/A	$269.13	DIN Rail terminal blocks, 115VAC power strip, DIN Rail grounding blocks.

Ref #	Item	Qty	Status	Contact	Part Number	S/N	Price	Notes
48	Power supplies	3	Installed	McMaster Carr	7009K71, 7010K58, 7009K73	N/A	$427.38	One 12VDC 2.5A power supply for most electronics, one 12VDC 8.5A power supply for oil pump, one 5VDC power supply for ignition and servos.
49	LN2 Supply Valves	2	Installed	Flow-Tite, Inc.	HPF51SS1GGL 15	N/A	$610.00	1/2" cyrogenic hand valves .
50	LN2 Supply Tank	2	In Use	Thanh Chu, Kimberly S Ehret, AFRL/Safety	Union Carbide PGS-45	044-004-U1, 044-009-AT2	$0.00	Older tanks with 200L capacity at 235 PSIG
51	Optical Compressor Speed Sensor	1	Not Ordered	Monarch Instruments	Model ROS-W	N/A	$0.00	This sensor has a speed rating of 1-250,000 RPM. This sensor is to detect shaft speed on the compressor.
52	Oil Cooler	1	Not Ordered	Derale	N/A	N/A	$0.00	For use on the compressor oil cooling system if temperature rise becomes a problem.
53	Air Supply Filter	1	Installed	McMaster Carr	4910K23, 5001K13, 4958K82	N/A	$100.22	Filter, regulator, and mounting bracket
54	Vibration Dampers	10	Installed	McMaster Carr	64875K9	N/A	$75.00	Vibration dampers for under the main base plate to isolate the chamber and dynamometer from the rest of the test stand.
55	Water Supply Filter	1	Installed	McMaster Carr	4448K36, 4422K61	N/A	$0.00	Used existing housing and filter element.
56	Oil Pump	1	Installed	Tilton	Model 40-524	05K20056	$0.00	Used Existing Equipment
57	Oil Supply Tank	1	Installed	Stef's Fabrication Specialists	N/A	N/A	$0.00	Used Existing Equipment
58	Oil Filter	1	Installed	N/A	Unknown	N/A	$0.00	Used Existing Equipment

Ref #	Item	Qty	Status	Contact	Part Number	S/N	Price	Notes
59	Pressure and Temperature Transducer Fittings	N/A	Installed	Swagelok, Cincinnati Valve and Fitting	Various	N/A	$1,068.40	Used existing components when possible
60	Fuel Valve Actuator Solenoids	2	Installed	Ingersoll Rand	A0059, 12VDC with 1/4" NPT fittings	N/A	$0.00	Used Existing Equipment
61	Fuel Valves and Actuators	2	Installed	Hoke	3-way hand valve with 1/4" NPT fittings	N/A	$0.00	Used Existing Equipment
62	Air Solenoid Valve	1	Installed	Ingersoll Rand	A0059, 12VDC with 1/4" NPT fittings	N/A	$0.00	Used Existing Equipment
63	Data Acquisition Chassis	1	Installed	National Instruments, Alex Stoermer, Alex.Stoermer@ni.com	Compact DAQ	150881A	$1099.00	8 slot chassis
64	Analog Input Module	1	Installed	National Instruments, Alex Stoermer, Alex.Stoermer@ni.com	NI 9205	N/A	$799.00	32 channel +/-10VDC analog input module
65	Analog Output Module	1	Installed	National Instruments, Alex Stoermer, Alex.Stoermer@ni.com	NI 9264	N/A	$900.00	16 channel +/- 10VDC analog output module
66	Thermocouple Module	1	Installed	National Instruments, Alex Stoermer, Alex.Stoermer@ni.com	NI 9213	N/A	$999.00	NI9213 16-channel thermocouple module

Ref #	Item	Qty	Status	Contact	Part Number	S/N	Price	Notes
67	Digital TTL Signal Module	1	Installed	National Instruments, Alex Stoermer, Alex.Stoermer@ni.com	NI 9401	N/A	$269.00	8 channel TTL Digital input/output module for flow meter signal
68	Solid State Relay Module	1	Installed	National Instruments, Alex Stoermer, Alex.Stoermer@ni.com	NI 9485	N/A	$319.00	High voltage +/- 60 VDC relay module
69	Analog Input Module	1	Installed	National Instruments, Alex Stoermer, Alex.Stoermer@ni.com	NI 9227	N/A	$ 999.00	NI9227, 4 channel universal analog input module for +/- 5 A rms
70	Battery	1	Installed	Advanced Auto	Autocraft Silver Battery, Group Size 58, 550 CCA, P/N 58-2	N/A	$86.99	
71	Compressor Cooling Oil	3	Installed	Auto Zone	Maxlife DEX-MERC ATF, VV322	N/A	$59.97	1 gal size, similar performance to fluid recommended by Vortron for compressor oil.
72	Window Gasket Material	2	Installed	McMaster Carr	95715K71, 95715K72	N/A	$164.42	Graphite sheet gasket material for windows and chamber ends.
73	Monitor and Keyboard	1 ea	Installed	Tiger Direct	Monitor: A179-2268 Keyboard: A68-1200	N/A	$169.98	Acer 22" LCD flat panel monitor with Adesso SlimTouch keyboard and touchpad combination
74	Mass Air Flow Sensor and Filter	1	Installed	Pro-M Racing LLC	Model 92	03A2794	$44.99	Used existing MAF but ordered a new filter
75	Electronics Rack	1	Installed	Rack Mount Solutions	ERK-2125 21U	N/A	$448.00	

Ref #	Item	Qty	Status	Contact	Part Number	S/N	Price	Notes
76	Electronics Rack Components	N/A	Installed	Parts Express and Rack Mount Solutions	Various	N/A	$402.16	Rack Rail 21U (P/N 262-394), 10-32 Rack Screws (P/N 262-590), Selves (P/Ns FVS1918-24 1U, 34-1058 1U)
77	Miscellaneous Supplies	N/A	Used or Installed	Various Suppliers	N/A	N/A	$649.45	Includes tooling, various bolts and fittings, extra materials, table replacement casters, etc.
78	Steam Ejector	1	Not Ordered	Fox Venturi Products, Larry Fox, 973 328 1011 ext 0	N/A	N/A	$0.00	4" x 4' steam ejector proposed to generate system pressures lower than 7 psia, quoted at $5500
79	Temporary 480V 3 Phase 50A Line	1	Installed	Wesco and HVM	N/A	N/A	$2,480.92	
						Total	$90,582.43	

Bibliography

1) United States Air Force Unmanned Aircraft Systems Flight Plan 2009-2047, Headquarters, United States Air Force, Washington DC, 18 May 2009.

2) Weatherington, Dyke, Unmanned Aircraft Systems Roadmap, 2005-2030, Deputy, UAV Planning Task Force, OUSD(AT&L) 2005.

3) Smith, G., Boruta, M., Jerovsek, J., Meitner, P., Meyer Nutating Disk Engine, a New Concept in Internal Combustion Engine Technology, AIAA 2007-5122, 43rd AIAA/ASME/SAE/ASEE Joint Propulsion Conference & Exhibit, Cincinnati, OH, 8-11 July 2007.

4) Haywood, John B., Internal Combustion Engine Fundamentals; McGraw-Hill, Inc., 1988.

5) http://www.marineengineeringonline.com/scavenging_in_diesel_engines.htm [cited 5 Dec 2010].

6) Cadou, C., Moulton, N., Menon, S., Performance Measurement and Scaling in Small Internal-Combustion Engines, AIAA 2003-0671, 41st Aerospace Sciences Meeting and Exhibit, Reno, NV, 6-9 January 2003.

7) Cadou, C., Sookdeo, T., Moulton, N., Leach, T., Performance Scaling and Measurement for Hydrocarbon-Fueled Engines with Mass Less than 1 Kg, AIAA 2002-3448, AIAA's 1st Technical Conference and Workshop on Unmanned Aerospace Vehicles, S, Portsmouth, VA, 20-23 May 2002.

8) Menon, S., Moulton, N., Cadou, C., Development of a Dynamometer for Measuring Small Internal-Combustion Engine Performance, Journal of Propulsion and Power, Vol. 23, No. 1, January-February 2007. DOI: 10.2514/1.19825

9) Cadou, C., Menon, S., Scaling of Losses in Small IC Aero Engines with Engine Size, AIAA 2004-690, 42nd AIAA Aerospace Sciences Meeting and Exhibit, Reno, NV, 5-8 January 2004.

10) Shin, Y., Chang, S.H., Koo, S.O., Performance Test and Simulation of a Reciprocating Engine for Long Endurance Miniature Unmanned Aerial Vehicles, Proceedings of Institution of Mechanical Engineers Vol. 219, Part D: Journal of Automobile Engineering, Pg 573-581, 6 Oct 2004.

11) Harari, R., Sher, E., The Effect of Ambient Pressure on the Performance Map of a Two-Stroke SI Engine, 930503, SAE International Congress & Exposition, Detroit, MI, Pg 115-123, 01 March 1993.

12) Watanabe, I., Kuroda, H., Effect of Atmospheric Temperature on the Power Output of a Two-Stroke Cycle Crankcase Compression Gasoline Engine, 810295, SAE International Congress and Exposition, Detroit, MI, 23-27 February 1981.

13) Flynn, P.F., Hunter, G.L., Farrell L.A., Durrett, R.P., Akinyemi, O.C., Westbrook, C.K., Pitz, W.J., The Inevitability of Engine-Out NOx Emissions from Spark-Ignition and Diesel Engines, 28th International Symposium on Combustion, Edinburgh, Scotland, 11 Jan 2000. US DOE Lawrence Livermore National Laboratory.

14) Chen, Rong-Horng, Chiang, Li-Bin, Wu, Ming-Hsun, Lin, Ta-Hui, Gasoline displacement and NOx reduction in an SI engine by aqueous alcohol injection; Fuel 89 (2010) pg 604-610.

15) Wilson, C., Performance of a Small Internal Combustion Engine Using N-Heptane and Iso-Octane, AFIT Thesis, AFIT/GAE/ENY/10-M28, Air Force Institute of Technology, Wright Patterson AFB, OH, March 2010.

16) Lee, K., Yoon, M., and Sunwoo, M., A Study on Pegging Methods for Noisy Cylinder Pressure Signal, Control Engineering Practice 16, pg 922 to 929, Elsevier Ltd., 28 Nov 2007.

17) Bertola, A., Stadler, J., Walter, T., Wolfer, P., Gossweiler, C., Rothe, M., Spicher, U., Pressure Indication During Knocking Conditions, Pressure Sensor, Kistler Instrumente AG, special print 920-349e-11.06, 2006.

18) Walter, T., Brechbühl, S., Gossweiler, C., Schnepf, M., Wolfer, P., Pressure Indicating with Measurement Spark Plugs on a DI-Gasoline Engine – State of Technology, Combustion Engines, Kistler Intrumente AG, special print 920-333e-09.04, 2004.

19) Revised Thermocouple Reference Tables, *Reference Tables N.I.S.T. Monograph 175 Revised to ITS-90*, pgs Z-204 to Z-205, http://www.omega.com/temperature/Z/pdf/z204-206.pdf cited [2 Jan 2011].

20) Beshia,S., Deniz, O., Chomiak, J., Gupta, A., An Experimental Study of the Variations in Cyclic Energy Release Rate in a Spark Ignition Engine, AIAA 89-2890, AIAA/ASME/SAE/ASEE 25th Joint Propulsion Conference, Monterey, CA, July 10-12, 1989.

21) Ceviz, M. A., Intake Plenum Volume and its Influence on the Engine Performance, Cyclic Variability and Emissions, Energy Conversion and Management 48 (2007) pgs 961-966.

22) Celik, M. B., Performance Improvement and Emission Reduction in Small Engine with Low Efficiency, Journal of the Energy Institute, Vol 80, No 3, pgs 175-180, 2007.

23) Turns, S. R. An Introduction to Combustion (2nd Ed.). New York: McGraw-Hill, Inc., 1996.

24) Kilpatrick, D.A., Calculation methodology for basic engine exhaust gaseous emissions parameters, "National Gas Turbine Establishment Memorandum M81002" Feb 1981, Controller HMSO London.

25) Procedure for the Analysis and Evaluation of Gaseous Emissions from Aircraft Engines, SAE Aerospace Recommended Practice ARP1533 Revision A; Issued 1996-01, Revised 2004-07.

26) Totten, G. E., Westbrook, S. R., and Shah, R. J., Fuels and Lubricants Handbook: Technology, Properties, Performance, and Testing, ASTM International, Glen Burnie, 2003.

27) NIST Chemistry Webbook. http://webbook.nist.gov [cited 22 Jan 2011].

28) Handbook of Aviation Fuel Properties(Second Printing). Prepared by the Coordinating Research Council, Inc., Society of Automotive Engineers, Inc., May 1984

29) National Energy Technology Lab, Office of Fossil Energy, U.S. Department of Energy, R & D Facts, Fischer-Tropsch Fuels April 2008 http://www.netl.doe.gov/publications/factsheets/rd/R&D089.pdf [cited 22 Jan 2011].

30) Korres, D.M. and Karonis, E. Lois. Use of Alternative Fuels on a Diesel Engine, AIAA 1st International Energy Conversion Engineering Conference, Portsmouth, VA, 2003.

31) Antonovski, Viktorio, Rotavera, Brandon M., Petersen, Eric L., Combustion Measurements of Synthetic Fuels at Gas Turbine Conditions, 43rd AIAA/ASME/SAE/ASEE Joint Propulsion Conference, AIAA-2007-5667, 8-11 July 2007, Cincinnati, OH.

32) Arpa, Orhan, Yumutas, Recep, Experimental investigation of Gasoline-Like Fuel obtained from waste lubrication oil on engine performance and exhaust emission, Fuel Processing Technology 91 (2010) pg 197-204.

33) National Oceanic and Atmospheric Administration, National Aeronautics and Space Administration, United States Air Force, U.S. Standard Atmosphere, 1976, Washington D.C., October 1976.

34) Moffat, R.J., Using Uncertainty Analysis in the Planning of an Experiment, Journal of Fluids Engineering, June 1985, Vol 107, pg 173-178.

35) Moffat, R.J., Describing the Uncertainties in Experimental Results, Experimental Thermal and Fluid Science, 1988; 1:3-17. Elsevier Science Publishing Co. Inc.

36) Kline, S.J., McClintock, F.A., Describing Uncertainties in Single-Sample Experiments, Mechanical Engineering, pg 3-8, Jan 1953.

37) Vortech Engineering, Inc., Compressor Performance Map, Model V5 K-trim, Test 1213F, 16 July 2010.

38) A-T Controls, Inc., Triac Division, "V" Series Control Port Ball Valves, 0308-V, http://download.a-tcontrols.com/pdf/Series-V.pdf [cited 21 February 2011].

39) Incropera, F.P., DeWitt, D.P., Bergman, T.L., Lavine, A.S., Fundamentals of Heat and Mass Transfer (6^{th} Ed.), New York: John Wiley and Sons, Inc., 2007.

40) ASME, Guide for Glass and Plastic Window Design for Pressure Vessels, 2.0/17606e011.doc, November 2008.

41) Riley, W.F., Sturges, L.D., Morris, D.H., Mechanics of Materials (5^{th} Ed.), New York: John Wiley and Sons, Inc., 1999.

Vita

Captain Peter John Schmick was born in St. Paul, Minnesota and graduated from Champlin Park High School in June 2000. He enrolled in undergraduate studies at Iowa State University in Ames, Iowa in the Fall of 2000. He majored in aerospace engineering with a minor in military studies. Capt Schmick was a graduate of the four year Air Force Reserve Officer Training Corps program at Detachment 250. He graduated with a B.S. in aerospace engineering and was commissioned in the United States Air Force in December 2004.

Peter's first assignment was at the Air Force Research Lab Propulsion Directorate Detachment 7 at Edwards AFB, CA. He served as a test stand engineer in the Experimental Demonstrations Branch on Test Stand 2A from 2005 until June 2007. After a short period working as the Predictive Avoidance engineer for the Airborne Laser Flight Test Squadron, he took over as the BMC4I integrated product team lead for the 417 FLTS. Following this assignment, he enrolled in the Graduate School of Engineering and Management at the Air Force Institute of Technology in August 2009, seeking a degree in Aeronautical Engineering. Upon graduating, he will be assigned to the AFRL Air Vehicles Directorate at Wright Patterson AFB.

REPORT DOCUMENTATION PAGE

Form Approved
OMB No. 074-0188

1. REPORT DATE *(DD-MM-YYYY)*	**2. REPORT TYPE**	**3. DATES COVERED** *(From – To)*
24-03-2011	Master's Thesis	August 2009 – March 2011

4. TITLE AND SUBTITLE

Effect of Atmospheric Pressure and Temperature on a Small Spark Ignition Internal Combustion Engine's Performance

5a. CONTRACT NUMBER

5b. GRANT NUMBER

5c. PROGRAM ELEMENT NUMBER

6. AUTHOR(S)

Schmick, Peter J., Captain, USAF

5d. PROJECT NUMBER

5e. TASK NUMBER

5f. WORK UNIT NUMBER

7. PERFORMING ORGANIZATION NAMES(S) AND ADDRESS(S)

Air Force Institute of Technology
Graduate School of Engineering and Management (AFIT/EN)
2950 Hobson Way, Building 640
WPAFB OH 45433-8865

8. PERFORMING ORGANIZATION REPORT NUMBER

AFIT/GAE/ENY/11-M28

9. SPONSORING/MONITORING AGENCY NAME(S) AND ADDRESS(ES)

Air Force Research Lab, Propulsion Directorate, Turbine Combustion Branch, 1790 Loop Road, Wright Patterson AFB, OH, Paul Litke, DSN 785-1673, paul.litke@wpafb.af.mil

10. SPONSOR/MONITOR'S ACRONYM(S)
AFRL/RZTC, SERL

11. SPONSOR/MONITOR'S REPORT NUMBER(S)

12. DISTRIBUTION/AVAILABILITY STATEMENT

APPROVED FOR PUBLIC RELEASE; DISTRIBUTION UNLIMITED.

13. SUPPLEMENTARY NOTES

The views expressed in this thesis are those of the author and do not reflect the official policy or position of the United States Air Force, Department of Defense, or the United States Government. This material is declared a work of the U.S. Government and is not subject to copyright protection in the United States.

14. ABSTRACT

The ever increasing use of man portable unmanned aerial vehicles, UAV, by the US military in a wide array of environmental conditions calls for the investigation of engine performance under these conditions. Previous research has focused on individual changes in pressure or temperature conditions of the air stream entering the engine. The need was seen for a facility capable of providing an environment representative of various simulated altitude conditions. A mobile test facility was developed to test small internal combustion engines with peak powers less than 10 hp. A representative engine was tested over a range of speeds from 2000 RPM to 9000 RPM at every 1000 RPM. The throttle was set to 50%, 75%, and 100% open at each of the speeds tested. The test engine was tested at environmental conditions representing sea level standard day conditions, 1500 m conditions and 3000 m conditions. The engine torque, fuel flow rate, and air flow rate were measured at each test point to determine the impact of combined pressure and temperature variations on engine performance. During the process of testing the engine and the test stand it was determined that the fuel to air ratio for the engine had a significant impact on engine operation. The test engine failed to under fuel rich or fuel lean conditions.

15. SUBJECT TERMS

Spark Ignition, Internal Combustion Engine, Altitude, BSFC, BMEP, Two-stroke

16. SECURITY CLASSIFICATION OF:			**17. LIMITATION OF ABSTRACT**	**18. NUMBER OF PAGES**	**19a. NAME OF RESPONSIBLE PERSON**
a. REPORT	**b. ABSTRACT**	**c. THIS PAGE**			Marc Polanka, PhD.
U	**U**	**U**	**UU**	166	**19b. TELEPHONE NUMBER** *(Include area code)* (937) 255-6565, ext 4714 (marc.polanka@afit.edu)

Standard Form 298 (Rev. 8-98)
Prescribed by ANSI Std. Z39-18